UNIVERSITA' DEGLI STUDI DI NAPOLI

FEDERICO II

FACOLTÀ DI INGEGNERIA

Dipartimento di Ingegneria chimica, dei Materiali e della Produzione industriale
DOTTORATO IN INGEGNERIA DEI MATERIALI E DELLE STRUTTURE
XXV CICLO

MULTIPLEXED MICROGELS FOR OLIGONUCLEOTIDES DETECTION

Ph.D. Thesis

ANNA ALIBERTI

Advisor: Professor Paolo A. Netti

Tutor: Assistant Professor Filippo Causa

MULTIPLEXED MICROGELS FOR OLIGONUCLEOTIDES DETECTION

by

ANNA ALIBERTI

In Partial Fulfillment of the Requirements for the Degree of

Doctor of Philosophy in

Engineering Materials and Structures

at the

Federico II University of Naples

April 2013

Advisor_____

Professor Paolo A. Netti

Tutor_____

Assistant Professor Filippo Causa

Chairman, Department Committee for Graduate Student_____

Professor Giuseppe Mensitieri

MULTIPLEXED MICROGELS FOR OLIGONUCLEOTIDES DETECTION

by

ANNA ALIBERTI

In Partial Fulfillment of the Requirements for the Degree of
Doctor of Philosophy in Engineering Materials and Structures

Abstract

The development of rapid detection strategies toward point-of-care applications has been receiving increasing attention due to the time and labor intensive protocols associated with well-established assays. In particular, assays that are free of separation, amplification, and other related operations are highly desirable.

In recent years, the use of encoded beads has received considerable attention due to their potential for measuring multiple analytes in solution. This can be achieved without the need for knowledge of their spatial position, as in the case of microarray technology. Encoded bead technology also relies on the solution kinetics rather than diffusion to a fixed surface as in the case of microarray technology, offering the possibility of developing rapid high throughput screening methods. Attempts to develop this technology tend to focus on the generation of featured barcodes both with a large number of identifications to increase the throughput and with novel functions to improve the assays.

This thesis describes a synthesis, characterization and unique properties of multi-responsive encoded core shell microgel. for the direct detection in multiplex of single strands nucleic acids (ssDNA, miRNA etc) at very low concentration

(femtomolar), without the need of other conventional tools such as PCR, Southern blot or microarray.

The encoded microgels are provided by a wide range of fluorescence-based codes with an innovative core-shell material architecture. However, compared to the already validated bead based detection systems, microgel composed by bio inert PEG are no fouling with minimal nonspecific binding that makes them favorable for assays in complex biological samples.

The platform assay, named MEDiA (**M**icrogel **E**nhanced **Di**splacement **A**ssay) consists of innovative probes, that mounted on PEG-encoded microgels, are able to capture and reveal the presence of the complementary oligonucleotides strand of DNA or miRNA through fluorescence emission.

The conjugation on particle surface brings a large number of fluorofore probes into a small region which significantly increases the fluorescence intensity and facilitates further manipulation.

Here we provide the proof of concept of the assay by using genetic material specific for viruses such as SARS, HIV, HCV and RNA, i.e. miRNAs.

The detection mechanism is based on a double strand displacement assay. Compared to other homogeneous assays for nucleic acids, ds displacement assay acts as integrated sensor that can i) be mounted on bead surfaces, ii) capture the target molecules and iii) highlight the binding event.

The evaluation of nucleotide concentration as well as the code is a result of fluorescence emission analysis over a fixed number of microgels.

The flexibility of the proposed platform could allow performing point of care analysis, both where the sensitivity is not a stringent requirement and both where an ultra-sensitive quantification is necessary by using fluorescent microscopy or miniaturized systems (lab-on-chip).

Acknowledgments

First, I would like to sincerely thank prof. Paolo Netti, for taking me into his research group and giving me a chance to work in his laboratory. I am extremely grateful to have had the fortunate opportunity to participate in such interesting and rewarding science. He was always passionate and enthusiastic about his research projects, he was very open to new ideas and showed me how exciting research can be.

I would like to express my special appreciation and thanks to my tutor Professor Filippo Causa, you have been a tremendous mentor for me. I would like to thank you for encouraging my research and for allowing me to grow as a research scientist. Your advice on both research as well as on my career have been invaluable.

Long discussions with Edmondo Battista have significantly improved my work and inspired many new research directions with his careful and instructive comments.

In particular, I am deeply grateful to Angela Cusano. To work with you has been a real pleasure to me, with heaps of fun and excitement. You have been a steady influence throughout my Ph.D. career; you have oriented and supported me with promptness and care, and have always been patient and encouraging in times of new ideas and difficulties; you have listened to my ideas and discussions with you frequently led to key insights. Your ability to select and to approach compelling research problems, your high scientific standards, and your hard work set an example. I admire your ability to balance research interests and personal pursuits.

In addition, I have been very privileged to get to know and to collaborate with many other great people at the IIT @CRIB center. I learned a lot from you about life, research, how to tackle new problems and how to develop techniques to solve them.

I want to thank the ’carmates’ friend Enza Torino for her support and the enjoyable discussions about life, Ph.D.s, politics, news, and all that.
Furthermore, I also want to thank all other friends who put up with me through the whole Ph.D. process and helped me with personal challenges. Thank you for sharing these years with me.
I would like to thank Antonio Massaro for his love and encouragement. And, thank you for your support when I have needed it the most. You have supported me, bearing the brunt of the frustrations, and sharing in the joy of the successes. Thank you with all my heart!
Finally, I would like to thank my mom, dad, and sister for their infinite support throughout everything. Grazie.

.

Table of Contents

List of Figures

List of Schemes

List of Tables

List of Abbreviations

DLS	dynamic light scattering
pNIPAm	poly(*N*-isopropylacrylamide)
VAA	vynil acetic acid
RCA	rolling circle amplification
QD	quantum dots
PEG	poly(ethyleneglycol)
Ag	antigen
Ab	antibody
qPCR:	quantitative polymer chain reaction
MB	molecular beacons
BPs	binary probes
ds assay	double strand displacement assay
dsDNA	double-stranded DNA
dsProbe	double-stranded probe
Kd	dissociation costant
RM	replica molding
PEGDMA	poly(ethylene glycol) dimethacrylate average
AAc	acrylic acid
KPS	potassium persulfate
EDC	1-ethyl-3-(3-dimethylaminopropyl) *carbodiimide*
PVA	Polyvinyl alcohol
AIBN	2,29-azobisisobutyronitrile
BPO	Benzoyl peroxide
DMSO	Dimethyl Sulfoxide
NaOH	Sodium Hydroxide
RhodamineB-acrylate	methacryloxyethyl thiocarbonyl rhodamine B

Fluorescein acrylate	fluoresceine *O*-methacrylate
D_h	hydrodynamic diameter
ζ	zeta potential
μ	electrophoretic mobility
λ	wavelength of incident light
η	viscosity (
ρ	density
v	particle volume
m_p	particle mass
R_h	hydrodynamic radius
DNA	Deoxyribose Nucleic Acid
Cy5	cyanine
BHQ	Black Hole quencher
nt	nucleotide
MEDiA	**M**icrogel **E**nhanched **Di**splacement **A**ssay
LOD	limit of detection
fM	femtomolar
pM	picomolar
CLSM	Confocal Laser Scanning Microscopy

CHAPTER I

INTRODUCTION

The work presented in this thesis revolves around the development of diagnostic tool through the combination of two prominent areas of research: hydrogel and oligonucleotide detection. In order to lay out a framework for the topics covered in the thesis, this chapter outlines: (1) the properties of hydrogel material that make them ideal for biological assay, (2) the existing strategies for multiplexed biomolecules detection, (3) the emerging clinically significance of oligonucleotides (DNA e/or RNA) detection.

1 Hydrogel Materials

1.1.1 Definition and classification of hydrogels

Hydrogels, by definition, are three-dimensional cross-linked polymeric networks that can imbibe large amounts of water.[1-4] These materials are generally classified into one of two categories based on their cross-linking chemistry.[5] The first category entails physical gels which are defined as polymeric networks that are bound together via polymer chain entanglement and/or non-covalent interactions that exist between polymer chains.[1,3,6,7] The attractive forces holding these networks together are typically based on hydrogen bonding, electrostatic or hydrophobic interactions and thus, the gels can be reversibly dissolved under certain conditions that would weaken these attractive forces, i.e. a change in pH.

In contrast to these weak physically cross-linked networks, the other general class of hydrogels is chemically cross-linked gels. These hydrogels exhibit improved stability due to the formation of covalent bonds between different polymer chains throughout the networks and display endurance with respect to network structure.[1,5,8] These gels are commonly formed through monomer polymerization in the presence of a cross-linking agent, which is typically a monomer with at least two polymerizable functional moieties.

Beyond this simple classification of hydrogel materials based on cross-linking chemistry, these networks can also be categorized on the basis of their responsivity or lack thereof.

Non-responsive gels are simple polymeric networks that dramatically swell upon exposure to water. Responsive gels, on the other hand, have added functionality and display changes in solvation in response to certain stimuli such as temperature,[9] pH,[10,11] ionic strength,[12-14] light,[15-19] and electric field.[20] Hence, this effect has broad implications in many arenas including biotechnology and biomedicine,[21] reversible volume changes (sometimes as large as several hundred times the original volume) in response to minute changes in external environmental conditions have been thoroughly reported for a variety of gels derived from polymeric networks.[20,21]

Yet another area in which hydrogel materials can be categorized is based on gel dimensions. Typically, hydrogels can be categorized as either macrogels or microgels. Macrogels are bulk, monolithic networks that typically range in size from millimeters or greater.[9] Microgels, on the other hand, are defined as colloidally stable, water swellable polymeric networks whose diameter typically ranges from 100 nm to 1 μm.[10] While microgels internally have the same gel structure as their macroscopic version, microgels and macrogels are physically different. Microgel particles have surface to volume ratios that are several orders of magnitude larger than those existing in bulk gels.[22] The synthesis of microgel particles typically involves a nucleation, aggregation and growth mechanism that ultimately results in a non-uniform distribution of polymer chains throughout the network.[22,23]

1.1.2 Synthesis and modification of microgels

The goals of microgel synthesis include controlling the particle size distribution, the colloidal stability, and the distribution of specific functional groups such as crosslinker, charged groups, or reactive centers for further chemical derivatization. The commonly adopted approach for microgel synthesis is (co)polymerization of vinyl monomers with cross-linker. It is convenient to divide the diverse range of microgel preparation strategies into three classifications based on the particle formation mechanism – those formed by homogeneous nucleation, those formed by emulsification, and those formed by complexation.

Homogeneous nucleation refers to those preparations in which microgel particles are generated from initially homogeneous (or nearly so) solutions. Emulsification refers to those methods where aqueous droplets of a pregel solution are formed in an oil or brine phase and, in the second step, the droplets are polymerized and/or cross-linked into a microgel. Finally, microgels can be prepared by mixing two dilute, water-soluble polymers that form complexes in water.

In particular for homogeneous nucleation, a solution of soluble monomer, including some type of cross-linking agent, is fed into the reactor and microgel particles form over the course of polymerization. A key requirement for discrete microgel particle formation is that the polymer formed must be insoluble under the polymerization (e.g., photo- and thermal-initiated polymerization). [41]

Figure 1.1 shows the mechanism of microgel formation under homogeneous condition. Sulfate radicals generated in solution initiate the homogeneous polymerization of monomer and crosslinker. However, the insolubility of the oligomer network under polymerization conditions causes the growing polymer chain to phase separate, forming precursor particles that are not colloidally stable. As the aggregated precursor particles coalesce, the charged chain ends tend to concentrate at the particle/water interface. Therefore, as the aggregates grow, the surface charge density increases until a point is reached

where the growing particle is colloidal stable with respect to similar sized or larger particles. These first formed stable particles are called primary particles. To achieve a monodisperse product, the primary particles must be formed at low monomer conversion. In later stages of polymerization, all newly formed precursor particles deposit onto existing stable microgels contributing to particle growth.

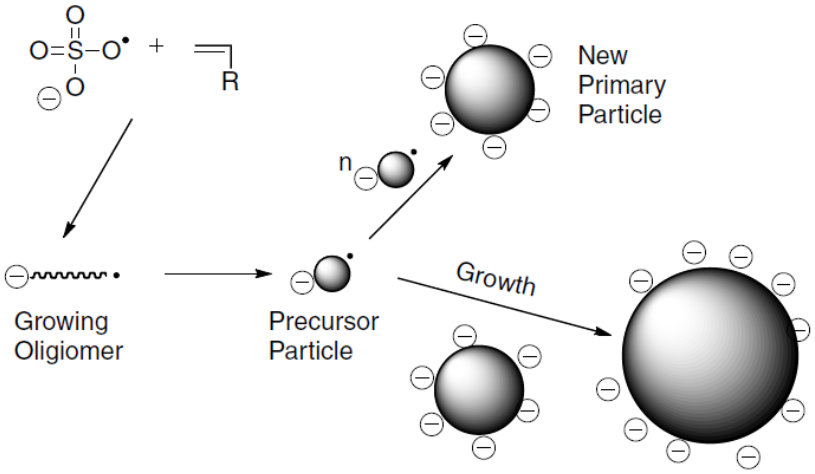

Figure 1.1 Microgel formation mechanism. Initially, unstable precursor particles aggregate to form new primary particles. At the end of nucleation stage, all new precursor particles are captured by existing stable particles.

There are few variables in the above microgel synthesis in this condition, thus it is difficult to obtain a wide range of average microgel diameters. Using a surfactant, it is possible to influence microgel particle nucleation and thus the final size. The role of surfactant is to stabilize the primary particles so that they are smaller than those prepared without. The smaller the primary particles, the higher the total number of primary particles that are initially formed, resulting in smaller microgels for the same dose of monomer.

1.1.3 Core/shell microgels

In addition to one-pot copolymerization, microgels with “core-shell”, topology were also prepared via two-step “seed-feed” polymerization. Almost all

kinds of functional groups could be incorporated into microgel particles by one-pot copolymerization, two-step "seed-feed" polymerization, and post-functionalization. [42]

The core/shell materials is the one that has hydrogel in both the core and the shell. Lyon' group first reported the synthesis of this type of hydrogel particles by two-stage polymerization.[42] In this method a polymer shell of the same or different structure or functionality of the core, is added onto preformed core particles thereby allowing control over the radial distribution of the functional groups in the particle. In a typical synthesis, preformed core particles are used as seed particles, followed by addition and initiation of the shell monomer solution. This method gives core/shell particles with no increase in polydispersity, as all oligomers formed in solution attached on pre-formed core particles. To prevent heteronucleation there are several important parameters that should be controlled, including the concentration of the core, initiator, surfactant and the shell monomer. The mechanism by which this reaction takes place is somewhat similar to that for the core microgels. The core particles tend to capture the growing oligomers, which results in the formation of the shell.

Core/shell particles prepared in this fashion can exhibit very interesting properties.[43-47] Since the shell can be synthesized using different comonomers than the core, the particles can show multiple phase transition behavior with temperature. Furthermore, depending upon the cross-linker density of the shell, compression or "shrink-wrapping" of the core can be observed due to a cross-link gradient in the shell.[43, 44, 46, 47]

The Lyon group has also used this synthetic method to make hollow hydrogel capsules. [48] To accomplish this, the core is fabricated with a degradable cross-linker and the shell with a non-degradable one. The degradable crosslinker that we have used contains a vicinal diol, which can be degraded by stoichiometric addition of periodate. After core degradation, the particles were cleaned extensively by centrifugation, after which dynamic light scattering (DLS) and fluorescence were used to confirm the hollow structure.

1.1.4 Modifications of microgels

For certain applications not all of the desired hydrogel functionalities can be added during the polymerization step. There are several reasons for this: the desired functionalities may not be stable during the polymerization step or the molecules are simply not polymerizable. This is especially true for most biomolecular structures from which hybrid gels would be prepared. To allow further functionalization of hydrogels, most often a small amount of comonomer with acidic or basic functionality is copolymerized during the polymerization step. These functional groups are then used for attachment of molecules that could not be directly incorporated by polymerization. [49]

Most of the standard techniques for coupling (conjugating) small molecules, peptides, oligonucleotides, and proteins are applicable to microgels [50]. Indeed, microgels offer important advantages: first, microgels can be centrifuged and readily redispersed, which facilitates cleaning (more on this later); second, subtle changes can be followed by dynamic light scattering, which is sensitive to swelling, microelectrophoresis, and to surface charge; third, microgels are generally more colloidally stable than latexes and other nanosized support particles.

The usual starting points for microgel derivatization are carboxyl or amine groups. Biotin, [51] streptavidin, [52] proteins, [53] and oligonucleotides [54] have been conjugated to microgels. Carbodiimide-based coupling chemistries seem to be the most popular. However, most publications do not include good descriptions of either the amounts or the location of coupled material.

Delair et al [54] reported the immobilization of DNA on microgels by post polymerization modification. Microgels composed of pNIPAm with an amine comonomer were synthesized. Single stranded DNA with an amine group at the 5' end was reacted with 1,4-phenylene diisocyanate in 1:2 ratio so that one of the isocyanates was coupled to the DNA, while the other one remained free. After purification, the DNA was coupled to the poly(*N*-isopropylacrylamide) (PNIPAM)

microgels by reacting the free isocyanate with the amines on the surface of the particles. The DNA particles were then used for detection of viral DNA and also for formation of two dimensional arrays on planar substrates.

Ali et al [55] reported the synthesis of VAA-PNIPAM carboxyl-containing microgel to conjugate a 5'-amine modified DNA. They investigate whether DNA-microgel conjugates were compatible with enzymatic reactions that are commonly used for manipulations of DNA in the design of DNA based bioassays or biosensors. It was demonstrated that DNA oligonucleotides covalently coupled to colloidal microgel can be manipulated by T4 DNA ligase for DNA ligation and by Phi29 DNA polymerase for rolling circle amplification (RCA). The work also show that the long single stranded RCA product can generate intensive fluorescence upon hybridization with complementary fluorescent DNA probe.

Pelton et al reported[52] the use of PNIPAM microgels as support particles for protein and oligonucleotide-based biosensors for paper-supported applications. They prepared paper strips printed with carboxylic microgels that were modified either with an antibody or with a DNA aptamer. They found that the antibody and the DNA aptamer retained their recognition capabilities when coupled to microgel. The printed microgel remains stationary during chromatographic elution while the microgel-supported molecular recognition elements are accessible to their intended targets present in the elution solution. The work indicates that microgels, large enough to isolate the biosensors from the paper surface, are sufficiently hydrophilic to be wetted during chromatographic elution, exposing the gel-supported affinity probes to their targets.

1.2 Multiplex assay

1.2.1 Beads *versus* planar array

In the field of medical diagnostics there is a growing need for inexpensive, accurate, and quick high throughput assays. Different recognition systems (based on immunological reactions, reactions of hybridization of nucleic acids or peptides) have been successfully used in combination with different transduction strategies (electrochemistry, optics) for multiplex detection systems in biomedical field. [56]

Multiplexed assays, where multiple tests or "panels" are performed on the same sample, offer the potential of performing a large number of different assays all in a single reaction vessel with volume equivalent to a single microtitre plate well therefore using smaller sample volumes than traditional ELISAs.

There are two broad classes of technologies used for multiplexing: planar arrays and suspension (particles based) arrays - both of which have application-specific advantages.

Planar-array technologies involve depositing two-dimensional grids of probe molecules (antibodies, oligonucleotides, drug candidates etc.) onto flat solid supports, each array location acting as a probe for a known target molecule. Although arrays are having a major impact on high-density screening, microarrays suffer from some disadvantages, including slow reaction kinetics, problems with localization of the biomolecules bound to the chip (making printing of high-density arrays complex), and inflexibility of probe combinations used in an assay. To overcome these issues, particles-based arrays have been developed. [57]

Particles-based arrays have significant advantages over planar arrays in terms of the way they are produced and used. Regardless of whether planar arrays are produced by photolithography or robotic spotting, there is a relatively low upper limit to the number of arrays that can be produced at the same time. Probe molecules must be attached to each spot of a planar array individually, whereas they can be conjugated to millions of microspheres at the same time, with a degree

of reproducibility that is impossible to reproduce in microarray production. Many of the problems that afflict planar arrays stem from the fact that all probe molecules must be attached to the array under the same conditions using the same surface chemistry, which may not be suitable for all of them. By contrast, individual probe molecules can be attached to separate batches of microspheres by a variety of proven chemistries under conditions that are optimum for each probe.

Planar arrays are often inflexible because they impose a predetermined panel of tests on the user, but when microspheres are used the panel can easily be changed by adding or subtracting microspheres with different probes.

The rates of hybridization and binding on planar arrays are limited by diffusion to the surface, but the kinetics of binding to microparticles can be accelerated by efficient mixing. Microspheres facilitate the separation and washing steps, and may even allow these to be eliminated altogether. They are inexpensive to produce in large numbers and allow minute sample volumes to be interrogated. The use of many microspheres for each target molecule in the same assay permits rigorous statistical scrutiny of the data and leads to high quality results. Particles can be analysed in microfluidic systems, providing a high throughput platform, which can be integrated into low-cost devices for biochemical research and point-of-care medical diagnostic applications. Potentially particles could be directed post analysis into different reaction vessels, for split-and-mix synthesis where molecules such as a peptides or oligonucleotides are progressively and combinatorially synthesized on the beads. [58-61]

1.2.2 The problem: encoding

When two-dimensional arrays are used to perform multiplexed assays the identity of each probe molecule is known from its location in the grid. This method of identification is known as positional encoding. (**Figure 1.2 a**)

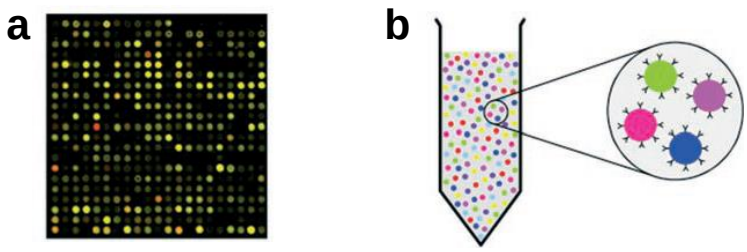

Figure 1.2 a) Conventional microarray consists of a two-dimensional grid of recognition molecules (antibodies, peptides, oligonucleotides etc.). The identity of the recognition molecules at each spot in the array is known from its location in the grid**. b)** A suspension array is composed of recognition molecules attached to encoded particles (in this image the particles are encoded with different colors). The identity of the recognition molecules attached to each particle is revealed by reading the particle code.

The benefits of using microspheres stem from their freedom to move in three dimensions, but this rules out positional encoding. Instead each microsphere must contain some form of code that identifies the probe molecules attached to it (**Figure 1.2 b**). Provided the probes can be identified, the target molecules bound to them can be identified in the same way as molecules bound to two-dimensional arrays.

A microparticle encoding technique must satisfy a number of requirements: it must be machine-readable by non-contact methods; suitable for encoding particles of tens of microns in size; unaffected by the biochemical reactions; robust, with low error rate; able to encode large numbers of particles, each with a unique code; implementable on materials which are compatible with biomolecule attachment and amenable to low-cost mass production (particularly important for diagnostic applications). A large number of techniques have been proposed for encoding beads: optical, graphical or physical.

1.2.3 Optical Encoding

Most of the suspension arrays described in the literature are composed of polymer microspheres internally doped with one or more fluorescent dyes. Polystyrene microspheres become swollen when suspended in an organic solvent, allowing the dye molecules diffuse into them, but when the microspheres are

transferred to an aqueous solution they shrink and the dye molecules become entrapped. By trapping dyes with different emission spectra at different concentrations (and thus intensities), microspheres with unique spectral codes are obtained. The number of codes depends on the number of dyes and intensities according to the formula: $C = N^{m-1}$ (where C=the number of codes, N=the number of intensity levels and m=the number of colors), but in practice other factors limit the number of spectrally distinct codes that can be generated. The dyes must be compatible in the swelling solvent and the doping process must be reproducible; this becomes more difficult as the numbers and concentrations of the dyes increase. For multiplexed detection a reporter dye is required and the region of the spectrum that is occupied by its emission profile is not available for encoding.

Luminex Corp (Austin, TX)[62,63] supplies microspheres that are encoded with organic dyes as part of their xMAP liquid array technology. They encode 5.5-μm microspheres with two dyes at ten different concentrations to produce up to 100 different sets of microspheres (**Figure 1.3 a**). Each set is matched to a different probe molecule that confers specificity on the microspheres in multiplexed assays (**Figure 1.3 b**).

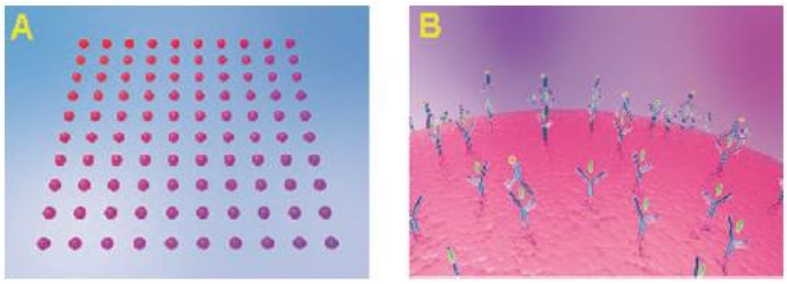

Figure 1.3 a) Suspension array composed of 100 sets of optically encoded microspheres. In this image one microsphere from each set has been organized into a two dimensional grid to emphasize the similarities and differences between suspension and planar arrays. Each set of microspheres in a suspension array is equivalent to one probe molecule in a planar array. Reading the code, rather than determining the position, reveals the identity of the probe molecules attached to the microspheres. **b)** Each set of microspheres in a suspension array has a different probe molecule attached to its surface.

Semiconductor quantum dots [64,65] are photoluminescent nanoparticles that have dimensions smaller than the exciton Bohr radius of the corresponding bulk material. For spherical CdS nanoparticles this limit is reached when the particles

have a diameter of less than 10 nm. The effect of quantum confinement gives rise to unique optical and electronic properties that are different from those of the component atoms or the bulk solids composed of them. These include narrow, quantum dots (QD) -size-tunable emission spectra (20–30 nm), and the possibility of exciting all colors at the same wavelength. Their narrow emission spectra allow 10–12 different colors to be resolved in the visible region (400–800 nm) with acceptable spectral overlap. These properties make QDs ideal for encoding. They can be incorporated into microspheres during synthesis or entrapped by solvent swelling methods similar to those used for fluorescent dyes. In theory, six colors at six different intensities would yield around 40 000 different codes, but in practice overlap between the different intensities is a major limitation (**Figure 1.4**). It is still necessary to use a reporter for multiplexed assays and this region of the spectrum is not available for encoding. [66]

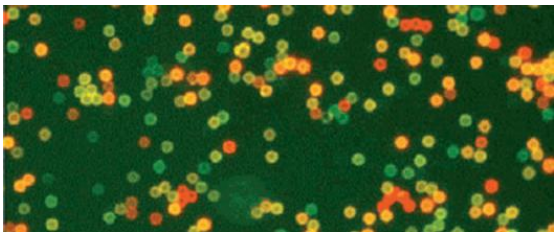

Figure 1.4 Microspheres encoded with different colors and ratios of semiconductor QDs

Although encoding microspheres with luminescent dyes or nanoparticles is the most popular method for producing encoded suspension arrays, a growing number of alternatives are being explored.

1.2.4 Graphical encoding

One of the earliest forms of encoding particles was based on microstructuring different materials, creating patterns which constitute a code.

Pregibon et al. [67] recently demonstrated the encoding, analyte attachment (to the particles) and reading of the codes all within a microfluidic system. The

method of manufacturing the encoded microparticles is shown in **Figure. 1.5 a**; two streams of the monomers of poly(ethyleneglycol) (PEG) flow together down a microfluidic channel, remaining separate due to laminar inside microchannels. One stream contains fluorescently labelled monomers, that form the code region, while the other contains monomers and a biological probe (for example an oligonucleotide) for use in an assay. The particles are defined and patterned using UV light passed through a mask and a reduction lens; regions of high UV intensity polymerize the monomers forming a solid particle from which the un-crosslinked monomer is subsequently rinsed, leaving holes that represent the desired code.

The region surrounding the holes representing the code digits is fluorescent, increasing the signal-to-noise ratio and allowing the code to be read simultaneously with the analysis of target attachment (**Figure 1.5 b**). The other half of the particle has the biological probe attached, for use in bead based assays using these particles.

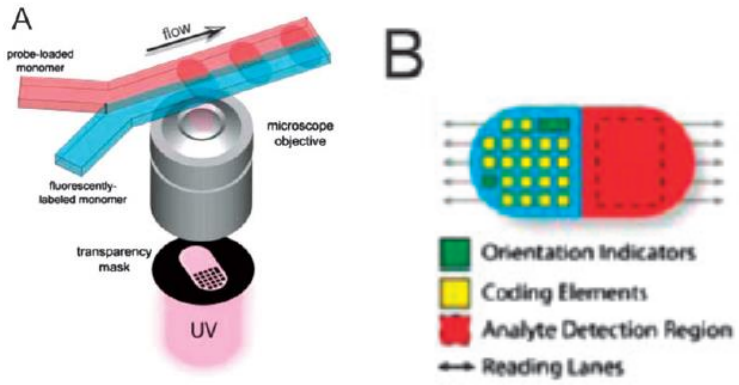

Figure 1.5 a) Particles manufactured in-flow from a PEG photopolymer. Two flow streams contain fluorescent labeled PEG for the code section of the particle and PEG with probe attached for the analyte section of the particle. **b)** The resulting particles contain a code featuring orientation digits and the code digits themselves, and an analyte region, both of which are read along the lines defined by the arrows.

The disadvantages of this method are the larger concentrations of probe molecules required to obtain a loading level similar to most other bead-based technologies (around 50 times larger), and the fact that the technology may be problematic for protein assays, because of the potential for UV-induced denaturation of the probes during particle formation.

1.2.5 Physical Encoding

Physical characteristics, such as size and refractive index, are usually the properties of entire particles and therefore do not offer much scope for multiplexing.

The Copalis system developed by DiaSorin was based on particle size.[68] Their dedicated flow cytometer was able to discriminate approximately 0.1-μm differences in bead diameter on the basis of low-angle light scattering. Immunoassays based on the measurement of scattered or absorbed light are an extension of the basic principles underlying latex agglutination tests. The change in the light scattered is used to measure the amount of antigen (Ag) or antibody (Ab) which causes the immunological Ab-Ag precipitation reaction or agglutination reaction (if latex is used).

In a basic light-scattering immunoassay, polyvalent antigens react with divalent antibodies to form large complexes, the antibody effectively forming a bridge between antigen molecules. A protein antigen, which can be considered multivalent, with possibly multiple copies of the same epitope as well as different epitopes, can produce a large immune complex made up of several molecules. When the sample contained the corresponding antibodies, the microspheres formed aggregates that were detected in the flow cytometer (**Figure 1.6**).

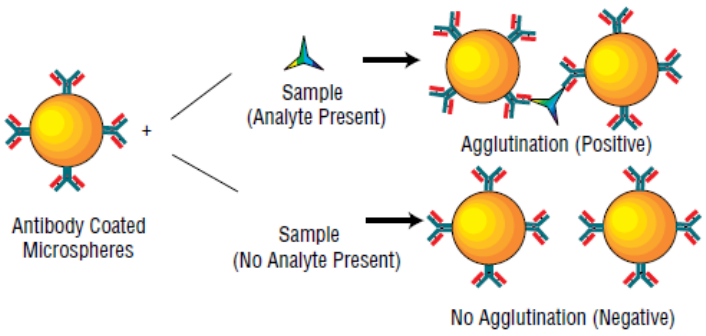

Figure 1.6 Direct agglutination assay

Although individual physical properties offer limited scope for multiplexing they can be combined with each other, and with other encoding strategies. Modern flow cytometers can decode particles on the basis of size and refractive index as well as photoluminescence. Microspheres have been encoded with up to six fluorescent dyes located in separate shells alternating with nonfluorescent spacer shells round a silica core. Microspheres prepared in this way display a diverse range of optical signatures derived from a combination of fluorescence wavelength and intensity, size and refractive index, but only those with a unique optical signatures are suitable for encoding.

1.3. Nucleic acids

1.3.1 Nucleic acid detection

Nucleic acids (DNA and RNA) are extremely attractive targets for diagnostics. They are highly specific, can be amplified to increase abundance in most applications, and can be labeled (for detection) using a number of approaches. Mutations (changes in nucleic acid sequence) can indicate disease. In addition to sequence, the abundance of nucleic acid targets is also of great importance. The up- or down- regulation of nucleic acid production is an important indicator for applications like drug discovery and cancer diagnostics.[70] Therefore, the assessment of both nucleic acid sequence and relative expression level is extremely important for diagnostics applications.

In particular, miRNAs play a crucial role in physiological as pathological processes. Most notably, this class of molecules has been implicated in development and progression of various types of cancers including breast, lung, ovarian, prostate, and liver cancers.[71] In addition, to serving as oncogenes and tumor suppressor genes, miRNAs have also been identified as significant agent in the development of HIV/AIDS, herpes virus infection, cardiovascular disease.[71-75]

This connection between aberrant expression of miRNAs and the emergence of disease states has led many researchers to look upon the 100 known human miRNAs as biomarker set that can be analyzed for diagnostic and prognostic purpose. Early efforts have demonstrated that profiling select sets of miRNAs offers a surprising wealth of information on the developmental lineage and differentiation state of tumors.

The stability of miRNAs in a wide range of biological contexts is another significant factor in their emergence as a new class of biomarker. It has been shown that their small size and association with both ribonucleoprotein complexes and exosomes can protect them from degradation by RNase. In recent years, circulating miRNAs have been discovered in several readily accessible biological fluids including serum, plasma and urine. Correlation between disease state and expression level of these circulating species suggest that miRNAs could be strong candidates for the development of noninvasive biomarker screens for the early, asymptomatic detection of tumor genesis and for monitoring of the treatment response.[76]

In any given diagnostic test, the targets (nucleic acids) must be manipulated, captured, or detected. For a test to be meaningful, it must be specific fot the target(s) of interest and sensitive enough to detect entities at physiologically-relevant quantities. Nucleic acids are a natural choice as recognition elements due to their intrinsic molecular base pairing ability. As bio recognition elements, nucleic acids offer a high degree of selectivity and stability. Oligonucleotide analysis is based on specific hybridization be-tween a single-stranded nucleic acid oligonucleotide “probe” sequence and the sample “target” sequence to be detected. The probe can be either free in solution or immobilized on a substrate (e.g. microparticles, optical fiber and glass slide). Target hybridization is often coupled to a signal generation scheme.

1.3.2 Current strategies for DNA and miRNA detection

A wide variety of probes have been designed and synthesized for detecting oligonucleotides *in vivo* and *in vitro*. [77]

To date the most widely used techniques in literature to study the expression profile of DNA and miRNAs, are based on microarray analysis. These approaches are particularly attractive for miRNA since they allow multiplexed detection of miRNAs.[78]

Microarray technologies are based on the hybridization between target molecules and their respective complementary probes. Oligonucleotide probes are immobilized on a support platform through a covalent link and fluorescent labeled nucleotides are hybridized with the array. The specific link between targets and probes generates fluorescent signals that are revealed and quantified as discrete spots on the slide. This technique is very attractive because it allows the analysis of a large number of nucleotides at the same time obtaining a DNA/RNA expression profile of specific samples.

The trickiest steps in microarray analysis are the design of probes used for capture of target molecules and labeling procedure of biological samples. Several modifications in both these steps have been introduced during the last years that have permitted to improve this technique. In particular, the probe design is influenced by a number of matters related to the nature of miRNAs. Indeed, miRNAs are small molecules that represent only a tiny fraction of total cellular RNA with many of them belonging to the same family and differ only by few nucleotides. These characteristics make it difficult to design multiple probes with a suitable melting temperature (Tm), thus optimizing hybridization conditions without compromising specificity. Microarrays are capable of a large degree of multiplexing, absolute quantification, and high sensitivity (in the 1 fg range) but require incubation for hours or days to achieve these limits. [79]

Other sensitive microRNA detection is typically performed with qPCR, which boasts near single- molecule sensitivity, high selectivity, and 10^7-fold dynamic range. [80] However, PCR amplification also has well-known drawbacks: it is sensitive to contamination, offers inaccurate quantification (limited to 2- to 4-

fold changes in expression), requires validated internal reference genes, and is not easily automated for use in clinical settings.[81-83]

In contrast, traditional northern blotting is highly-quantitative yet takes days to complete and requires large amounts of sample (~10 μg of total RNA).[84] Sequencing is emerging as a unique platform for small RNA discovery but is ill-suited to diagnostics because it is sample-hungry, requires expensive equipment and reagents, and can take up to 2 weeks to complete. [85]

On the other hand, development of rapid detection strategies toward point-of-care applications has been receiving increasing attention due to the time and labor intensive protocols associated with most of the existing assays. In particular, assays that are free of separation, amplification, and bacterial culture are highly desirable.

Several approaches couple signal generation to the hybridization event for the detection of unlabeled nucleic acids in solution, and some of these have been adapted to particle based assay. [86]

Of these, molecular beacons (MBs), binary probes (BPs) and double strand displacement assay (Ds) have shown particular applicability to specific problems such as mRNA tracking, single nucleotide polymorphism, and polymerase chain reaction quantization.[87,88]

Molecular beacons are single-stranded probes with a stem-loop structure that recognize a specific target molecule. The complementary sequence to the target is in the loop of the molecule, while the stem is formed by the annealing of two complementary sequences with a fluorophore linked to the end of one arm and a quencher linked to the end of the other one. Molecular beacons emit fluorescence only when they hybridize with the target, undergoing a spontaneous conformational reorganization that forces the fluorophore and the quencher to move away from each other. This approach is very sensitive to mismatches and, since probes can be linked with different fluorophores, is also helpful to simultaneously detect different target miRNAs. Various assays were then published using the molecular beacons technology, ranging from mRNA in situ visualization [89,90] to nucleic acid sequence-based amplification detection [91], and

multiplex detection of four pathogenic retroviruses. [92] In other applications, molecular beacon probes were designed for use as DNA biosensors by binding molecular beacons to beads (*BEADCONS*) allowing the specific detection of viruses complementary sequences. [93]

BPs, [87,88] on the other hand, consists of two fluorophore-containing oligonucleotide strands that hybridize to adjacent regions of a target sequence, thus favoring energy transfer between the neighboring fluorophores. These probes have been extensively studied and modified to enhance their detection characteristics using different dye combinations, three-dye arrays, excimer-forming molecules and metal complexes.

Double-stranded DNA (dsDNA) probe is a homogeneous assay for rapid detection of specific nucleic acid sequences and can potentially be applied for pathogen identification. [94-98]

In the dsDNA sensing scheme, it is possible to identify two different steps: the primary duplex formation, and the related, but distinct process of strand displacement. In a strand displacement event, the target strand must replace the original partner strand of the initial or primary duplex to form a new or secondary duplex. This exchange of partner strands can be reported by either a signal-on event (e.g. a quenched fluorophore becomes fluorescent following duplex formation with a target) or a signal-off event (e.g. the initial duplex contains a fluorescently labeled strand that is removed as a secondary duplex forms). Successful displacement is promoted if the target of interest has a greater affinity for one of the strands in the initial duplex or double-stranded probe (dsProbe). Thus, in terms of effective reporting, the ideal dsProbes possess (i) sufficient base-pair matches to remain thermally stable in the absence of a target of interest, but (ii) fewer base-pair matches than the target of interest. [99]

Compared to other homogeneous assays for nucleic acids, such as a molecular beacon, advantages of dsDNA probes include the possibility of adjusting the quencher-to fluorophore ratio for noise minimization and the flexibility of modifying the lengths of the quencher sequence and the sticky end for improving the specificity and kinetics of the assay. The dsDNA probes have been

demonstrated in various biomedical applications, including detection of single nucleotide mismatches, quantification of PCR products, and quantification of DNA binding proteins.[100]

In addition, to make easier the detection of circulating miRNAs, new techniques have been recently developed (**Figure 1.7**) . By performing miRNA detection through an electrochemical geno-sensor, Lusi *et al.* [101] were able to directly detect miRNAs without the need of PCR and a labeling reaction, with an assay simple, very fast and ultrasensitive (detection limit of 0.1 pmol). Further developing these and other approaches will certainly enable the application of circulating miRNAs as biomarkers for cancer diagnosis.

However, a common drawback of all these approaches remains the lack of a house-keeping miRNA for normalization of circulating miRNAs that, in contrast to tissue or cellular miRNAs, cannot be normalized against U6 since it is present in a very low concentration in serum and plasma.[102] Nevertheless, the normalization of the volume of serum or plasma samples has been proposed as an effective way to overcome such problems. The best approach is to normalize experimental miRNA data using spiked-in synthetic, nonhuman mature miRNA from *C. elegans* or plants as control.[103]

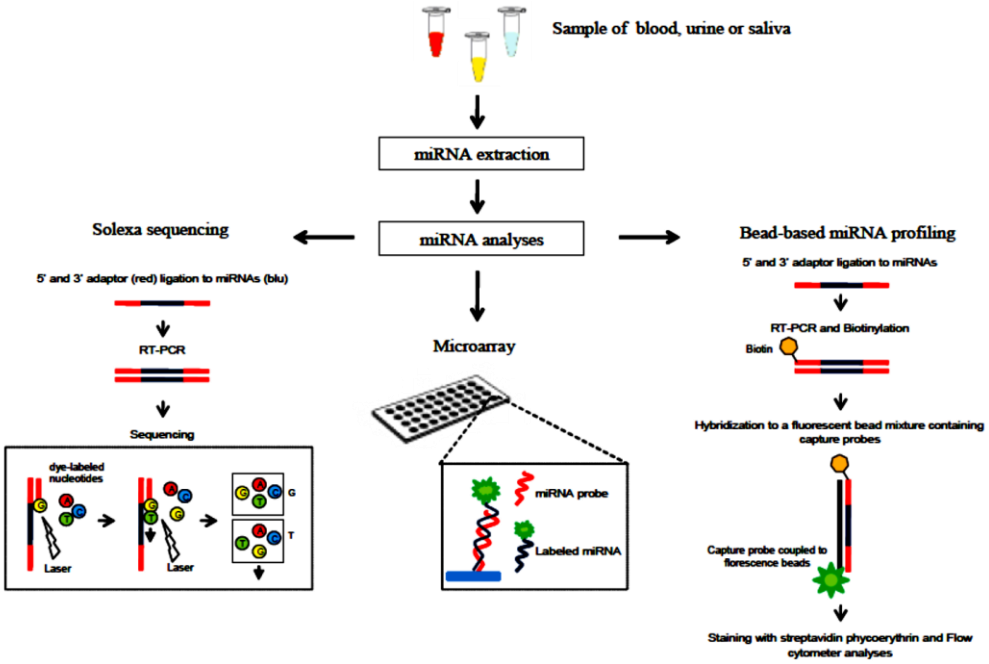

Figure 1.7 Main methods used for miRNA detection.

1.3.3 Thermodynamics of hybridization on solid surface

The most important parameter in determining sensitivity and specificity of any given hybridization is the dissociation costant (Kd) of the nucleic acid complexes involved. for a system with target T, probe P, and target-probe complex TP, the dissociation constant is given by ratio of their equilibrium concentrations ([mol/L]) as:

$$Kd= [T][P]/[TP] \quad (1\text{-}1)$$

As such, when complex formation is favorable, Kd, is very small. While complex formation (for oligomers 20bp or longer) in solution is very favorable (Kd ~ 10^{-12}- 10^{-20}), it is well know that solid surface methods suffer from drammatrically inhibited kinetics (Kd ~ 10^{-7}). [104-105] The reason for this is that there is an energy cost associated with transferring target molecules into probe forest on solid surface where they can then associate with their complement strands.

1.3.4 Hydrogel substrate for nucleic acid detection

As an alternative to solid surface, hydrogel based substrates have been used for biomolecule detection. Hydrogels are a class of polymeric materials that are bio-friendly with three dimensional structures that characteristically retain water. Mirzabekov's group has done a considerable amount of work in producing "MAGIC" and "IMAGE" chips, [106-107] which are gel-based analogs of traditional microarrays (**Figure 1.8**).

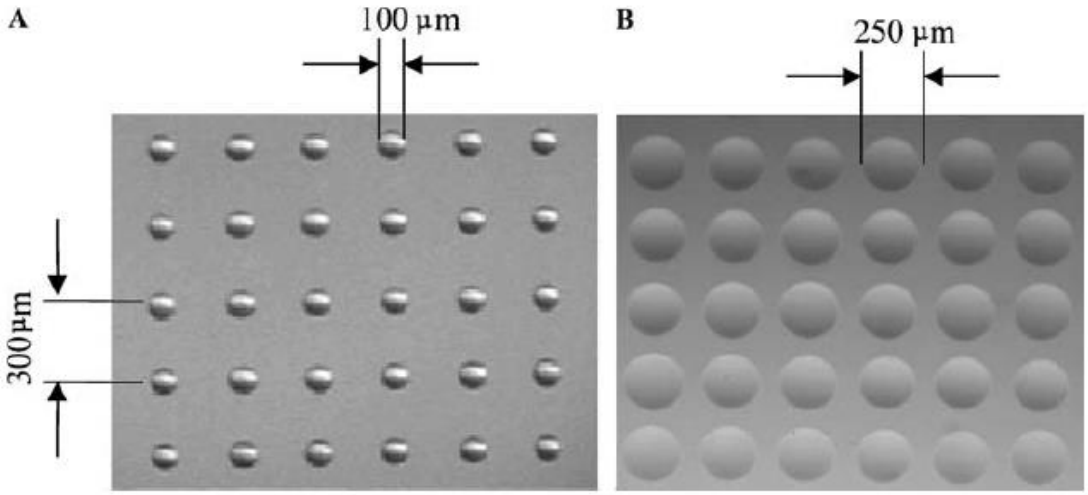

Figure 1.8 Photographs of the microchip gel elements in transmitted light. Drops of polymerization mixture were applied with 150-lm robot pin and polymerized **a)** on hydrophobic glass surface treated with Bind Silane and **b)** on hydrophilic surface treated with 3-aminopropyl triethoxysilane.

The most significant advantage of hydrogel systems over solid-substrate is that while hybridization thermodynamics are greatly suppressed on solid surfaces, hybridization in gels closely resembles solution kinetics. In addition to favorable thermodynamics, gel arrays also offer a much higher effective probe density due to their 3D structure [106] and a broad range of material and linkage chemistries. Planar hydrogel arrays have shown a great enhancement of both signal and signal and sequence discrimination over their solid counterparts.

Although several materials have been used in hydrogel synthesis, those made of poly(ethylene glycol) (PEG) precursor provide a non-fouling surface to maximize assay specificity. Bio-inert substrates provide a favorable envoirment that is chemically transparent to biological species. In addition, PEG oligomers are available in a broad range of molecular weight and functionalities, providing versatility in material design.

Lewis *et al* [108] identify and investigate several critical parameters in the fabrication of single-stranded DNA conjugated poly- (ethylene glycol) (PEG) microparticles based on replica molding (RM) for highly uniform and robust nucleic acid hybridization assays. The effects of PEG-diacrylate, probe DNA, and photoinitiator concentrations on the overall fluorescence and target DNA penetration depth upon hybridization are examined. Fluorescence and confocal

microscopy results illustrate high conjugation capacity of the probe and target DNA, femtomole sensitivity, and sequence specificity (**Figure 1.9**).

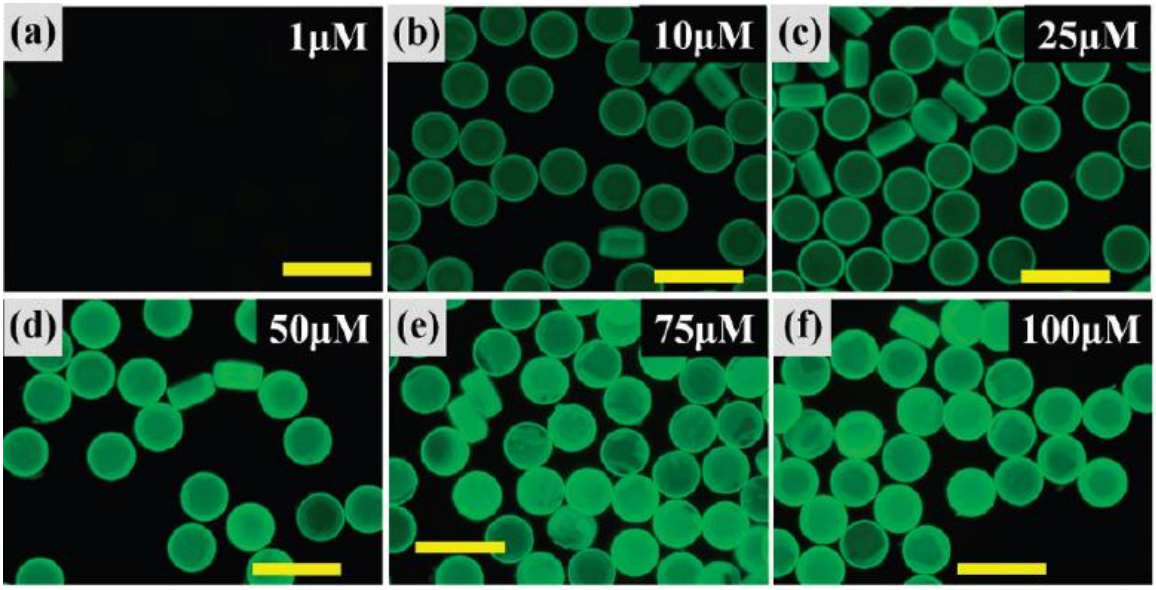

Figure 1.9 . Effect of probe DNA concentration. Fluorescence micrographs (a-f) of microparticles upon target DNA hybridization. Scale bars represent 200 μm.

Combined, these findings demonstrate a significant step toward simple, robust, and scalable procedures to manufacture highly uniform and high capacity hybridization assay particles in a well-controlled manner.

Because of their wide availability, bio-friendly nature, and favorable hybridization characteristics, hydrogels are ideal substrates for bioassay and many other biological applications.

1.4. Aim of the work

The aims of this PhD work are to provide an encoded microgel carriers for the direct detection in multiplex of single strands nucleic acids (ssDNA, miRNA), ranging from 20 to 100 bases, at very low concentration (femtomolar), without the need of other conventional tools such as PCR, Southern blot or microarray.

The assays set up consists of innovative probes, that mounted on encoded microgels, are able to capture and reveal the presence of the complementary oligonucleotides strand of DNA or miRNA through fluorescence emission.

The mechanism is based on a double strand displacement assay. The encoded microgels are provided by a wide range of fluorescence-based codes with an innovative material architecture. The evaluation of nucleotide concentration as well as the code is a result of fluorescence emission analysis over a fixed number of microgels.

Bibliography

[1] Hoffman, A. S. *Adv. Drug Delivery Rev.* **2002**, *54*, 3-12.

[2] Drury, J. L.; Mooney, D. J. *Biomaterials* **2003**, *24*, 4337-4351.

[3] DeRossi, D.; Kajiwara, K.; Osada, Y.; Yamauchi, A. *Polymer Gels: Fundamentals and Biomedical Applications*; Plenum Press: New York, 1991.

[4] Dhara, D.; Nisha, C. K.; Chatterji, P. R. *J. Macromol. Sci., Pure Appl. Chem.* **1999**, *A36*, 197-210.

[5] Hennink, W. E. *Adv. Drug Delivery Rev.* **2002**, *54*, 13-36.

[6] Akiyoshi, K.; Kang, E. C.; Kurumada, S.; Sunamoto, J.; Principi, T.; Winnik, F. M. *Macromolecules* **2000**, *33*, 3244-3249.

[7] Collier, J. H.; Hu, B. H.; Ruberti, J. W.; Zhang, J.; Shum, P.; Thompson, D. H.; Messersmith, P. B. *J. Am. Chem. Soc.* **2001**, *123*, 9463-9464.

[8] Eddington, D. T.; Beebe, D. J. *Adv. Drug Delivery Rev.* **2004**, *56*, 199-210.

[9] Li, Y.; Tanaka, K. *J. Chem. Phys.* **1990**, *92*, 1365-1371.

[10] Jones, C. D.; Lyon, L. A. *Macromolecules* **2000**, *33*, 8301-8306.

[11] Moselhy, J.; Wu, X. Y.; Nicholov, R.; Kodaria, K. *J. Biomater. Sci., Polym. Ed.* **2000**, *11*, 123-147.

[12] Duracher, D.; Sauzedde, F.; Elaiessari, A.; Perrin, A.; Pichot, C. *Colloid Polym. Sci.* **1998**, *276*, 219-231.

[13] Duracher, D.; Sauzedde, F.; Elaiessari, A.; Pichot, C. *Colloid Polym. Sci.* **1998**, *276*, 920-929.

[14] Snowden, M. J.; Chowdhry, B. Z.; Vincent, B.; Morris, G. E. *J. Chem. Soc.- Faraday Trans.* **1996**, *92*, 5013-5016.

[15] Sershen, S. R.; Westcott, S. L.; Halas, N. J.; West, J. L. *J. Biomed. Mater. Res.* **2000**, *51*, 293-298.

[16] Sershen, S. R.; Westcott, S. L.; West, J. L.; Halas, N. J. *Appl. Phys. B* **2001**, *73*, 379-381.

[17] Sershen, S. R.; Westcott, S. L.; Halas, N. J.; West, J. L. *Applied Physics Letters* **2002**, *80*, 4609-4611.

[18] Suzuki, A.; Tanaka, T. *Nature* **1990**, *346*, 345-347.

[19] Suzuki, A.; Ishii, T.; Maruyama, Y. *J. Appl. Phys.* **1996**, *80*, 131-136.

[20] Tanaka, T.; Nishio, I.; Sun, S. T.; Ueno-Nishio, S. *Science* **1982**, *218*, 467-469.

[21] Kishi, R.; Miura, T.; Kihara, H.; Asano, T.; Shibata, M.; Yosomiya, R. *J. Appl. Polym. Sci.* **2003**, *89*, 75-84.

[22] Saunders, B. R.; Crowther, H. M.; Morris, G. E.; Mears, S. J.; Cosgrove, T.; Vincent, B. *Colloids Surf. A* **1999**, *149*, 57-64.

[23] Wu, X.; Pelton, R. H.; Hamielec, A. E.; Woods, D. R.; McPhee, W. *Colloid Polym. Sci.* **1994**, *272*, 467-477.

[24] Peppas, N.; Hilt, J. Z.; Khademhosseini, A.; Langer R. *Adv. Mater.* **2006**, *18*, 1345–1360.

[25] Merrill, E.; Salzman, E.; Wan, S.; Mahmud, N.; Kushner, L.; Lindon, J.; Curme, J. *Trans.—Am. Soc. Artif. Intern. Organs* **1982**, *28*, 482.

[26] *Biomaterials Science: An Introduction to Materials in Medicine* (Eds: B. D. Ratner, A. S. Hoffman, F. J. Schoen, J. E. Lemons), 2nd ed., Elsevier Academic, Amsterdam, The Netherlands **2004**.

[27] Whitesides, G. M.; Ostuni, E.; Takayama, S.; Jiang, X. Y.; Ingber, D. E. *Annu. Rev. Biomed. Eng.* **2001**, *3*, 335.

[28] West, J.; Hubbell, J. *React. Polym.* **1995**, *25*, 139.

[29] West, J.; Hubbell, J. *Macromolecules* **1999**, *32*, 241.

[30] Hern, D. L.; A. Hubbell, J. *J. Biomed. Mater. Res.* **1998**, *39*, 266.

[31] Huh, K.; Bae, Y. *Polymer* **1999**, *40*, 6147.

[32] N. A. Peppas, P. Bures, W. Leobandung, H. Ichikawa, *Eur. J. Pharm. Biopharm.* **2000**, *50*, 27.

[33] Jeong, B.; Kim, S.; Bae, Y. *Adv. Drug Delivery Rev.* **2002**, *54*, 37.

[34] Miyata, T.; Uragami, T.; Nakamae, K. *Adv. Drug Delivery Rev.* **2002**, *54*, 79.

[35] Khare, A. R.; Peppas, N. A. *J. Biomater. Sci., Polym. Ed.* **1993**, *4*, 275.

[36] Scott, R.; Peppas, N. *Macromolecules* **1999**, *32*, 6149.

[37] Podual, K.; Peppas, N. *Polym. Int.* **2005**, *54*, 581.

[38] Kim, S. W.; Bae, Y. H.; Okano, T. *Pharm. Res.* **1992**, *9*, 283-290.

[39] Ulijn, R. V.; Bibi, N.; Jayawarna, V.; Thornton, P. D.; Todd, S. J.; Mart, R. J.; Smith, A. M.; Gough, J. E. *Mater. Today* **2007**, *10*, 40-48.

[40] Hoffman, A. S. *Adv. Drug Deliv. Rev.* **2002**, *54*, 3-12.

[41] Fernandez-Nieves, A.; Wyss, H.; Mattsson, J. and Weitz D.A. Microgel Suspensions: Fundamentals and Applications, **2011.**

[42] Jones, C. D.; Lyon, L. A. *Macromolecules* **2000**, *33*, 8301-8306.

[43] Tian, P.; Wu, Q. L.; Lian, K. *J. Appl. Polym. Sci.* **2008**, *108*, 2226-2232.

[44] Suzuki, D.; Kawaguchi, H. *Langmuir* **2005**, *21*, 8175-8179.

[45] Suzuki, D.; Kawaguchi, H. *Colloid Polym. Sci.* **2006**, *284*, 1443-1451.

[46] Suzuki, D.; Kawaguchi, H. *Langmuir* **2006**, *22*, 3818-3822.

[47] Hantzschel, N.; Zhang, F. B.; Eckert, F.; Pich, A.; Winnik, M. A. *Langmuir* **2007**, *23*, 10793-10800.

[48] Hu, X.; Tong,Z. and Lyon, L.A *J. Am. Chem. Soc.* **2010**, *132*, 11470–11472

[49] H. Maeda, L. W. Seymour and Y. Miyamoto, *Bioconjugate Chemistry*, 1992, **3**, 351-362.

[50] Hermanson, G.T. *Bioconjugate Techniques*, **1996**, Academic Press, San Diego, CA.

[51] Nayak, S. and Lyon, L.A. *Angew. Chem., Int. Ed.*, **2004**, *43*, 6706–6709.

[52] Su, S., Ali, M.M., Filipe, C.D.M., Li, Y. and Pelton, R *Biomacromolecules*, **2008**, *9*, 935–941.

[53] Hamerska-Dudra, A., Bryjak, J., and Trochimczuk, A.W. *Enzyme Microb. Technol.*, **2007**, *41*, 197–204.

[54] Delair, T., Meunier, F., Elaissari, A., Charles, M.H., and Pichot, C. *Colloids Surf. A*, **1999**, *153*, 341–353.

[55] Ali,M.; Su, S.; Filipe,C.; Pelton, R. and Li, Y. *Chem. Commun*., **2007**, 4459–4461.

[56] Birtwell, S. and Morgan, H. *Integr. Sam Biol*., **2009**, *1*, 345-362.

[57] Wilson, R.; Cossins A.; Spiller, D. *Angew. Chem. Int. Ed*. **2006**, *45*, 6104– 6117

[58] Meza, M. B. *Drug Discovery Today*, **2000**, *1* (HTS Suppl.), 38 – 41.

[59] Rao, R. S.; Visuri, S. R.; McBride, M. T.; Albala, J. S.; Mathews, D. L.; Coleman, M. A.; *J. Proteome Res.* **2004**, *3*, 736 – 742.

[60] Probst, M.; Rothe, G.; Schmitz, G. *J. Lab. Med*. **2003**, *27*, 182 – 187.

[61] Braeckmans,K.; De Smedt,S.; Leblans, M.; Pauwels, R.; Demeester, *J. Nat. Rev. Drug Discovery* **2002**, *1*, 447 –456.

[62] Vignali, D. *J. Immunol. Methods* **2000**, *243*, 243 – 255.

[63] Kellar, K.; Iannone, M. *Exp. Hematol*. **2002**, *30*, 1227 – 1237.

[64] Sutherland, A. *Curr. Opin. Solid State Mater. Sci*. **2002**, *6*, 365 –370.

[65] Chan,W.; Maxwell,D.; Gao,X.; Bailey,R:; Han, M.; Nie, S.M. *Curr. Opin. Biotechnol.* **2002**, ***13***, 40 – 46.

[66] Gao,X.; Nie,S.M. *Anal. Chem.* **2004**, *76*, 2406 – 2410.

[67] Pregibon, D. and Doyle P. *Anal Chem*. **2009**, *81*, 4873–4881

[68] Benecky, M.; Post,D.; Schmitt, S.; Kochar, M. *Clin. Chem.* **1997**, *43*, 1764 – 1770.

[69] Lawrie, G.; Battersby,B.; Trau, M.; *Adv. Funct. Mater*. **2003**, *13*, 887 – 896.

[70] Segal,E.; Friedman, N.; Koller, D.; and Regev, A. *Nature Genetics*, **2004**, *36*, 1090-1098.

[71] Esquela-Kerscher, A. and Slack, F. *Nat. Rev. Cancer*, **2004**, ***6***, 259-269.

[72] Provost, P. *Brain Res.***2010**, *1338*, 58-66.

[73] Small, E.; Frost, R.; Olson, E. *Circulation*, **2010**, *121*, 1022-1032.

[74] Cullen, B. *Nat. Genet.* **2006**, *38*, S25-S30.

[75] Cullen, B. *Nature*, **2009**, *457*, 421-425.

[76] Mitchell, P.S. et al *Proc. Natl. Acad. Sci. USA*, **2008**, *105*, 10513-10518.

[77] Catuogno, S.; Esposito, C.; Quintavalle, C.; Cerchia, L.; Condorelli, G. and de Franciscis , V. *Cancers*, **2011**, *3*, 1877-1898

[78] Wark, A.W.; Lee, H.J.; Corn, R.M. *Angew Chem. Int. Ed. Engl.* **2008**, *47*, 644-652.

[79] Garcia-Schwarz, G. and Santiago, J. *Anal. Chem.* **2012**, *84*, 6366−6369.

[80] Chen, C.; Ridzon, D. A.; Broomer, A. J.; Zhou, Z.; Lee, D. H.; Nguyen, J. T.; Barbisin, M.; Xu, N. L.; Mahuvakar, V. R.; Andersen, M. R.; Lao, K. Q.; Livak, K. J.; Guegler, K. J. *Nucleic Acids Res*. **2005**, *33*, e179.

[81] Corless, C. E.; Guiver, M.; Borrow, R.; Edwards-Jones, V.; Kaczmarski, E. B.; Fox, A. J. *J. Clin. Microbiol.* **2000**, *38*, 1747−1752.

[82] Bustin, S. A.; Nolan, T. *J. Biomol. Tech.* **2004**, *15*, 155−155.

[83] Benes, V.; Castoldi, M. Methods **2010**, *50*, 244−249.

[84] Cissell, K. A.; Shrestha, S.; Deo, S. K. *Anal. Chem*. **2007**, *79*, 4754−4761.

[85] Baker, M. *Nat. Meth*. **2010**, *7*, 687−692.

[86] Nolan, J. and Mandy, F. *Cytometry Part A*, **2006**, *69A*, 318–325.

[87] Tyagi, S.; Kramer, F. *Nat. Biotech.* **1996**, *14*, 303-308.

[88] Marras, S.A.E.; Tyagi, S.; Kramer, F.R. *Clinica. Chimica. Acta* **2006**, *363*, 48-60.

[89] Matsuo, T. *Biochim. Biophys. Acta*, **1998**, *1379*, 178–184.

[90] Sokol, D.L.; Zhang, X.; Lu, P. and Gewirtz, A.M. *Proc. Natl Acad. Sci. USA*,**1998**, 95, 11538–11543.

[91] Leone, G.; van Schijndel, H.; van Gemen, B., Kramer, F.R. and Schoen,C. *Nucleic Acids Res*., **1998**, *26*, 2150–2155.

[92] Vet, J.A.; Majithia, A.R.; Marras, S.A.; Tyagi,S.; Dube,S.; Poiesz, B.J. and Kramer, F.R. *Proc. Natl Acad. Sci. USA*, **1999**, *96*, 6394–6399.

[93] Horejsh,D.; Martini,F.; Poccia,F.; Ippolito, G. *Nucleic Acids Research*, **2005**, *33*, 2-7.

[94] Nutiu, R.; Li, Y. F. *Angew. Chem., Int. Ed.* **2005**, *44*, 1061–1065.

[95] Li, N.; Ho, C. M. *J. Am. Chem. Soc.* **2008**, *130*, 2380–2381.

[96] Li, Q. Q.; Luan, G. Y.; Guo, Q. P.; Liang, J. X. *Nucleic Acids Res.* **2002**, *30*, e5.

[97] Gidwani, V.; Riahi, R.; Zhang, D. D.; Wong, P. K. *Analyst* **2009**, *134*, 1675–1681.

[98] Meserve, D.; Wang, Z.; Zhang, D. D.; Wong, P. K. *Analyst* **2008**, *133*, 1013–1019.

[99] Baker, B. and Milam, V. *Nucleic Acids Research*, **2011**, 1–13

[100] Riahi, R.; Mach,K.; Mohan, R.; Liao, J. and Wong P. *Anal. Chem.* **2011**, *83*, 6349–6354

[101] Lusi, E.A.; Passamano, M.; Guarascio, P.; Scarpa, A.; Schiavo, L. *Anal. Chem.* **2009**, *81*, 2819-2822.

[102] Brase, J.C.; Wuttig, D.; Kuner, R.; Sultmann, H. *Mol. Cancer* **2010**, *9*, 306.

[103] Kroh, E.M.; Parkin, R.K.; Mitchell, P.S.; Tewari, M. *Methods* **2010**, *50*, 298-301.

[104] Wark, A.; Lee, H.; Corn, R. *Angew. Chem., Int. Ed.* **2008**, *47*, 644-652.

[105] Levicky, R. and Horgan, A. *Trends in Biotechnology*, **2005**, *23*, 143-149.

[106] Rubina ,A.; Pan'kov, S.V; Dementieva, E.I; Pen'kov, D.N; Mirzabekov, A. *Analitical Biochemistry*, **2004**, *325*, 92-106.

[107] Sorokin, N.V.; Mirzabekov, A. *Journal of Biomolecular Structure and Dynamics* **2003**, 2 , 279-288.

[108] Lewis, C.; Choi, C.; Lin, Y.; Lee, C. and Yi, H. *Anal. Chem.* **2010**, *82*, 5851–5858.

CHAPTER II

Encoded microgels synthesis and characterization

2.1 Introduction

Free radical polymerization procedure has been used for the preparation of hydrogel with core/shell structures. The core-shell strategy is of particular interest because it permits independent tuning of the core and shell properties and either to introduce spatially localized chemical functionalities to the particle.

The first application of core-shell structure involved the fluorescence spectral encoding. Our encoding method makes use of multiple fluorescent dyes (with no overlapped emission spectra) in which several alternating fluorescent and non-fluorescent concentric hydrogel shells are synthesized around a core particle by using a fluorescent acrylate dyes. In particular, this technique avoided the difficulties related to the mixing of organic fluorescent dyes by physically separating them into different shells.

The process resulting in a population of multi-fluorescent hydrogels particles which display a diverse range of fluorescence emissions and intensities: the ratio of emission spectra of the two dyes (rhodamine and fluoresceine) represents the barcode of a single microgel particles.

Narrowly distributed spherical core-shell hydrogels were prepared by a multi-steps polymerization procedure. Core particles composed of poly(ethylene glycol) dimethacrylate (PEGDMA) and rhodamine B acrylate monomer were prepared by

free-radical precipitation polymerization. The core served as a seed for the subsequent polymerization of PEGDMA non fluorescent shell, resulting in core/shell microgels. By varying the surfactant and monomer concentrations, particle size was controlled while maintaining excellent monodispersity. Finally, a second fluorescent and containing carboxy groups shell was added to these core particles to facilitate subsequent bioconjugation and to complete the barcode.

2.2 Experimental

2.2.1 Materials

Poly(ethylene glycol) dimethacrylate average Mn 550 (PEGDMA), Acrylic acid (AAc), potassium persulfate (KPS), fluoresceine O-methacrylate, 1-ethyl-3-(3-dimethylaminopropyl) carbodiimide (EDC), polyvinyl alcohol 40-88 (PVA), 2,29-azobisisobutyronitrile (AIBN), Benzoyl peroxide (BPO), Dimethyl Sulfoxide (DMSO), Sodium Hydroxide (NaOH) and MES were all purchased from Sigma-Aldrich (St. Gallen, CH) and used as received. The dye Methacryloxyethyl thiocarbonyl rhodamine B was obtained from Polyscience Inc. Tris buffer 1M, pH 8 was supplied by Applichem GmbH (Darmstadt, DE).
Water for all reactions, solution preparation, and polymer purification was distilled and filtered through a 0.2 μm filter to remove particulate matter.

2.2.2 Core double shell microgels synthesis

- **Core synthesis**

PEG microgels were prepared by free-radical precipitation polymerization, using 1% (w/v) total monomer concentration. Polymerization was carried out in a

three-neck, 100 mL round-bottom flask to which a filtered, aqueous solution of all monomers and 1% (w/v) PVA were added. This solution was heated to ~ 70 ºC while being purged with N_2 gas and stirred vigorously for ~ 1 h. Then the reaction was immediately initiated by injection of KPS aqueous solution (to make a final KPS concentration of 2mM). The solution turned turbid, indicating successful initiation. Methacryloxy thiocarbonyl rhodamine B, dissolved in dimethyl sulfoxide (0.1mL) and diluted with water (1.9mL), was then added to the stirred mixture at final concentration ranging from 0.005-0.3mM to obtain different dye amount. The solution was allowed to heat and stir for an additional 7 h while being purged with N_2 gas. The microgels were dialyzed for 15 days against to distilled water, purified several times by centrifuging for 15 minutes at 12000 rpm and resuspending in deionized water to remove unreacted monomers, oligomers and surfactants and stored at 4 °C until further use.

- **1st Shell synthesis**

The Rhodamine-labelled microgel was resuspended in deionized water to a concentration of 10 mg/mL. These microgels were then used as seed particles, upon which a PEGDMA cross-linked shell was added. A solution of Rh-labelled core microgels (100mg, 10 mL) in deionized water (25 mL) was heated to 70 ºC under a gentle stream of N_2. Separately, PEGDMA (240 mg) was dissolved in water (10 mL), purged with N_2 at room temperature and then slowly added to the heated core solution. After the temperature remained stable at 65 ºC for ~ 1 h, 2 ml of aqueous solution of KPS (final concentration of 1mM) was added to initiate the polymerization. The reaction was allowed to proceed for 6 h. The microgels were purified several times by centrifugation (15 minutes at 9000 rpm) and resuspended in deionized water.

- **2nd Shell synthesis**

A solution of core 1st shell microgels (10 mL, [C]=10mg/ml) in deionized water (25 mL) was heated to 65 ºC, followed by the slow addition of 10 mL of aqueous monomer solution containing PEGDMA (240 mg) and AAc (12,5 mg). After the temperature remained stable at 70 ºC for ~ 1 h, 2 ml of aqueous solution of KPS (final concentration of 1mM) was added to initiate the polymerization. Fluoresceine O-methacrylate diluted in water (2mL), was then added to the stirred mixture at final concentration ranging from 0.05-0.2mM to obtain different dye amount. The reaction was allowed to proceed for 6 h. The microgels were dialyzed for 15 days, purified several times by centrifugation (for 15 minutes at 6500rpm) and resuspended in deionized water to remove unreacted monomer, oligomers and surfactants, then stored at 4 °C prior to use until further use.

2.2.3 Characterization methods

2.2.3.1 Particle size and size distribution

Measurements were conducted using Dynamic light scattering (Malvern Zetasizer Nano ZS instrument, 633 nm laser, 173° scattering angle) which allowed calculation of the intensity-average diameter of the particles via the Stokes-Einstein equation. The hydrodynamic diameter (D_h) was determined in the presence of 10^{-3}M KCl as the background electrolyte or at different pH using a diluite microgels solution 0,1% w/v. A total of 5 runs (each comprised of 3 cycles) were conducted; the experimental uncertainties represent the standard error of the mean of 5 replicate runs.

2.2.3.2 Zeta Potential and Electrophoretic Mobility

Measurements were conducted using a Malvern Zetasizer Nano ZS instrument (Malvern Instruments Ltd, Worcestershire, UK). Polystyrene cuvettes were used as sample holders and were rinsed twice with the sample solution before use.

For a charged particle, moving with respect to the solution phase, the potential at the shear surface, with respect to the bulk solution, is usually referred to as the "zeta (ζ) potential".[1] The following **Scheme 2.1** demonstrates the concept of ζ potential.

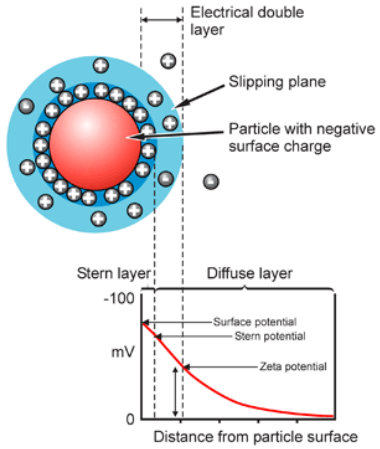

Scheme 2.1 Schematic representation of zeta potential from Malvern Instruments Ltd.(http://www.malvern.com/LabEng/technology/zeta_potential/zeta_potential_LDE.htm)

It is difficult to measure ζ potential directly, and therefore it is estimated indirectly by electrophoresis. In a chamber with parallel oppositely charged electrode, a charged particle is subjected to a uniform electric field *E*, causing it to move towards the oppositely charged electrode. The particle attains a constant velocity *v* when the viscous drag force balances the electric force. The velocity *v* could be used to calculate the electrophoretic mobility μ, which depends on the size, shape, and charge of the particle.

$$v=\mu E \qquad (2\text{-}1)$$

The electrophoretic mobility μ can be related to the ζ potential using various models. [1]

For highly polar solvents such as water, the simplest model relates the zeta potential to the mobility in terms of the viscosity ηs, and the relative permittivity ε_r, of the continuous phase via the Smoluchowski equation, [2]

$$\mu = \varepsilon_0 \varepsilon_r \zeta / \eta_s \qquad (2\text{-}2)$$

where ε_0 is the permittivity *in vacuo*. The problem then becomes measuring the speed of small particles.

The movement of particles can be followed using laser Doppler electrophoresis (LDE). When light is scattered from a moving particle, its frequency will be shifted by an amount depending on the speed and direction of the movement. In the absence of a charge-induced particle flow, the observed frequency broadening is solely due to the Brownian motion of the particles and can be used to calculate the diffusion coefficient and hence hydrodynamic diameter.

When an electrical field is applied to a charged particle, its net motion vector becomes a sum of coherent (charge dependant) and incoherent (Brownian motion). The electrical properties of the scattering particle can then be calculated if these terms can be distinguished. In brief, laser Doppler electrophoresis measures small frequency shifts in the scattered light that arise due to the movement of particles in an applied electric field.

The frequency shift Δf is equal to:

$$\Delta f = 2v \sin(\theta/2)/ \lambda \qquad (2\text{-}3)$$

where v is the particle velocity, θ scattering angel, and λ the wavelength of incident light. However, the signal (coherent) to noise (incoherent) ratio becomes progressively smaller for low mobility particles. The charge-induced movement of the particles could be increased, and therefore be more easily measured, by increasing the time they are exposed to the voltage gradient or increasing the magnitude of that gradient. Unfortunately long experiments can lead to an

accumulation of particles at one of the electrodes and high voltages can lead to Joule heating—either effect would disrupt measurement.

Until recently these limitations made measurement of the charge of low mobility colloids extremely difficult. In phase analysis light scattering (PALS), a laser beam is split, a frequency modulation is applied to a portion of the light and it is then used to generate a scattering pattern from a suspension of particles. The scattered light is recombined with the original (unmodulated) beam. Light scattered from even a stationary.

A Malvern Zetasizer based upon PALS was used to determine the ζ potential of microgel particles in the very dilute regime (0.1wt%) at 20 °C.

The zeta potential, ξ, and electrophoretic mobility, determined in the presence of 10^{-3}M KCl as the background electrolyte or at different pH at 0.1% *w/*v microgel concentration were calculated via Smoluchowski equation by software.

The experimental uncertainties represent the standard error of the mean of 5 runs (each comprised of 50 cycles).

2.2.3.3 Titration

Potentiometric titrations were performed using Compact Titrator G20 (Mettler Toledo AG, Analytical Schwerzenbach, CH). Samples were prepared by suspending 0.050g of microgel in 50 mL of 10^{-3}M KCl solution. Titrations were run in a thoroughly cleaned, 100 mL beaker fitted with a pH electrode and NaOH (0.1 M, freshly prepared from Standard volumetric concentrates) was used as titrant.

During the titration, pH was measured as the function of the volume of delivered standard NaOH solution. After each 50 μL of titrant was delivered into the microgel dispersions, followed by magnetic stirring until the pH value was stable and recorded. The total volume of standard NaOH solution delivered at equivalence point was used to calculate the carboxyl content of microgels.

2.2.3.4 Viscometry and particle mass determination:

Ubbelohde viscometer was used for determining intrinsic viscosity of different microgel preparation.

A capillary viscometer measures a viscosity as defined in the Wells-Brookfield handout, although no parallel plates or force determinations are involved. Capillary viscometry is conceptually simple: the time it takes a volume of polymer solution to flow through a thin capillary is compared to the time for a solvent flow. The flow time (t) for either is proportional to the viscosity (η), and inversely proportional to the density (ρ).

$$t_{solvent} = \frac{\eta_{solvent}}{\rho_{solvent}} \tag{2-4}$$

$$t_{sol'n} = \frac{\eta_{sol'n}}{\rho_{sol'n}} \tag{2-5}$$

We define the relative viscosity to be the ratio $\eta_{sol'n} / \eta_{solvent}$. For most polymer solutions at the concentrations of interest, $\rho_{sol'n} / \rho_{solvent} \approx 1$. Thus, to a very good approximation, the relative viscosity is a simple time ratio:

$$\eta_{rel} = t_{sol'n} / t_{solvent} \tag{2-6}$$

In this work, the flowing time of diluted microgel solution at different concentration was measured. Each time is an average of 5 run measurements.

For the particle mass determination, the bachelor Einsten fitting was performed on two microgel sets.

2.2.3.5 Spectrofluorymetry

2300 EnSpire multilabel reader (Perkin-Elmer, Waltham, MA) was used to measure the fluorescence emission intensity and to record the fluorescence emission spectra.

To evaluate the effect of the initiatior on the dye emission, solutions 10uM of rhodamineB-acrylate and fluoresceine o-methacrylate monomer were put in contact with initiator solutions of BPO, AIBN, and KPS ([initiator]= 2mM) and heated at 65°C for 4 hours. The solution emission spectra were examined by fluorescence spectrophotometry, excitating the rhodamine B monomer at λ= 543 nm and fluorescein acrylate monomer at λ= 488 nm.

To quantify the fluorescence emission of the encoded microgel, all microgel sets were excited at $\lambda ex_{Fluoresceine}$=488 and $\lambda ex_{Rhodamine}$=540 nm .

The number of the counts emission and the emission spectra for the two single dyes were recorded at the same particle concentration: [C] = 1mg $_{microgel}$/ml; V= 100µl, Tris HCl pH 8 buffer.

2.2.3.6 CLSM imaging for fluorescence quantification

30 µl of microgels diluted solutions were loaded onto µ-slide channels (Ibidi, Martinsried, DE), illuminated at confocal laser scanning microscope Leica SP5 using Helium neon laser 543 nm and 633 nm, Argon laser 488 nm and fluorescence images of microgel were collected. Objective: HCX PL APO CS 100.0x1.40 oil, section thickness 1µm, scan speed 8000 Hz, Excitation Laser Argon 488 nm, $\lambda em_{fluoresceine}$ range 500-530 nm, Excitation Laser Helium neon 543 nm, $\lambda em_{Rhodamine}$ range 560-620 nm, image size 77.5x77.5 µm ^{2}.

For microgel experiments, 200 microparticles were selected for each sample (i.e. different target concentrations) to be analyzed and their fluorescence quantified.

All captured images were analysed with a public domain image-processing Image J (version1,43i, NIH, Bethesda, MD). Briefly the images were thresholded by Otsu algorithm and then processed with the Image J Analyze Particles function to computationally determine the number of single fluorescent particles sizing in the range of 1µm.

The fluorescence mean and standard deviation of each sample were calculated and a t-student test was used to compare them (p value < 0.05). The experimental uncertainty represents the standard error of the mean of three replicates measurements.

2.3 Results and discussion

Here we report the synthesis of core-double shell hydrogel by free-radical polymerization. In this approach, a free-radical initiator is used to initiate the reaction, while a surfactant is used to stabilize the growing polymer globule. Classically, one would expect that increasing both the surfactant and initiator concentrations would lead to a reduction in particle size. [3] Potassium persulfate (KPS), 2,29-azobisisobutyronitrile (AIBN), and Benzoyl peroxide (BPO) are a free radical initiator, and as the reaction is heated, they create free radicals and hence growing oligoradicals that act as nucleation sites onto which growing polymer can add.[4] The nature of initiator can affect both the size both number of particles that can potentially be formed. Since the monomer is being consumed by more growing particles under such conditions, the final particle size will be smaller as the same amount of monomer is spread among more particles.

The second control parameter to be explored is that of surfactant concentration. Polyvinyl alcohol (PVA) is the surfactant used in the particle syntheses described below. PVA acts to stabilize the growing nuclei against aggregation early in the reaction. Thus, at lower concentration of PVA, particles formed in the early stages of the reaction aggregate to form larger particles, decreasing the number of particles that are formed in a reaction. Conversely, an increase in concentration of PVA increase the stability of the early nuclei, allowing them to grow without extensive aggregation and therefore increasing the particle number while decreasing the final particle size. Because of the simplicity of these reaction design considerations, these control parameters are commonly used to control particle size. [3]

The selection of a suitable initiator is very important if fine and stable PEG particles are to be obtained. The concentration and decomposition rate of the initiator and temperature are expected to affect the rate of production of free radicals in the medium, determining thus nucleation in dispersion polymerization.

In this study, regular spherical PEG particles were obtained only using the BPO and KPS initiator. If AIBN initiated the polymerization instead of BPO and KPS, an agglomerated product resulted.

This fact can be explained by two reasons. The decomposition rate of the last mentioned compound was probably too high (the half-lives being 289 or 293 min, respectively, at 90 °C) compared with BPO (half-life 1,049 min at 65 °C). Only a moderate rate of radical generation, achieved with BPO, could ensure a relatively short nucleation stage and proper adsorption of stabilizer so that spherical particles were formed.[5]

In addition, the superiority of KPS in the polymerization of PEGDMA to AIBN can consist in that persulfate radicals are known to be more effective than cyanoalkyl radicals.

At this point, to prepare fluorescent hydrogel particles with different range of fluorescence emissions and intensities (the fluorescence spectral code), we choose methacryloxyethyl thiocarbamoyl rhodamine B and fluoresceine O-methacrylate as fluorescent acrylate dyes (**Figure 2.1**):

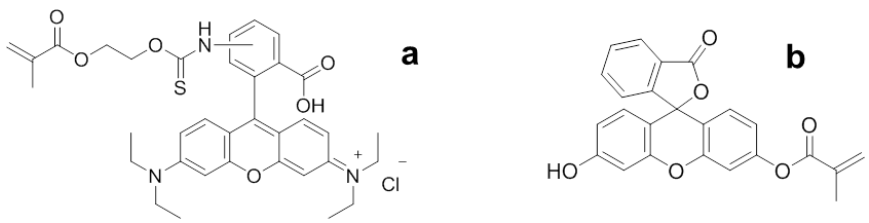

Figure 2.1 Fluorescent acrylate dyes structures: **a)** Methacryloxyethyl thiocarbamoyl rhodamine B; **b)** Fluorescein O-methacrylate

Before starting the synthetic procedure with the rhodamine-acrylate monomer and fluoresceine acrylate monomer, fluorescence emission spectra in presence of two

possible initiators BPO and KPS was recorded. The aim of these tests was to verify the fluorescence stability of the acrylate dye.

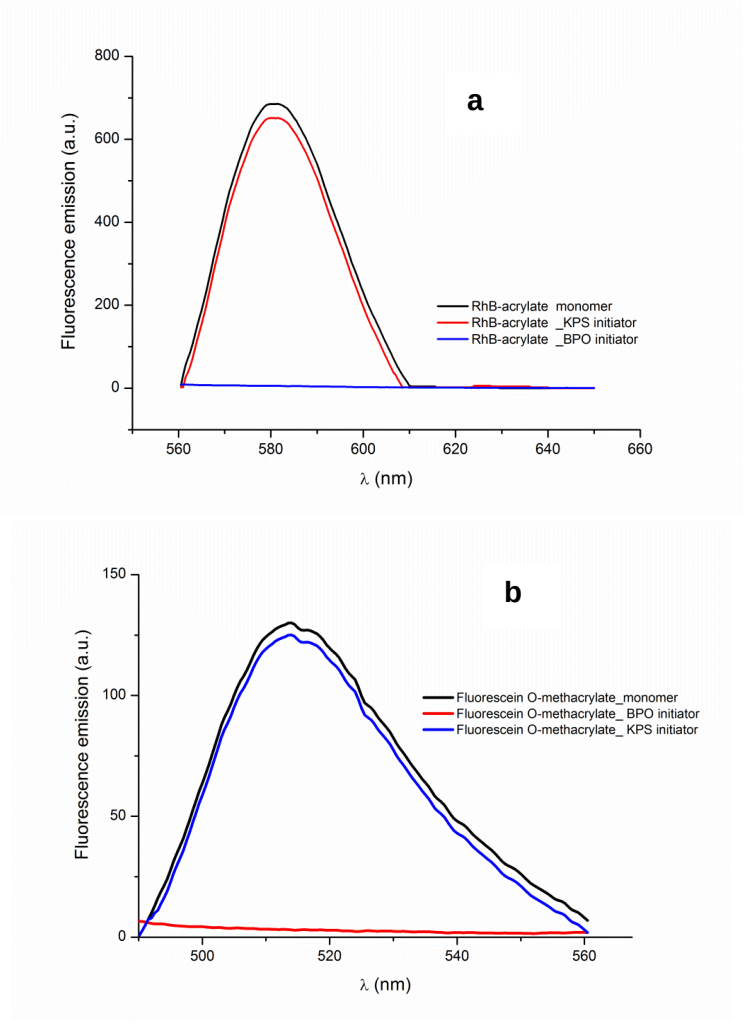

Figure 2.2 Fluorescence emission spectra of **a)** rh-acrylate monomer and **b)** fluorescein acrylate monomer with different initiator

As it shown in **Figure 2.2**, the fluorescence emissions spectra of the fluorescent acrylate monomers (both rhodamine and fluoresceine), are stable in presence of KPS initiator, but disappeared with BPO: the benzoyl-peroxyde radical interacts with the fluorescent monomer and destroys the rhodamine and fluorescein fluorophore.[6] So, KPS is the initiator choice for the polymerization optimization.[7-9]

PEG-RhB-labelled microgel core has been synthesized by radical polymerization of the fluorescent monomer within the core during the polymerization (**Scheme 2.2**).

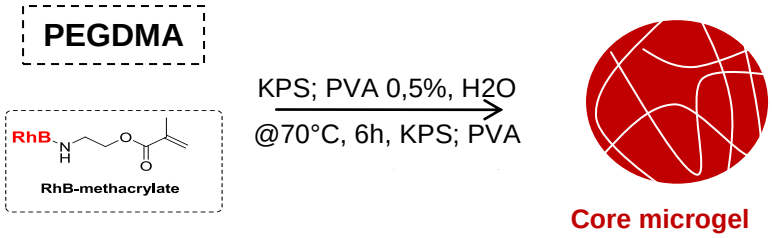

Scheme 2.2 Core synthesis scheme

The optimized parameters for the controlled core synthesis are reported in **Table 2.1**. To obtain fuorescent particles, rhodamine monomer is added during the polymerization after about 15 minutes from the introduction of the initiator.

Changing the concentration of the rhodamine-acrylate monomers, the resultant microgels have different emission intensities related to the rhodamine concentration in the core.

Sample	PEGDA [%w/v]	KPS [mM]	RhB-methacrylate [mM]	PVA [%w/v]
Core microgel (Rh_1)	1	0,1	0,005	1
Core microgel (Rh_2)	1	0,1	0,01	1
Core microgel (Rh_3)	1	0,1	0,1	1
Core microgel (Rh_4)	1	0,1	0,3	1

Table 2.1 Rh_xCore particles synthesis parameters

To follow the growing of microgels particles, dynamic light scattering was used to measure the particles size increase along the time.

We have evaluated the reaction's kinetic to study the core particle growth at different the different rhodamine-acrylate monomer concentrations. As it shown in

Figure 2.3, the particles size for each core microgel preparation increased until the final size of 450-500 nm after addition of the fluorescent acrylate monomer.

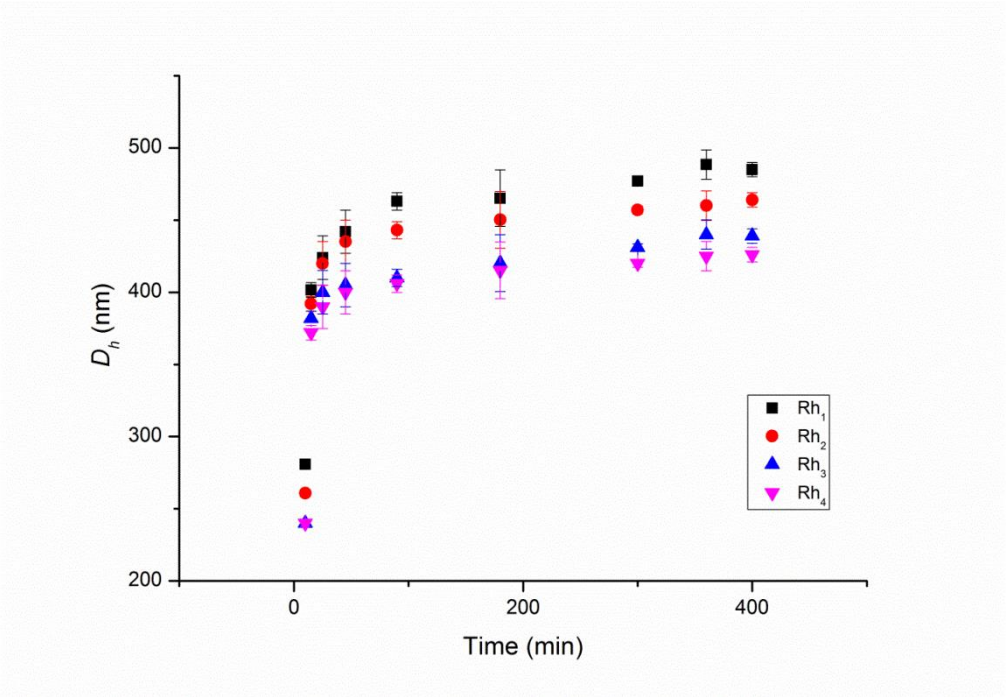

Figure 2.3 Kinetic study of particles' growth at different Rh-acrylate concentration

Non-fluorescent layers has been synthesized around the fluorescent core using a seeded polymerization procedure (**Scheme 2.3**).

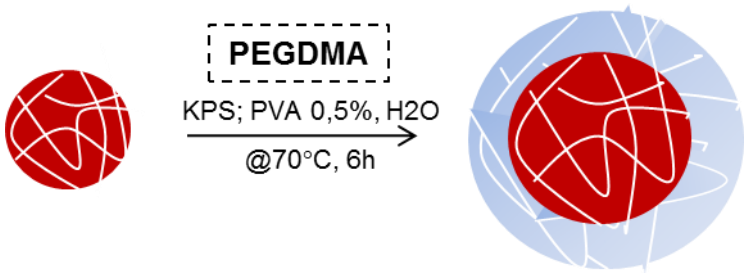

Scheme 2.3 Core-1st shell microgel synthesis scheme

The optimized reaction procedure and conditions for the core-1st shell microgels synthesis are summarized in the **Table 2.2**.

Sample	Core microgel [g]	PEGDMA [%w/v]	KPS [mM]	PVA [%w/v]
Rh_1Core-1st shell	0,100	0,5	0,015	0.05
Rh_2Core-1st shell	0,100	0,5	0,015	0.05
Rh_3Core-1st shell	0,100	0,5	0,015	0.05
Rh_4Core-1st shell	0,100	0,5	0,015	0.05

Table 2.2 Rh_xCore- 1st shell microgel synthesis parameters

Finally, the outer fluorescent shell layer was build up around the core-1st shell microgel using PEGDMA monomer, fluoresceine acrylate monomer, and acrylic acid (AAc) monomer to introduce carboxylic group on the surface (**Scheme 2.4**).[10]

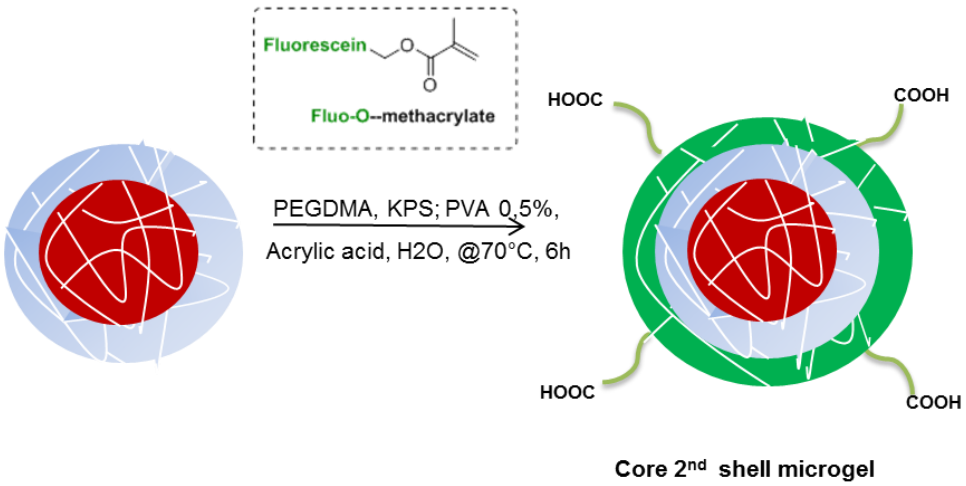

Scheme 2.4 Core-2nd shell microgel synthesis scheme

In particular, to obtain particles with different "bar code", we carried on different particles preparation with three different fluoresceine acrylate monomer concentration (**Table 2.3**).

Sample		Core-1st shell microgel [g]	PEGDMA [%w/v]	AAc [mM]	Fluo-acrylate [mM]	KPS [mM]	PVA [%w/v]
Rh_4Core-F_1 2nd shell	Rh_4Core-1st shell	0,200	0,5	2	0.05	0,05	0.05
Rh_1Core-F_2 2nd shell	Rh_1Core-1st shell	0,200	0,5	2	0,1	0,05	0.05

Rh_2Core-F_2 2nd shell	Rh_2Core-1st shell	0,200	0.5	2	0,1	0,05	0.05
Rh_1Core-F_3 2nd shell	Rh_1Core-1st shell	0,200	0,5	2	0,2	0,05	0.05
Rh_3Core-F_3 2nd shell	Rh_3Core-1st shell	0,200	0,5	2	0,2	0,05	0.05
Rh_4Core-F_3 2nd shell	Rh_4Core-1st shell	0,200	0.5	2	0,2	0,05	0.05

Table 2.3 Rh_x core F_y2nd shell synthesis parameters

Dynamic light scattering was used to measure the overall hydrodynamic diameter (*Dh*) of the carriers after each synthetic step. As reported in **Table 2.4**, *Dh* of each particles set increases from the core to the second shell synthesis.

Sample	Size (*Dh*, nm)
core Rh_1	488±2
Rh_1Core-1st shell	735±6
Rh_1Core-F_2 2nd shell	1021±83
Rh_1Core-F_3 2nd shell	1098±37
core Rh_2	464±3
Rh_2Core-1st shell	734±20
Rh_2Core-F_2 2nd shell	1053±44
core Rh_3	424±20
Rh_3Core-1st shell	714±20
Rh_3Core-F_3 2nd shell	1075±56
core Rh_4	422±20
Rh_4Core-1st shell	703±12
Rh_4Core-F_1 2nd shell	1081±61
Rh_4Core-F_3 2nd shell	1078±58

Table 2.4 Hydrodynamic diameter (D*h*) measurements of the different microgel sets at 0.1 wt% in distilled water.

For a deeply characterization of our microgel sets and to determine the particle mass increasing during the polymerization procedure, we measure the viscosity η of microgel solutions relative to that of water ηo with an Ubbelohde tube immersed in a water bath at temperature of 25° C. The particle volume fraction is obtained from the relative viscosity $\eta_r=\eta/\eta_o$ of dilute suspensions at different polymer concentrations *c*. [11-12]

Using the Einstein-Batchelor relation:

$$\eta_r = 1+2{,}5\ (k*c)+B\ (k*c)^2 \qquad (2\text{-}7)$$

we fit the data at fixed temperature to obtain the intrinsic volume fraction

$$k = \zeta/c. \quad (2\text{-}8)$$

Since the solution density is essentially equal to that of water, 1=g /cm^3, the intrinsic volume fraction becomes:

$$k = \zeta/c = \nu/m_p \quad (2\text{-}9)$$

with ν the particle volume and m_p its mass.

We carried on Ubbelohde viscosity measurements for two sets of encoded microgels (**Figure 2.4 a, b**).

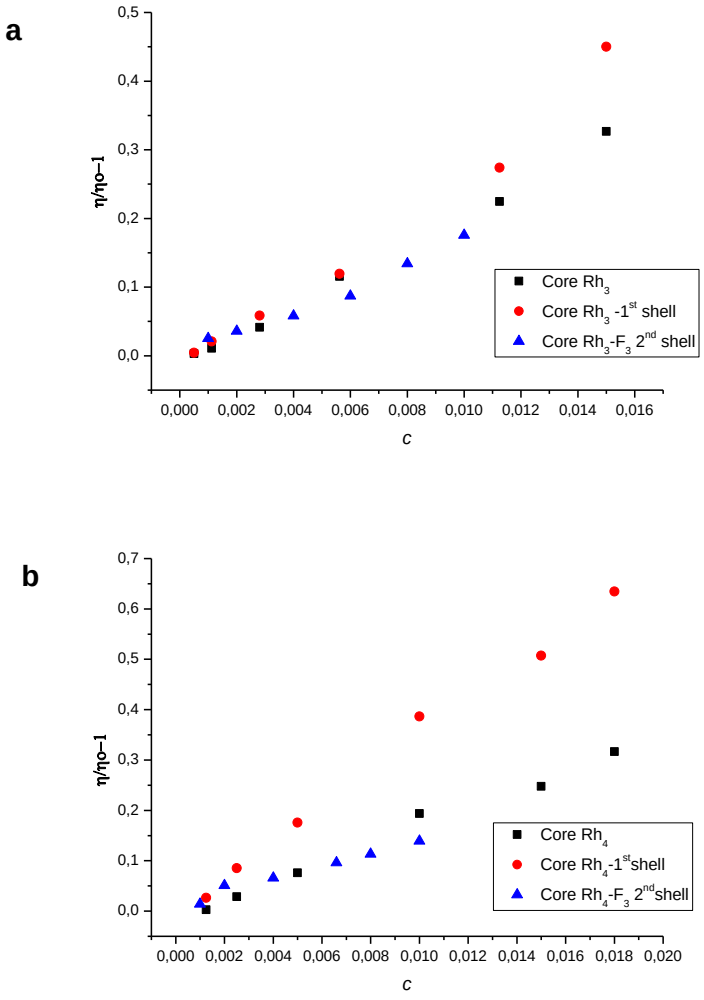

Figure 2.4 Ubbelhode viscosity measurements for two sets of encoded microgel:**a)** Core Rh_3-F_3 2nd shell; **b)** Core Rh_4-F_3 2nd shell

From viscometry we find k values and from dynamic light scattering measurements the volume of the particles ν, from which we get the particle mass after each polymeration steps. (**Table 2.5**)

Sample	K	Size (*Rh*, nm)	*mp* (g)	n°microgels/mg $_{microgel}$
core Rh_3	7,3	212±10	$5{,}5\cdot10^{-15}$	$1{,}8\cdot10^{11}$
Rh_3Core-1st shell	9,0	357±10	$2{,}1\cdot10^{-14}$	$4{,}7\cdot10^{10}$
Rh_3Core-F_3 2nd shell	6,0	537±23	$1{,}1\cdot10^{-13}$	$9{,}3\cdot10^{9}$
core Rh_4	5,7	211±20	$6{,}8\cdot10^{-15}$	$1{,}5\cdot10^{11}$
Rh_4Core-1st shell	10,2	351±6	$1{,}7\cdot10^{-14}$	$5{,}7\cdot10^{10}$
Rh_4Core-F_3 2nd shell	5,2	536±24	$1{,}2\cdot10^{-13}$	$8{,}0\cdot10^{9}$

Table 2.5 Particles mass determination from Hubbelhode viscometry measurements

As shown in **Table 2.5**, the particles mass increased one hundred times form the core carrier to the final carrier. These data, as well as the size measurements, confirm the growth of outer shell layers around the core particle, rather than the generation of new blank microgels particles without an inner core during the polymerization reactions.

Acid-base titration was used to determine the amount of AAc in copolymeric microgels based on the neutralization of carboxylic acid by hydroxide. Potentiometric titrations were performed on each microgel system using 100 mM sodium hydroxide as the base.

An example of an obtained potentiometric titration curve of microgel particle (Core Rh_3-F_3 2nd shell) can be seen in **Figure 2.5** .

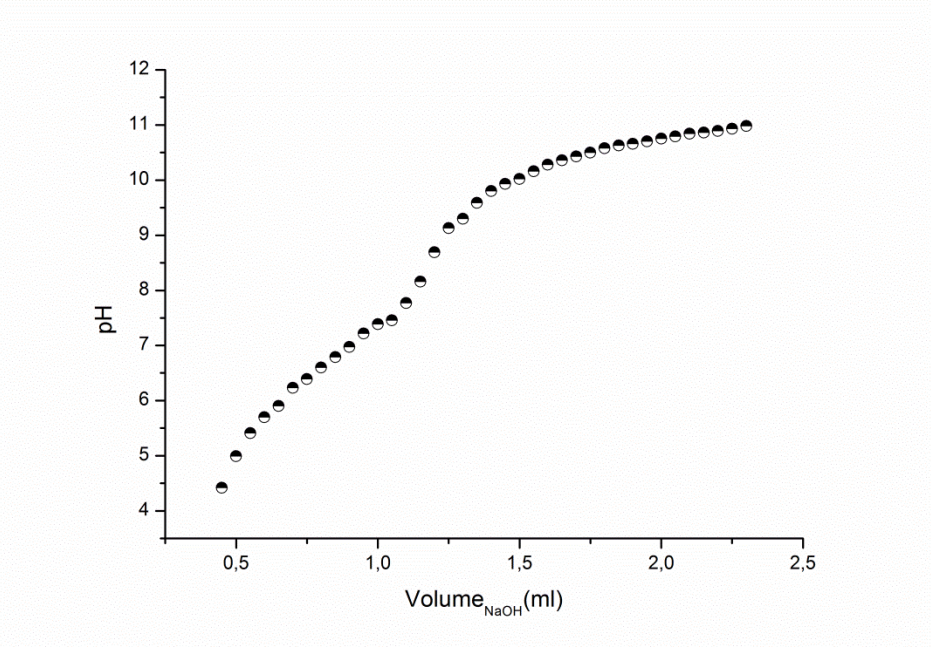

Figure 2.5 The acid-base titration curve of Core Rh_3-F_3 2nd shell microgel dispersion (50 mg microgel dispersed in 50 mL deionized water) titrated by 0.1 M NaOH standard solution at room temperature. Note that the pH value jumps from 8.3 to 8.9.

In microgel titration, ions are not restricted to the aqueous bulk phase (as with conventional colloids) since the gel phase is ion-permeable. Diffusion limitations associated with the penetration of titrant ions into the microgel bulk demand the use of much longer pH stabilization times for full equilibration of the titrant to be achieved between the aqueous bulk phase and the gel. This is especially true if titratable functional groups reside within the bulk of the particles. In our experiment, each titrant adding was followed by magnetic stirring until the pH value was stable and then recorded. [13-15]

Noticed the equivalent point volume (V_{eq}) and the weight of microgel for preparation of dispersions, so the content of AAc in the microgel is calculated as follows:

$$\text{moles}_{AAC} = V_{eq}\,(L) \cdot [NaOH]\ \text{mol/L}$$

where [NaOH] = titrant concentration

The results are illustrated in **Table 2.6**

Sample	-COOH content (·10^{-6} mol/mg microgel)
Rh_1Core-F_2 2nd shell	1.0±0.4
Rh_1Core-F_3 2nd shell	1.0±0.3
Rh_2Core-F_2 2nd shell	1.5±0.2
Rh_3Core-F_3 2nd shell	1.4±0.2
Rh_4Core-F_1 2nd shell	1.2±0.1
Rh_4Core-F_3 2nd shell	1.1±0.3

Table 2.6 -COOH content determination by potentiometric titration for the sets of microgel

Electrophoresis and dynamic light scattering can be used to correlate the progression of -COOH ionization with changes in the surface charge and the particle size, respectively, of the microgels.

The pH-responsive swelling behavior is due to the the increasing degree of deprotonation of AAc monomers, thereby reducing the hydrogen bonding between carboxylic acid and increasing the electrostatic repulsion between anionic carboxylate groups and osmotic pressure of microgels. Hence, the average hydrodynamic diameter of microgel particles increases, thereby reducing the van der Waals attractions between particles. **Figure 2.6** demonstrate the increase of unperturbed hydrodynamic diameter of Core Rh_3-F_3 2nd shell microgel particles with the increase of pH values under the same ionic strength.

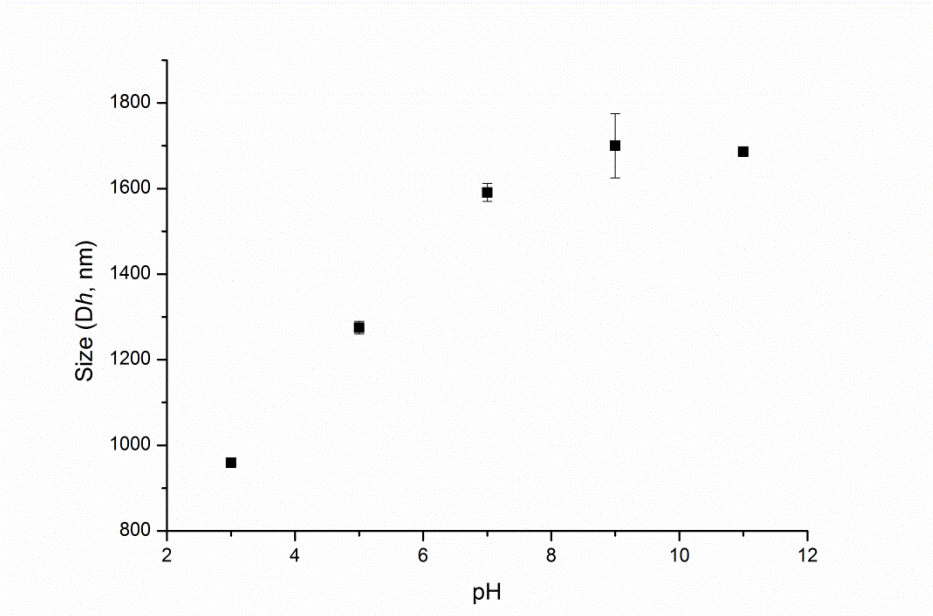

Figure 2.6 The hydrodynamic diameter (D*h*) of microgel particles measured by dynamic light scattering in buffers with pH values ranging from 3.0 to 11 at 25°C.

The measurement of charge properties is clearly important in any attempt to estimate electrostatic interactions between microgel particles. The ζ potential of microgel-encoded sets is reported in **Table 2.7**:

Sample	ζ potential (mv)
Rh_1Core-F_2 2nd shell	-13,9±0,5
Rh_1Core-F_3 2nd shell	-13,8±0,9
Rh_2Core-F_2 2nd shell	-14,1±0,4
Rh_3Core-F_3 2nd shell	-14,7±0,8
Rh_4Core-F_1 2nd shell	-15±0.3
Rh_4Core-F_3 2nd shell	-14,5±0,5

Table 2.7 ζ potential measurement of encoded microgels

Additionally, the ζ potential of microgel dispersions was measured at different pH values.

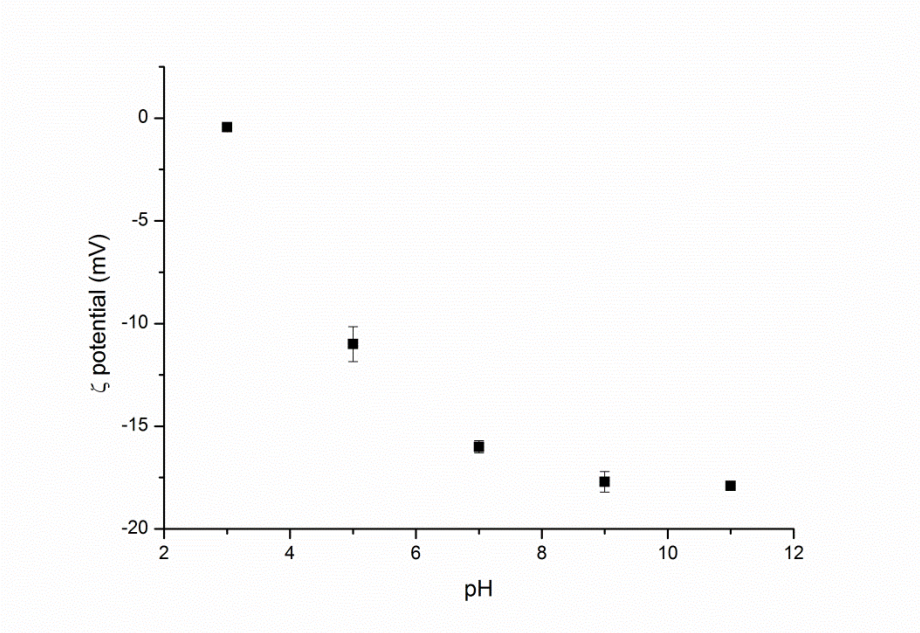

Figure 2.7 The ζ potential of microgel particles (0.1 wt%) from pH 3.0 to 11 at 20 ºC. With increasing pH, the absolute value of the ζ potential increases due to deprotonation of AAc units on the microgels.

Figure 2.7 shows the change of ζ potential with the increase of pH values. Because of the anionic carboxylate and sulfate groups on the surface of core-double shell microgel particles, the ζ potential of particles are negative. With the increment of pH, the deprotonation of carboxylic acid leads to more anionic

carboxylate groups, thereby increasing the absolute value of ζ potential. However, when pH reach 5.5, the ζ potential of particles reach a plateau, probably indicating that the majority of carboxylic acid groups have been deprotonated at that pH.

Figure 2.8 shows the pH dependence of the electrophoretic mobility measured at 25 °C.

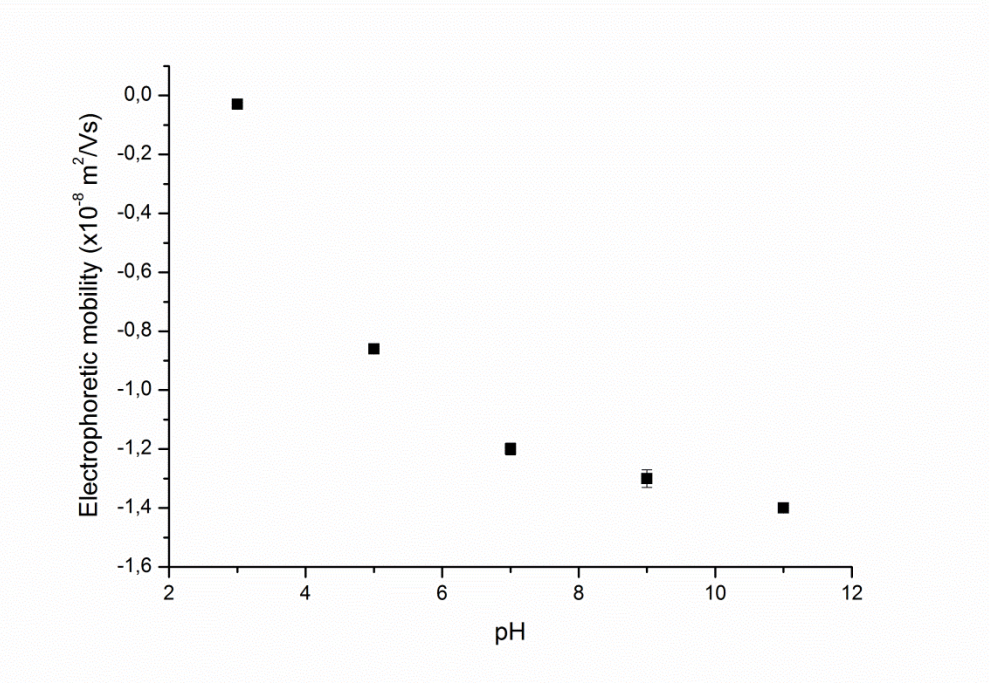

Figure 2.8 Electrophoretic mobility versus pH profiles for Core Rh_3-F_3 2nd shell microgels 0.1 wt% in buffers with pH values ranging from 3.0 to 11 at 25°C.

The mobility and particle size of the microgels system are strongly pH dependent, with both the particle size and absolute electrophoretic mobility increasing continuously between pH 3 and pH 9 and plateauing at higher pH values. This ionization profile corresponds directly to that observed in the titration, which indicated ionization of -COOH groups in the range 4.4 < pH < 8.6. The slightly lower absolute mobility values recorded at pH 3 and pH 11 are likely a result of charge screening at the higher ionic strength demanded for measurements at these pH values.

A difference is also observed in the total number of charges located on the microgel surface systems. **Table 2.8** compares the calculated surface charges and functional group contents of the evaluated microgels.

sample	El. mobility pH 5 (x10^{-8} m^2/Vs)	El. mobility pH 9 (x10^{-8} m^2/Vs)	Microgels size pH 5 (*Rh*, nm)	Microgels size pH 5 (*Rh*, nm)	Surface charge pH 5 (n°/microgel)	Surface charge pH 9 (n°/microgel)	-COOH content (mol/$g_{microgel}$)
Core Rh_3-F_3 2nd shell	-0.86±0.006	-1.3±0.03	635±7	850±15	636±150	1126±103	(1,4±0.2)·10^{-6}

Table 2.8 Estimated surface charges of microgels at pH 5 and pH 9 compared with the total functional group content of each microgel

From the mobility results and corresponding particle size data, the total number of charges attributable to -COOH groups on the surface of each microgel can be approximated using hard sphere colloid equations.[16] The measured electrophoretic mobility is related to the zeta potential through the Henry equation (2-10).

$$\zeta = 3\mu\eta / 2\varepsilon_0\varepsilon_r f(\kappa R) \qquad (2\text{–}10)$$

Here, R is the microgel radius, η is the solution viscosity, k is the inverse Debye length, ε_0 is the permittivity of a vacuum, ε_r is the medium dielectric constant, and $f(\kappa R)$ is Henry's function for a 1:1 electrolyte

Using the zeta potential as an approximation of the surface potential Ψ_0, the surface charge density (σ) can be estimated using the Grahame equation (2–11)

$$\sigma = \zeta\varepsilon_0\varepsilon_r(\kappa R+1) \qquad (2\text{–}11)$$

The total numberof charges on the surface of each microgel particle (Q) can subsequently be estimated by multiplying by the surface area of the microgel and dividing by the elementary charge; the final relationship is shown as (2–12).

$$Q = 6\pi R\mu\eta(\kappa R+1)/ e(f(\kappa \qquad (2\text{–}12)$$

Upon changing the pH from 5 to 10, the surface charge density of microgels increases 2-fold the hydrodynamic diameter increases 34%. Since functional group ionization is the only mechanism of pH-induced swelling for these microgels, the swelling behavior of the microgels is related to the number and the distribution of ionizable functional groups reside in the bulk of the microgel.

Infact, if charged groups are distributed throughout the particle, ion-ion repulsion would have a minimal effect on the swelling of the microgel since the local polyanion concentrations would be relatively low (i.e., a similar number of charges are distributed over a much larger volume). Thus, a lower degree of swelling would be expected for such microgels at high pH. Instead, for our microgels, the surface charge increasing and the swelling effect results are consistent with the clustering of -COOH groups near the microgel surface.

The fluorescence characteristics of the core shell microgels were examined by fluorescence spectrophotometry and fluorescence microscopy. [17-19]A specific signal of fluorescence emission is associated to every shell. The emission spectra of rhodamine and fluoresceine reported in **Figure 2.9** confirm that the fluorescence emission intensity of the microgel depends from the dye content in its architecture.

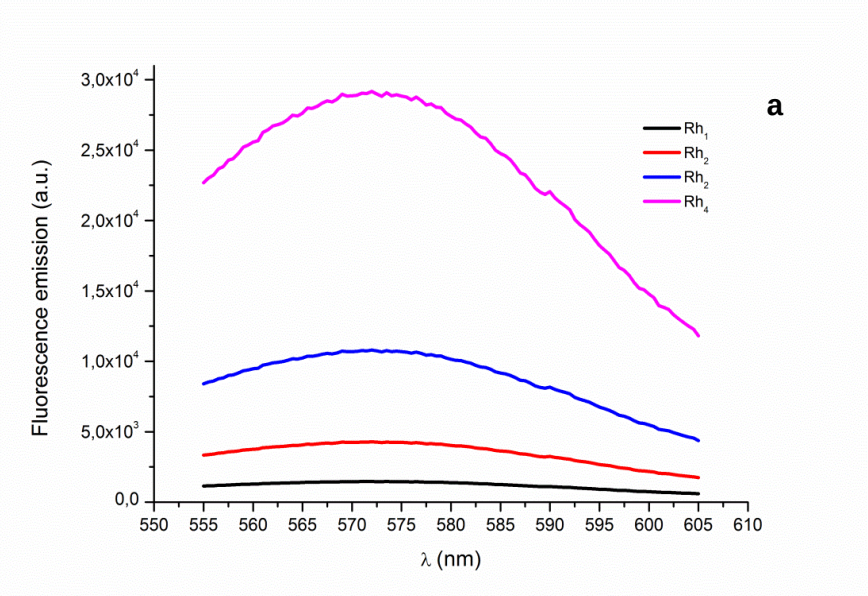

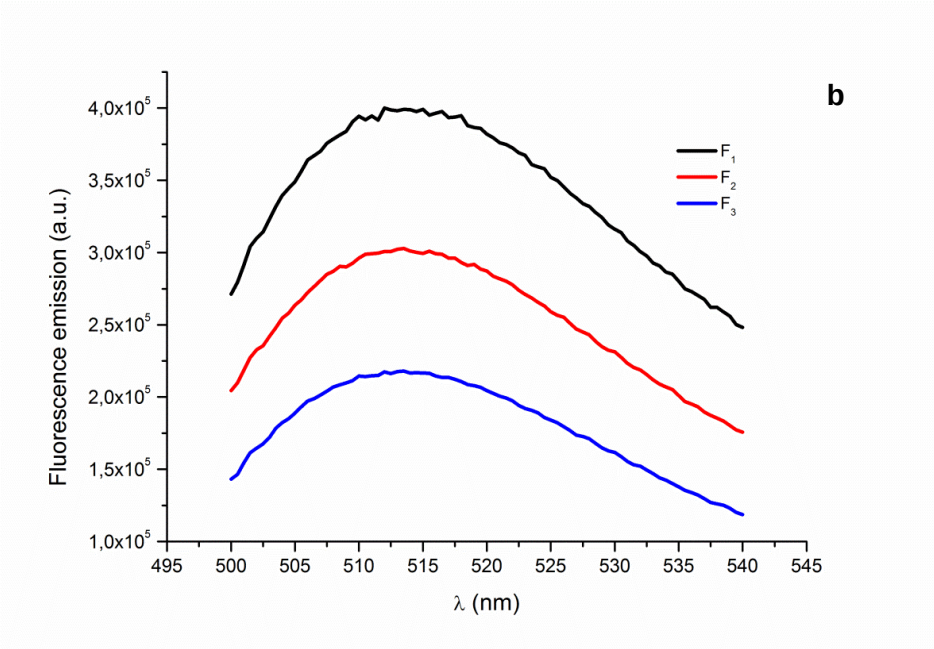

Figure 2.9 Emission spectra for the different level of dyes content in the encoded microgel **a)** rhodamine**; b)** fluoresceine

The process resulted in a population of multi-fluorescent hydrogels particles which displayed a diverse range of fluorescence emissions and intensities: a specific emission ratio of Fluoresceine/Rhodamine B dyes provided each microgels type with a unique "bar code".[20-26]

To evaluate the encoding capability of our strategy, using a label counter spectrophotometer, all the sets of particles were excited at 488 and 543 nm and the number of counts emission for the two single dyes were recorded at the same particles concentration.[27-33] As shown in **Figure 2.10 a**, the number of counts emission for the dyes depends on their concentration level inside the particles layer. The ratio of the two dyes emission counts corresponds to the "barcode": all the values presents significant statistical difference according to *t*-student test ($p<0.05$) and six "barcodes" are distinguishable (**Figure 2.10 b**).

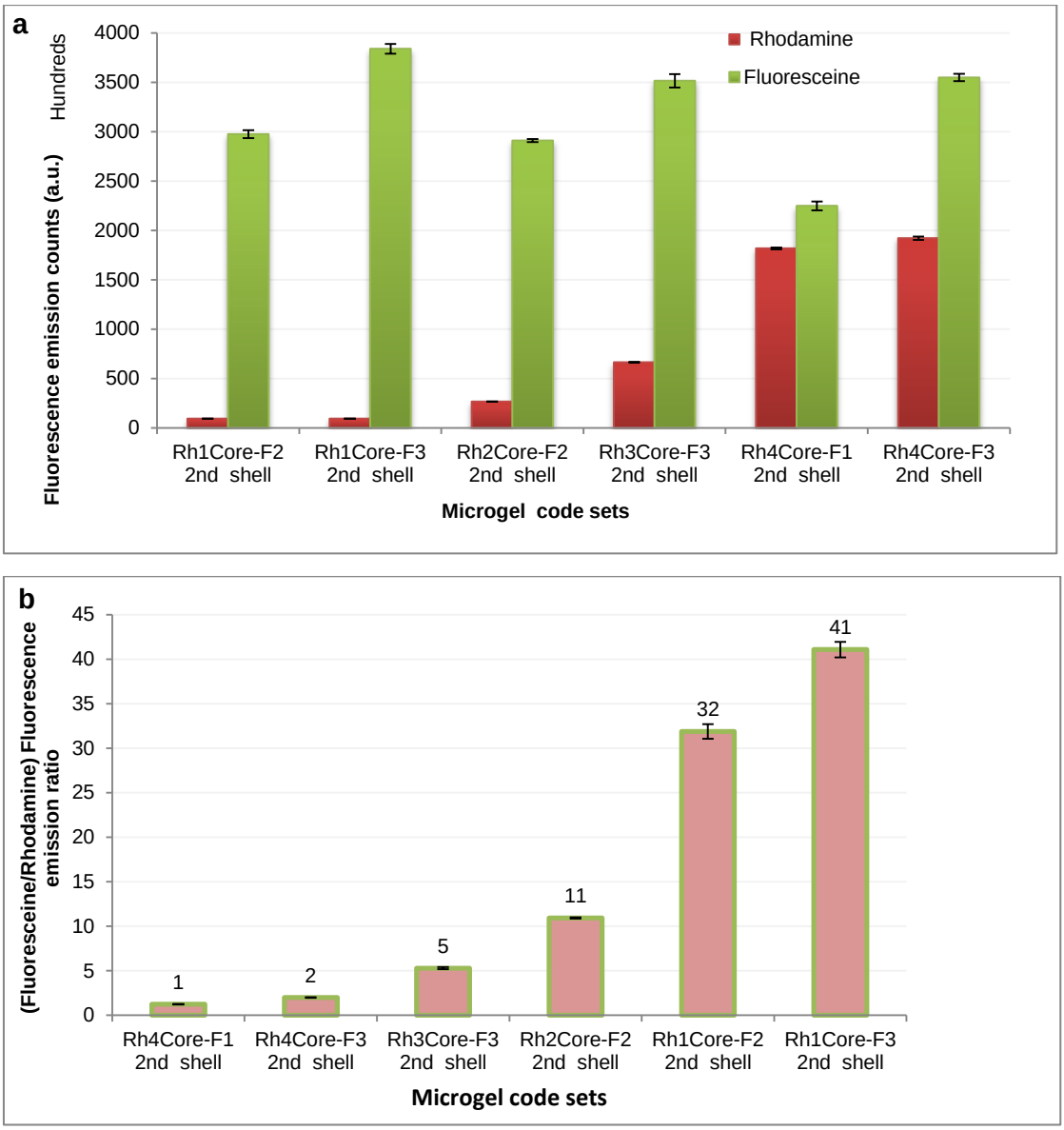

Figure 2.10 a) Rhodamine and fluoresceine emission counts; **b)** Fluo /Rh emission ratio by label counter analysis: [microgel]= 1mg /ml, V= 100ul, buffer Tris HCl pH8

The encoded microgels were also analyzed by confocal laser scanner microscopy.

The fluorescence microscope image (**Figure 2.11 a**) shows the dual fluorescent performance of the microgel when were excited by 488 and 543nm wavelength lasers. The green and red emissions originate from rhodamine B and the fluorescein dyes in the core and shell layer, respectively.

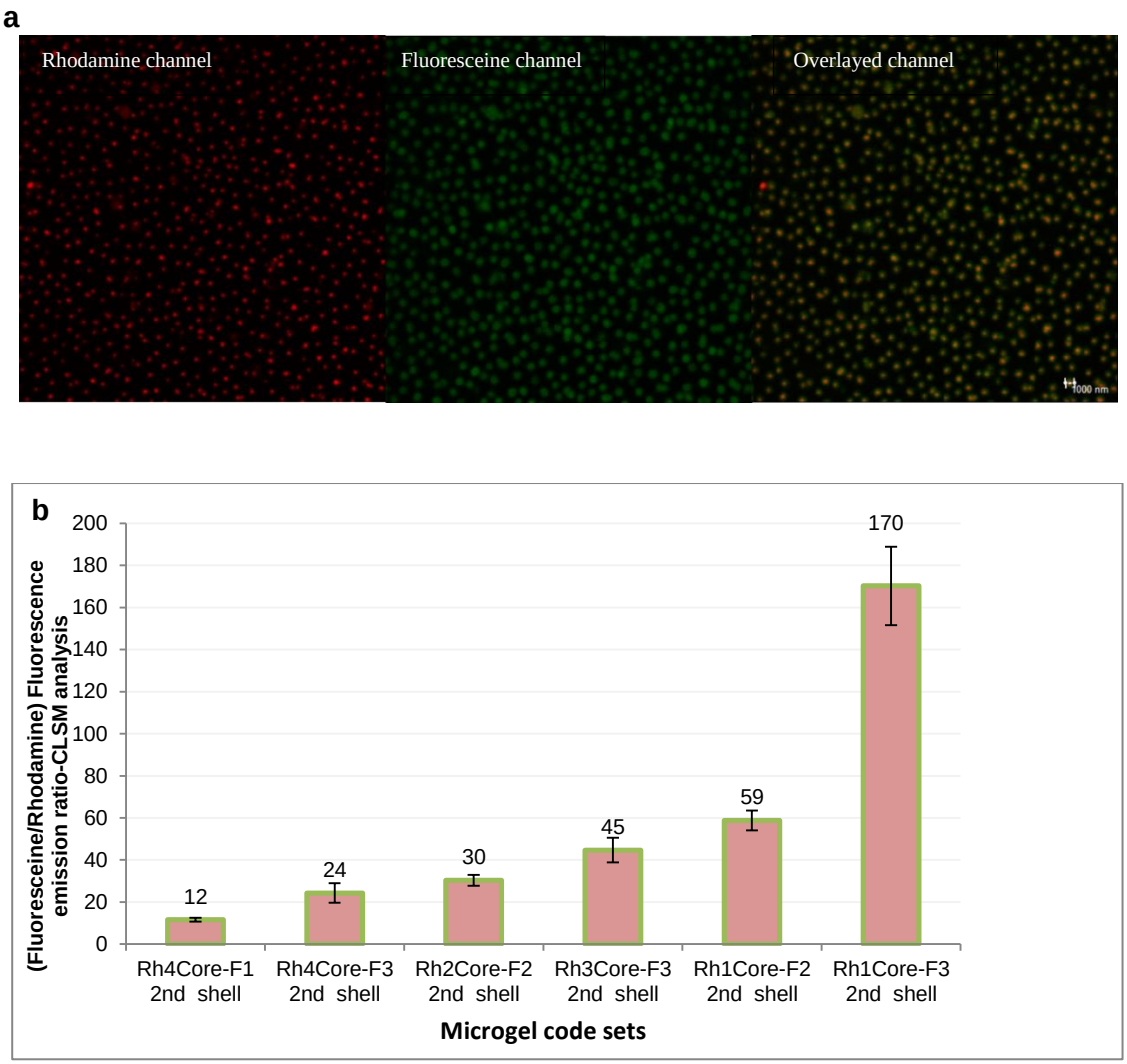

Figure 2.11 a) The fluorescence microscope image of the microgel Rh_3 Core-$F_2$2nd shell when were excited by 488 and 543nm wavelength lasers. **b)** Fluo /Rh emission ratio by CLSM image analysis; **c)** CLSM image of a mixing solution of three different code

From the CLSM image analysis, we have evaluated the fluoresceine/rhodamine emission ratio (**Figure 2.11 b**), and we are able to distinguish and visualize by

fluorescence imaging the different encoded microgel correspondent to the different dye level in their core shell architecture(**Figure 2.11 c**).

2.4 Conclusion

This chapter gave a broad overview of synthesis, characterization and unique properties of multi-responsive encoded core shell microgel. Core shell encoded microgels were obtained via multi step ammonium persulfate-initiated radical polymerization at fixed temperatures. Microgel particles are both fluorescent and pH-responsive.

The presence of –COOH functional group allow us the following coniugation of probe molecules for multiplex assay.

Regarding the encoding capability, multi-fluorescent hydrogel particles with different range of fluorescence emissions and intensities (the fluorescence spectral code) have been characterized. The fluorescent dyes are located in separate shells alternating with non-fluorescent spacer shells round a hydrogel core. Microspheres prepared in this way display a diverse range of optical signatures derived from the fluorescence emission ratio of fluoresceine/rhodamine.

Bibliography

[1] Hunter, R. J. *Foundations of Colloid Science*; 2nd ed., **2001**, Oxford University Press: Oxford, Great Britain,.

[2] Smoluchowski, M. v. *Handbuch der Electrizität und des Magnetismus*; Barth: Leipzig, **1921**; *2*.

[3] G. Odian, Principles of Polymerization, 4th Edition, **2004**.

[4] Kolthoff, I. M.; Miller I. K. *J. Am. Chem. Soc.*, **1951**, *73*, 3055–305.

[5] Wilson, G.; Henderson, J.; Caruso, M. *Journal of Polymer Science: Part A: Polymer Chemistry*, **2010**, *48*, 2698–2708.

[6] Nandi, P. K. ;Nandi, U. S. *J. Phys. Chem.*, **1965**, *69* , 4071–4076

[7] Hu, X.; Tong, Z.; Lyon, A. *J. Am. Chem. Soc.*, **2010**, *132*, 11470–11472

[8] Nayak, S.; Lyon, L. A. *Angew. Chem., Int. Ed.* **2005**, *44*, 7686–7708.

[9] Blackburn, W. H.; Dickerson, E. B.; Smith, M. H.; McDonald, J. F.; Lyon, L. A. *Bioconjugate Chem.* **2009**, *20*, 960–968.

[10] Blackburn, W. H.; Lyon, L. A. *Colloid Polym. Sci.* **2008**, *286*, 563-569.

[11] Romeo, G.; Imperiali, L.; Kim, J.; Weitz, D. *J. Chem. Phys.* **2012**, *136*, 124905 -124909

[12] Romeo, G.; Fernandez-Nieves, A.; Wyss, H.; Acierno, D.; Weitz, D. *Adv. Mater.* **2010**, *22*, 3441–3445

[13] Hoare, T.; Pelton, R. *Langmuir* **2004,** *20*, 2123-2133

[14] Hoare, T.; Pelton, R. *Macromolecules* **2004,** *37*, 2544-2550

[15] Suzuki, H.; Wang, B.; Yoshida, R.; Kokufuta, E. *Langmuir* **1999**, *15*, 4283.

[16] Wiersema, P. H.; Loeb, A. L.; Overbeek, J. Th. G. *J. Colloid Interface Sci.* **1996**, *22*, 78.

[17] Xiao, X. C.; Chu, L. Y.; Chen, M.; Wang, W. S.; Li, Y. *Adv. Funct. Mater*. **2003**, *13*, 847.

[18] Li, X.; Zuo, J.; Guo,Y.; Yuan, X. *Macromolecules* **2004**, 37, 10042.

[19] Yang, W. J.; Trau, D.; Renneberg, R. ; Yu, N. T.; Caruso, F. *J. ColloidInterface Sci*. **2001**, *234*, 356.

[20] Pan,X.; Ju, J.; Zhan,J.; Wu, W. *Macromol. Chem. Phys*. **2010**, *211*, 2347–2355

[21] *Sun, H.; Poulsen, A.; Gu, H.; Almdal, K. Chem. Mater.*, **2006**, 18 (15), pp 3381–3384.

[22] He, H.; Mortellaro, M. A.; Leiner, M. J. P.; Fraatz, R. J.; Tusa, J. K *J. Am. Chem. Soc.* **2003**, *125*, 1468.

[23] Stojanovic, M. N.; de Prada, P.; Landry, D. W. *J. Am. Chem. Soc.* **2000**, *122*, 11547.

[24] Minta, A.; Tsien, R. Y. *J. Biol. Chem.* **1989**, *264*, 19449.

[25] Fehr, M.; Frommer, W. B.; Lalonde, S. *Proc. Natl. Acad. Sci. U.S.A.* **2002**, *99*, 9846.

[26] Wang, L.; Yang, C.; Tan, W. *Nano Lett.* **2005**, *5*, 37.

[27] Tan, M.; Wang, G.; Hai, X.; Ye, Z.; Yuan, J. *J. Mater. Chem.* **2004**, *14*, 2896.

[28] Clark, H. A.; Hoyer, M.; Philbert, M. A.; Kopelman, R. *Anal. Chem.* **1999**, *71*, 4831.

[29] Clark, H. A.; Kopelman, R.; Tjalkens, R.; Philbert, M. A. *Anal. Chem.* **1999**, *71*, 4837.

[30] Brasuel, M.; Kopelman, R.; Miller, T. J.; Tjalkens, R.; Philbert, M. A. *Anal. Chem.* **2001**, *73*, 2221

[31] Xu, H.; Aylott, J. W.; Kopelman, R.; Miller, T. J.; Philbert, M. A. *Anal. Chem.* **2001**, *73*, 4124

[32] Ji, J.; Rosenzweig, N.; Griffin, C.; Rosenzweig, Z. *Anal. Chem.* **2000**, *72*, 3497.

[33] McNamara, K. P.; Nguyen, T.; Dumitrascu, G.; Ji, J.; Rosenzweig, N.; Rosenzweig, Z. *Anal. Chem.* **2001**, *73*, 3240

Chapter III

ds Displacement assay design

3.1 Introduction

The ability to specifically and quantitatively detect nucleic acids is of great importance in various biomedical applications. In this chapter we report he design and optimization of a double-stranded molecular probe for homogeneous detection of specific nucleotide sequences. The probes are labeled with either a fluorophore or a quencher such that the probe hybridization brings the two labels into close proximity, and this diminishes the fluorescence signal in the absence of a target. In the presence of a target, the fluorophore probe is thermodynamically driven to unzip from its hybridized form and bind with the target.

By proper design of the sequence, the probe discriminates the target nucleotide in a single step in non-specific nucleic acids mixtures and in the presence of interfering proteins commonly found in complex biological matrixes (Human Serum).

3.2 Experimental

3.2.1 Materials

DNA and RNA oligonucleotides were purchased from Diatech Pharmacogenetics srl, (Ancona, IT) with HPLC purification. All nucleotides were suspended in

rnase-free water molecular grade (Applichem) and diluted to the appropriate concentration.

The buffer solution for the dsDNA probe contains 10 mM Tris HCl pH 8 and 200 mM NaCl. Human serum was supplied by Lonza, For RNA displacement experiments, human serum was thawed on ice and lysed with an equal volume of 2x denaturating solution (Ambion).

3.2.2 Characterization methods

3.2.2.1 Optimization Quencher/fluorophore ratio

In order to conduct the assay, 20 pmol of tail-Cy5 DNA were mixed at a 0.5-to-10 ratio of quencher DNA in Tris HCl pH 8 buffer in a final volume of 200µL. Each sample was loaded onto a 96-well microplate and the fluorescence emission intensity was measured in 2300 EnSpire multilabel reader (Perkin-Elmer, Waltham, MA) by setting the λex_{Cy5}=633 and λem_{Cy5}=654.

The residual Cy5 emission intensities upon the quenching event were normalized versus the DNA tail Cy5 emission for each ratio point. The experimental uncertainty represents the standard error of the mean of three replicates assay.

3.2.2.2 Quenching kinetic

20 pmol of tail-Cy5 DNA were mixed to 20 pmol of quencher DNA (molar ratio 1/1) in Tris HCl, pH 8 buffer in a final volume of 200µL. Each sample was loaded onto a 96-well microplate and the fluorescence emission intensity was measured in 2300 EnSpire multilabel reader (Perkin-Elmer, Waltham, MA) by setting the λex_{Cy5}=633 and λem_{Cy5}=654.

The fluorescence quenching was monitored at 30-60 minutes step until any variation in fluorescence recovery was recorded. The residual Cy5 emission

intensities upon the quenching event were normalized versus the DNA tail Cy5 emission for each ratio point. The experimental uncertainty represents the standard error of the mean of three replicates assay.

3.2.2.3 Homogeneous displacement assay

20 pmol of tail-Cy5 DNA were mixed to 20pmol of quencher DNA in Tris HCl, pH 8 buffer. 20 pmol of DNA or RNA target were added to such solutions in a final volume of 200μL. Quenched samples were used as reference in order to evaluate the displacement efficiency. The specificity of double strand probes was evaluated by using scrambled or non-specific sequences. The selectivity of the assay was investigated in presence of an interfering agent (Human Serum).
Each sample was loaded onto a 96-well microplate and the fluorescence emission intensity was measured in 2300 EnSpire multilabel reader (Perkin-Elmer, Waltham, MA) by setting the λex_{Cy5}=633 and λem_{Cy5}=654.
The experimental uncertainties indicated represent the standard deviation of three replicates.

3.2.2.4 Displacement kinetic of HIV DNA, miR21 DNA/RNA target in homogeneous assay

20 pmol of tail-Cy5 DNA were mixed to 20 pmol of quencher DNA in Tris HCl, pH 8 buffer. For each assay 20 pmol of HIV-DNA, miR21 DNA/RNA target respectively were added to such solutions in a final volume of 200μL and the fluorescence recovery was monitored at 30-60 minutes step until any variation in fluorescence recovery was recorded. Quenched samples were used as reference in order to evaluate the displacement efficiency. The Cy5 emission intensities upon the displacement event were normalized versus the DNA tail Cy5 emission for

each time point. The experimental uncertainty represents the standard error of the mean of three replicates assay.

3.3 Results and discussion

The use of fluorescent nucleic acid hybridization probes that generate a fluorescence signal only when they bind to their target enables real-time monitoring of nucleic acid detection assays. Fluorescent nucleic acid hybridization probes are available in a wide range of different fluorophore and quencher pairs.[1] Multiple hybridization probes, each designed for the detection of a different nucleic acid sequence and each labeled with a differently colored fluorophore, can be added to the same nucleic acid amplification reaction, enabling the development of highthroughput multiplex assays.

In order to develop robust, highly sensitive and specific real-time nucleic acid detection assays it is important to carefully select the fluorophore and quencher labels of hybridization probes.

Selection criteria are based on the type of hybridization probe used in the assay, the number of targets to be detected.

Quenching of a fluorophore can occur as a result of the formation of a non-fluorescent complex between a fluorophore and another fluorophore or non-fluorescent molecule. This mechanism is known as ‘‘contact quenching’’, ‘‘static quenching,’’ or ‘‘ground-state complex formation.’’ In contact quenching, two molecules interact by proton-coupled electron transfer through the formation of hydrogen bonds. In aqueous solutions, electrostatic, steric, and hydrophobic forces control the formation of hydrogen bonds. When this complex absorbs energy from light, the excited state immediately returns to the ground state without emission of a photon and the molecules do not emit fluorescent light. A characteristic of contact quenching is a change in the absorption spectra of the two molecules when they forma complex. Among the hybridization probes that use this mechanism of energy transfer are strand-displacement probes.

‘‘Strand-displacement probe’’ assays utilize two complementary oligonucleotide probes, one probe labeled with a reporter fluorophore, and the other probe labeled with a non-fluorescent quencher moiety (**Fig. 3.1**). [2,3]

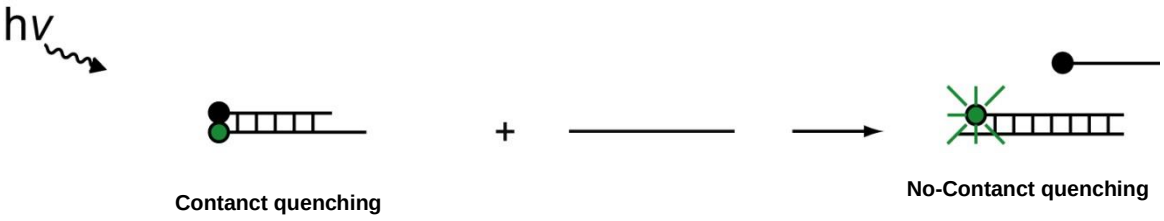

Figure 3.1 Strand displacement probe scheme

When the two probes are hybridized to each other, the fluorophore and quencher are in close proximity and contact quenching occurs, resulting in low-fluorescence emission. In the presence of a target nucleic acid, one of the probes forms a more stable probe-target hybrid, resulting the two probes being separated from each other. As a consequence of this displacement, the fluorophore and the quencher are no longer in close proximity and fluorescence of the reporter fluorophore increases.

For the design of fluorescent hybridization probes that utilize contact quenching, any non-fluorescent quencher can serve as a good acceptor of energy from the fluorophore. However, it is reported in literature that Cy3 and Cy5 are best quenched by the BHQ-1 and BHQ-2 quenchers (**Figure 3.2**) [4].

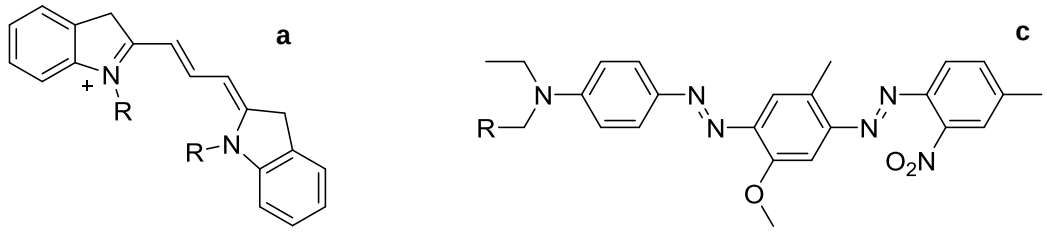

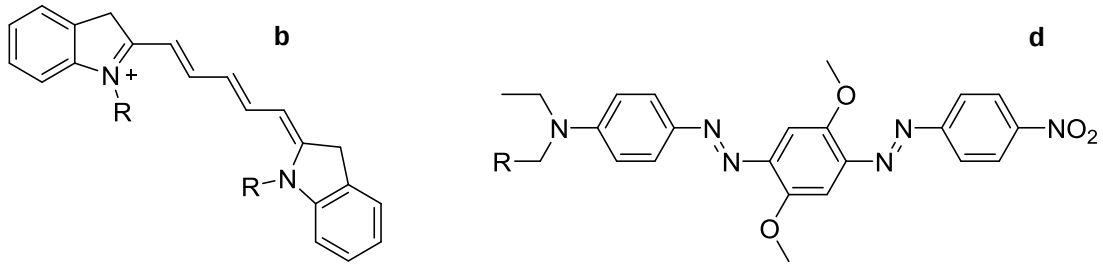

Figure 3.2 Moleculare structure of Cy3 (a), Cy5 (b), BHQ_1 (c), BHQ_2 (d).

On this basis, we developed an alternative molecular binding scheme using two single-stranded probes for rapid quantification of specific nucleic acid molecules.

In this sensing scheme, a single strand DNA ("ssDNA tail"), with a Cy5 fluorochrome molecule on the 3' position and with an ammine group on the 5' position for the following covalent immobilization on the encoded microgel surface, is designed.

A quencher strand (23-39 nt) internally modified with a fluorescence quencher Black Hole Quencher (BHQ) was designed to partially hybridize the tail. To maximize the quenching process, BHQ molecules as dark quenchers will be placed internally the capture probe strand in a position complementary to fluorophore one. When the two strands partially hybridize to form a duplex, Cy5 and BHQ come in close proximity and fluorescence quenching occurs resulting in 11-27 pending nucleotides. [5]

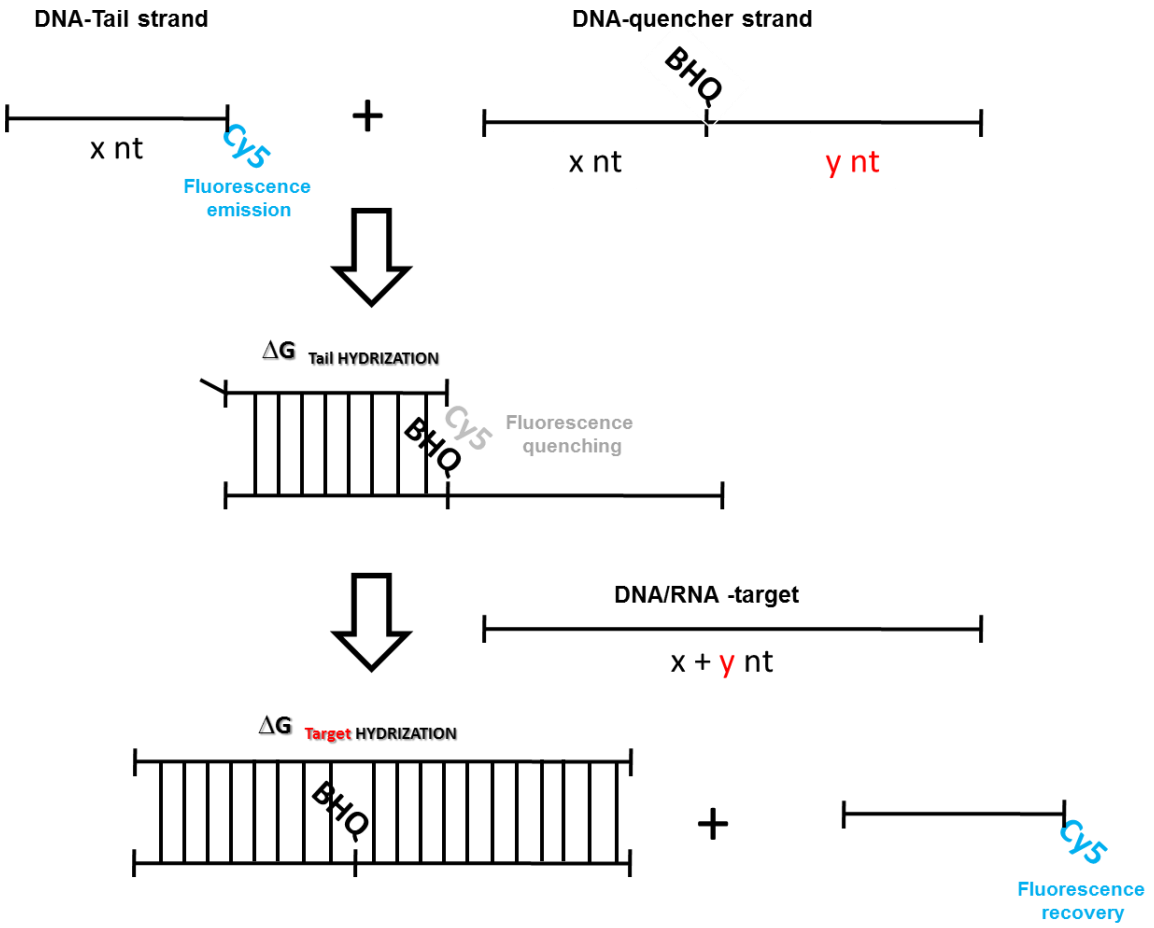

Figure 3.3 ds Probe design for detecting specific nucleic acid sequences. In the existence of target, the fluorophore probe is thermodynamically driven to hybridize the target, which replaces the quencher probe**.**

In presence of the target, hybridization occurs between the target and the fully complementary quencher (23-39 nt) starting from the quencher pending nucleotides and leading to a branch migration. As a consequence, this displacement leaves behind the tail strand, the Cy5 and BHQ are no longer in close proximity and Cy5 fluorescence emission is recovered (**Figure 3.3**).

The length of tail is chosen in order to have the appropriate difference in free energy between the tail/quencher and the target/quencher duplex. In this way, the strand displacement mechanism is "fueled" by the free energy released from the fully complementary base pairing occurring between the quencher probe and its corresponding RNA/DNA target.

The double strand displacement event can be tuned throw a rational design of the double strand sequence. During the strand displacement the target strand

must replace the original partner strand of the primary duplex to form a secondary duplex. The success of this event is promoted if the target of interest has a greater affinity for one of the strands in the initial duplex. Thus, for an effective reporting system, the ideal double strand probes possess sufficient base pair matches to remain thermally stable in absence of target of interest but fewer base pair matches than the target. [6-8]In order to estimate the performance of a probe design the free energy change, which is directly related to the equilibrium constant by the equation $K= e^{-\Delta G/RT}$, should first be estimated based on the probe sequences and length. [9] On these bases different sets of tail-quencher probe were designed in order to evaluate the effect of free energy change on the displacement event and the stability of secondary duplex (Data not shown). In **Table 3.1** and **Table 3.2** are reported the sequence and thermodynamic parameters of the DNA probes used in this study.

Probe name	Sequence	Length (nt)	ΔG (Kcal/mol)[a]
HIV probes [b]			
HIV tail-Cy5	5' Cy5 ACT GCT GTT AAA C6 NH_2-3'	12	Tail hybridization 11.2
HIV quencher	5' TTT AAC AGC AG BHQ TGA GTT GAT ACT ACT GGC CTA ATT CCA 3'	39	Target hybridization 50.9
HIV-target	5' TGG AAT TAG GCC AGT AGT ATC AAC TCA ACT GCT GTT AAA 3'	39	
			Displacement 39.7
HCV probes [c]			
HCV tail-Cy5	5' Cy5 TTC CGG TGT ACT-C6 NH_2-3'	12	Tail hybridization 13.3
HCV quencher	5'-AGT ACA CCG GABHQ TTG CCA GGA CGA CCG GGT CCT TT-3'	35	Target hybridization 53.7
HCV-target	5'- AAA GGA CCC GGT CGT CCT GGC AAT TCC GGT GTA CT -3'	35	
			Displacement 40.4
SARS probes [d]			
SARS tail-Cy5	5' Cy5 GGC TCC AGT ATA -C6 NH_2-3'	12	Tail hybridization 11.9
SARS quencher	5'- TAT ACT GGA GCBHQ ATT GTC TAC CTG AAC ACT ACC GCG T -3'	37	Target hybridization 52.4
SARS -target	5'- ACG CGG TAG TGT TCA GGT AGA CAA TGG CTC CAG TAT A -3'	37	
			Displacement 40.5
HIV100 probes [e]			
HIV 100-R[a]	5'TGGAATTAGGCCAGTAGTATCAACTCAACTGCTGTTAAATGGCA GTCTAGCAGAAGAAGAGGTAGTAATTAGATCTGTCAATTTCACGG ACAATGCTAA-3'	99	
HIV100-M[a]	5'TACAAATGTCAGCACAGTACAATGTACACATGGAATTAGGCCAG TAGTATCAACTCAACTGCTGTTAAATGGCAGTCTAGCAGAAGAAG AGGTAGTAAT-3'	99	
HIV 100-L[a]	5'TAATAAGACGTTCAATGGAACAGGACCATGTACAAATGTCAGCA CAGTACAATGTACACATGGAATTAGGCCAGTAGTATCAACTCAAC TGCTGTTAAA-3'	99	

Table 3.1 Sequence, modifications and thermodynamic parameters of the DNA probes used in this study.

[a]ΔG values are calculated using *Oligocalc* software (http://www.basic.northwestern.edu/biotools/oligocalc.html)

[b] HIV sequence source: HIV 1 (GenBank: AF033819.3 position 6520-6559);

[c] HCV sequence source: HCV-1a (M67463.1 position 160-195)

[d] SARS sequence source: Human coronavirus 229E, complete genome, (GenBank AF304460 position 16710-16747)

[e] HIV100R, HIV100 M and Hiv 100 L were designed including the HIV DNA target complementary sequence at the 5'end, in the middle and the 3'end of the 100 nucleotide sequence. The underline sequences indicate the HIV DNA target complementary portion.

Probe name	Sequence[b]	Length (nt)	ΔG (Kcal/mol)[a]	
miR21 probes				
miR21 tail-Cy5	5' Cy5 GACTGATGTTGA NH_2-3'	12	Tail hybridization	11.2
miR21 quencher	5' TCAACATCAGTBHQTGATAAGCTA -3'	22	Target hybridization	
miR21-target DNA	5' TAGCTTATCAGACTGAUGTTGA-3'	22		25.1
miR21-target RNA	5' UAGCUUAUCAGACUGAUGUUGA-3'	22		24.8
			Displacement	13.6 (13.9)
miR210 probes				
miR210 tail-Cy5	5' Cy5 ACAGCGGCTGA NH_2-3'	11	Tail hybridization	13.9
miR210 quencher	5' TCAGCCGCTGBHQCACACGCACAG-3'	22	Target hybridization	
miR210-target DNA	5'CTGTGCGTGTGACAGCGGCTGA-3'	22		33.3
miR210-target RNA	5'CUGUGCGUGUGACAGCGGCUGA-3'	22		34.9
			Displacement	21.0 (19.4)
miR196a-5p probes				
miR196a-5p tail-Cy5	5' Cy5 CATGTTGTTGGG NH_2-3'	12	Tail hybridization	11.2
miR196a-5p quencher	5' CCCAACAACATBHQAAACTACCTA-3'	22	Target hybridization	
miR196a-5p-target DNA	5'TAGGTAGTTTCATGTTGTTGGG-3'	22		26.1
miR196a-5p-target RNA	5'UAGGUAGUUUCAUGUUGUUGGG-3'	22		25.8
			Displacement	14.6 (14.9)

Table 3.2 Sequence of the RNA probes used in this study to test the specificity and selectivity of the double strand DNA detection system
[a]ΔG values are calculated using *Oligocalc* software (http://www.basic.northwestern.edu/biotools/oligocalc.html)
[b] miR21-target RNA , miR210-target RNA and miR196a-5p source: http://www.mirbase.org

The performance of the double strand displacement assay was first evaluated in homogeneous conditions (ds displacement assay) to prove its specificity and selectivity by spectrofluorometer measurements . In such condition we evaluated the ability to detect single, synthetic DNA target sequences derived from typical or non-coding genome region of three RNA virus: HIV, HCV, SARS.[10, 11]

In order to assess the assay versatility and robustness, the ds displacement assay ability to detect RNA target was explored. miR21, mir210 and miR196a-5p sequence were chosen as RNA target model[12] since they have been identified as biomarker of pancreatic cancer disease, when simultaneously over-expressed. [13]

In general, the optimization of the assay performance including (i) the signal to-noise ratio, (ii) hybridization condition (probe sequence and hybridization time), (iii) the selectivity tests in presence of complex matrix.[14]

The disassociation of the free fluorophore probe from the quencher probe is a major source of the background noise and represents a major factor that limits the overall sensitivity of the dsDNA assay.[15,16] In order to minimize the background level, the concentration of the quencher probe relative to the concentration of the fluorophore probe (quencher to- fluorophore ratio) was adjusted systematically to minimize the concentration of free fluorophore probe in the solution. The background fluorescence generally diminishes with the quencher-to-fluorophore ratio.

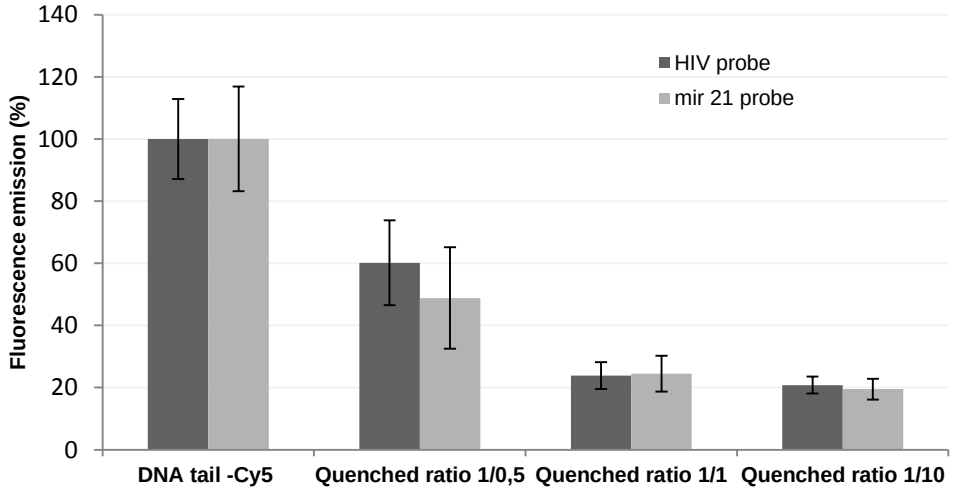

Figure 3.4 Quencher /fluorophore ratio optimization

As reported in **Figure 3.4**, HIV DNA and mir 21 DNA probes were chosen as model to evaluate the effect of fluorophore/quencher ratio on the background minimization. The fluorescence intensity is quite minimized when the quencher-to fluorophore ratio reaches 1-to-1 ratio and a further increase in the ratio does not show significant reduction of the fluorescence intensity. However, a higher quencher-to-fluorophore ratio can affect the probe sensitivity and shifts the dynamic range to the higher target concentration.

Incubation time for the tail-quencher probe hybridization also plays a role on the overall assay efficiency. [17,18]

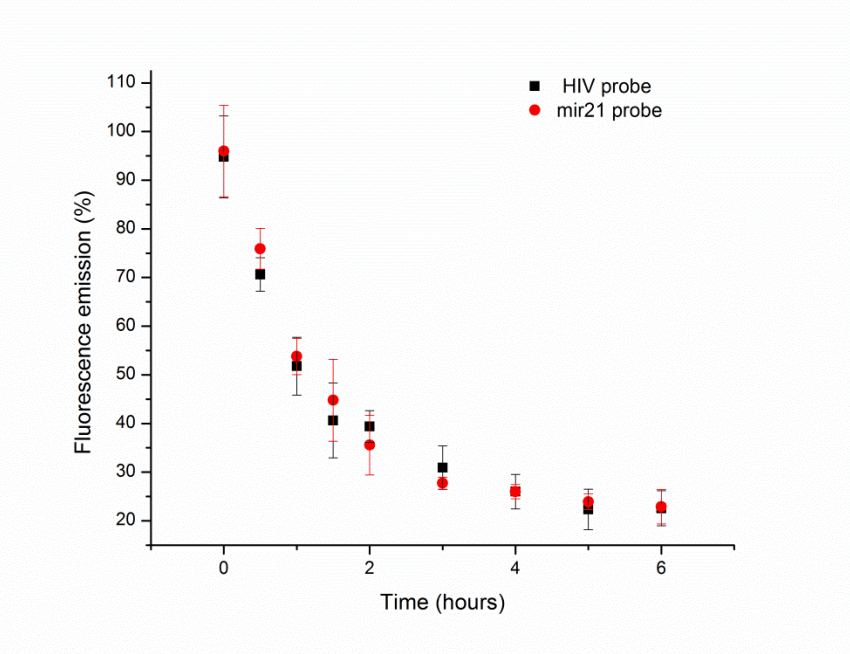

Figure 3.5 Kinetic study of incubation time for the tail-quencher probe hybridization

Fluorescence quenching obtained after incubation for six hours were shown in **Figure 3.5**. It was observed that the fluorescence decreased until reached the minimum value at five hours of incubation.

To get further insight into the kinetics of the displacement assay with respect of different target length and secondary ds strand nature (homoduplex *vs* heteroduplex) we collected time dependent fluorescence recovery of ds HIV and ds miR21 ds displacement assay in presence of the relative targets (**Figure 3.6**) .

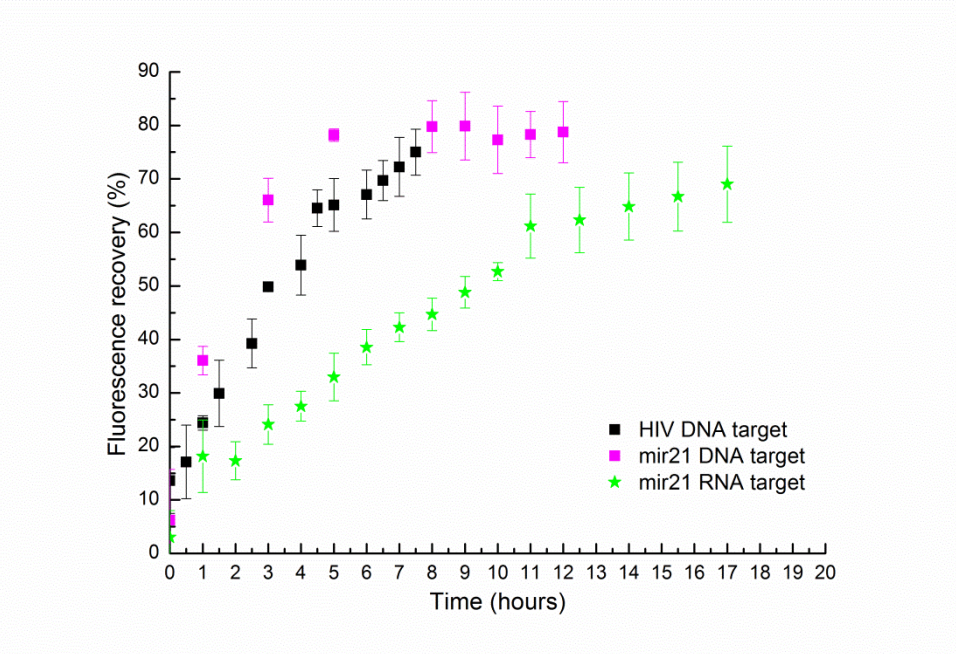

Figure 3.6 Displacement kinetic of HIV DNA, miR21 DNA/RNA target in homogeneous assay. Fluorescence recovery was monitored at 30-60 minutes step until any variation in fluorescence recovery was recorded. Quenched samples were used as reference in order to evaluate the displacement efficiency. The Cy5 emission intensities upon the displacement event were normalized versus the DNA tail Cy5 emission for each time point.

Since in the miRNA detection assay the displacement leads to the formation of a DNA-RNA heteroduplex whose thermodynamic stability could affect the assay efficiency in this case the kinetic rate was studied both in presence of RNA target and the homologous DNA. As reported in **Figure 3.6** the displacement rate is the same in presence of DNA target (HIV-DNA target and mir21 DNA target) and thus not affected by the length of the pending tail (27nt vs 10nt). For both assays a complete displacement is achieved in 6 hours. Instead the miR21 RNA target needs 12 hours to lead to the complete formation of heteroduplex. [19-21]

The performance of the dsDNA probe was first characterized to evaluate the use of the assay for rapid molecular analysis without target amplification at nanomolar concentration by spectrofluorometer measurements (molar ratio tail/quencher/target 1/1/1).

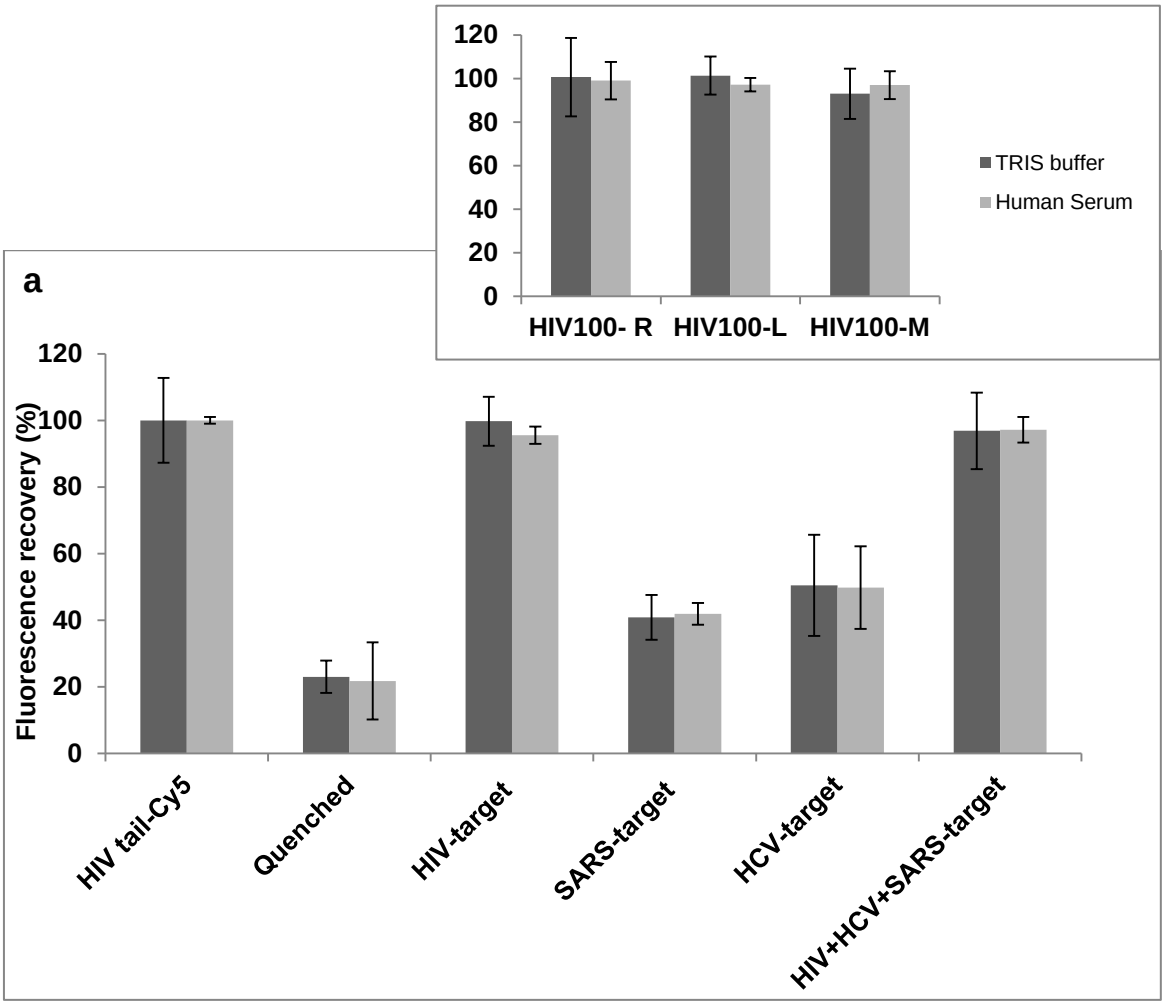
a
Fluorescence recovery (%)
120
100
80
60
40
20
0
HIV tail-Cy5
Quenched
HIV-target
SARS-target
HCV-target
HIV+HCV+SARS-target
HIV100- R
HIV100-L
HIV100-M
TRIS buffer
Human Serum

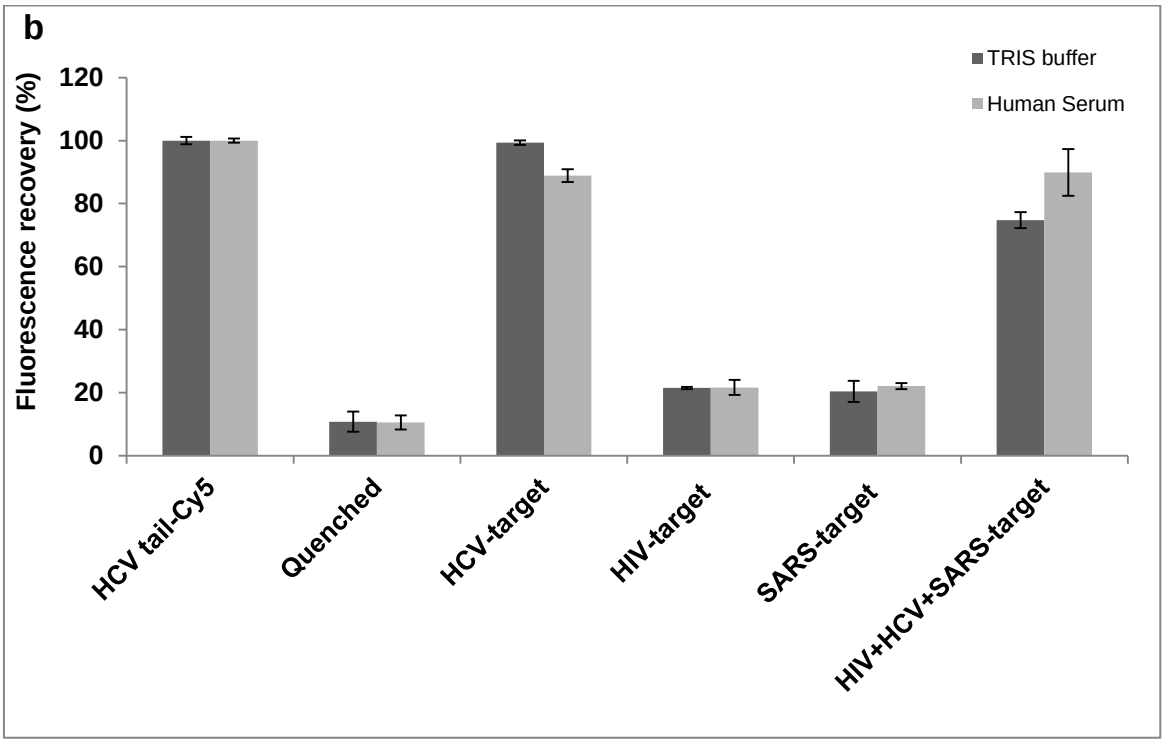
b
Fluorescence recovery (%)
120
100
80
60
40
20
0
HCV tail-Cy5
Quenched
HCV-target
HIV-target
SARS-target
HIV+HCV+SARS-target
TRIS buffer
Human Serum

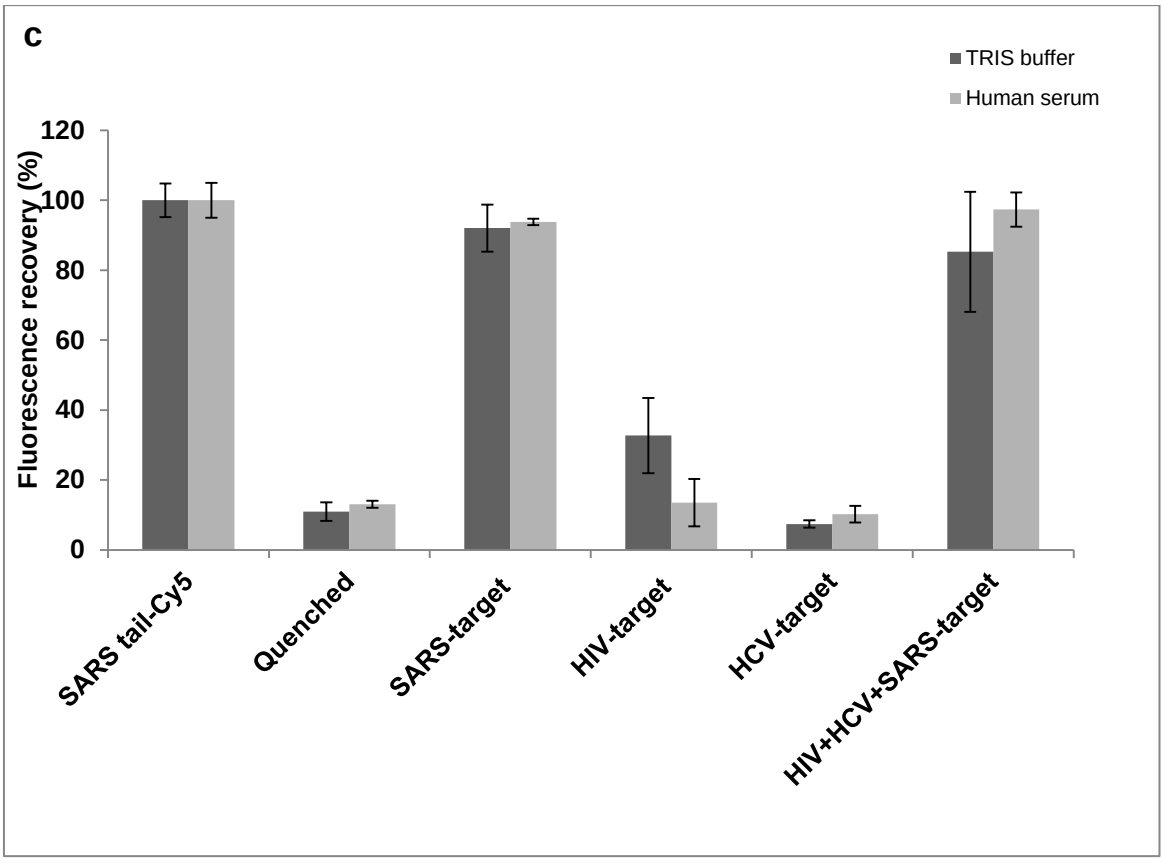

Figure 3.7 ds displacement assay performance for viral DNA target detection. Specificity of the ds displacement assay for HIV **(a)** , HCV **(b)**, SARS **(c)** virus DNA are tested in homogeneous assay in presence of corresponding DNA target by spectrofluorometer measurements. The selectivity of the specific target is investigated in a mixture of non-specific nucleic acids (HIV+HCV+SARS target) or in presence of interfering agent (Human serum). The Cy5 fluorescence recovery of the HIV ds probe when the target sequence is flanked by non specific genomic portions (HIV-100M) or when it carries nucleotide genomic tail longer than 60 nt (HIV-100R and HIV-100L) is reported in the panel **a** inset. The Cy5 emission intensities are normalized versus the DNA tail-Cy5 emission. The experimental uncertainty represents the standard error of the mean of three replicates assay.

Figure 3.7, panel a, b, c shows high displacement efficiency in presence of the corresponding target after six hours incubation, even when diluted in a mixture of non-specific nucleic acids (HIV+HCV+SARS target) and in the presence of interfering proteins commonly found in human serum. For the HIV strand detection further analyses on the specificity were performed. The effect on the displacement of longer strands, flanking the complementary sequence, was investigated. The complementary HIV target sequence allows the full displacement even within (HIV100-M) or flanking (HIV100-R and HIV100-L) genomic portions longer than 60 nt (**Figure 3.7 a inset**). **Table 3.1** reports the HIV100 sequences.

To verify the ability of the our ds displacement assay for miRNAs detection, the displacement performance is evaluated by comparing the fluorescence recovery in presence of RNA target (heteroduplex formation) to the one measured for the homologous DNA target. The specificity was also investigated by the displacement target ability in a mixture of non-specific miRNAs (miR21+miR210+miR196a-5p target) or in presence of interfering agent (Human serum).

Figure 3.8 a, b, c shows that ds displacement assay is able to detect all the miRNAs targets with efficiency comparable to the one observed in presence of the homologous DNA target , even though with a slower kinetic rate.[22]

One of the major applications of miRNAs detection method is detection in the complex matrix like human serum. Therefore, to show that our strategy will work in a complex matrix, and to show that nonspecific hybridization does not occur between non-complementary nucleic acid and the quenched probes, we tested the performance of the assay in human serum. We would expect the assay to yield similar results to that obtained when it is performed in the hybridization buffer.

The results obtained yielded the same emission profile as that seen previously with the hybridization in a buffer matrix for all the miRNAs probes. Therefore, hybridization between the non-complementary nucleic acid and the quenched probes either does not occur, or does not significantly affect the fluorescence recovery, indicating that this detection assay is compatible in more complex matrices containing non target nucleic acid. (**Figure. 3.8**).

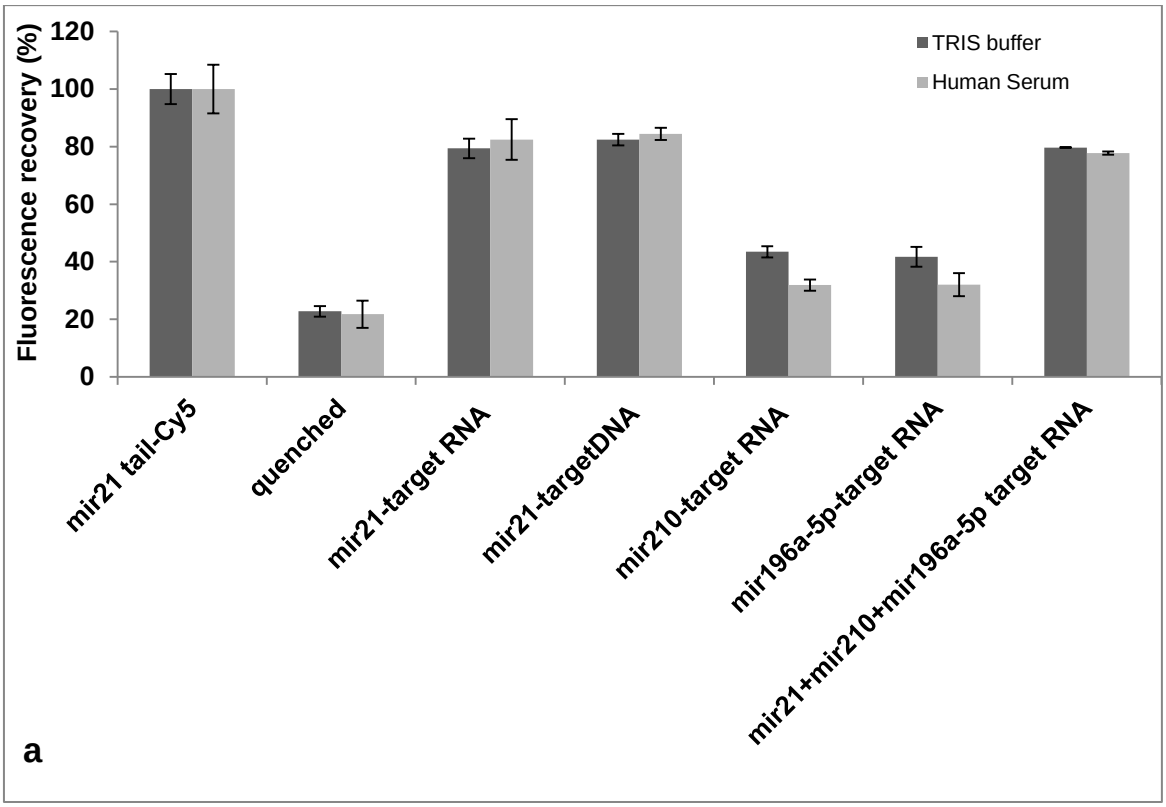
Fluorescence recovery (%)
120
100
80
60
40
20
0
TRIS buffer
Human Serum
mir21 tail-Cy5
quenched
mir21-target RNA
mir21-targetDNA
mir210-target RNA
mir196a-5p-target RNA
mir21+mir210+mir196a-5p target RNA
a

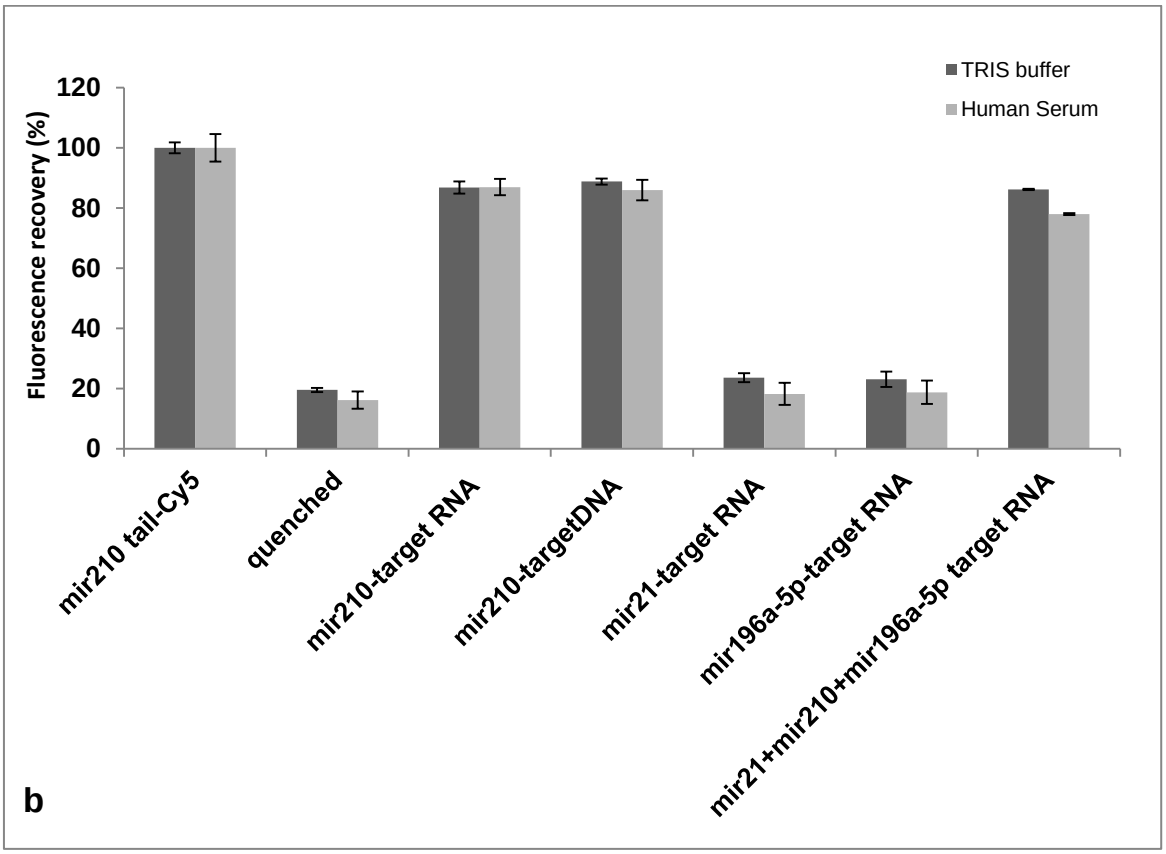
Fluorescence recovery (%)
120
100
80
60
40
20
0
TRIS buffer
Human Serum
mir210 tail-Cy5
quenched
mir210-target RNA
mir210-targetDNA
mir21-target RNA
mir196a-5p-target RNA
mir21+mir210+mir196a-5p target RNA
b

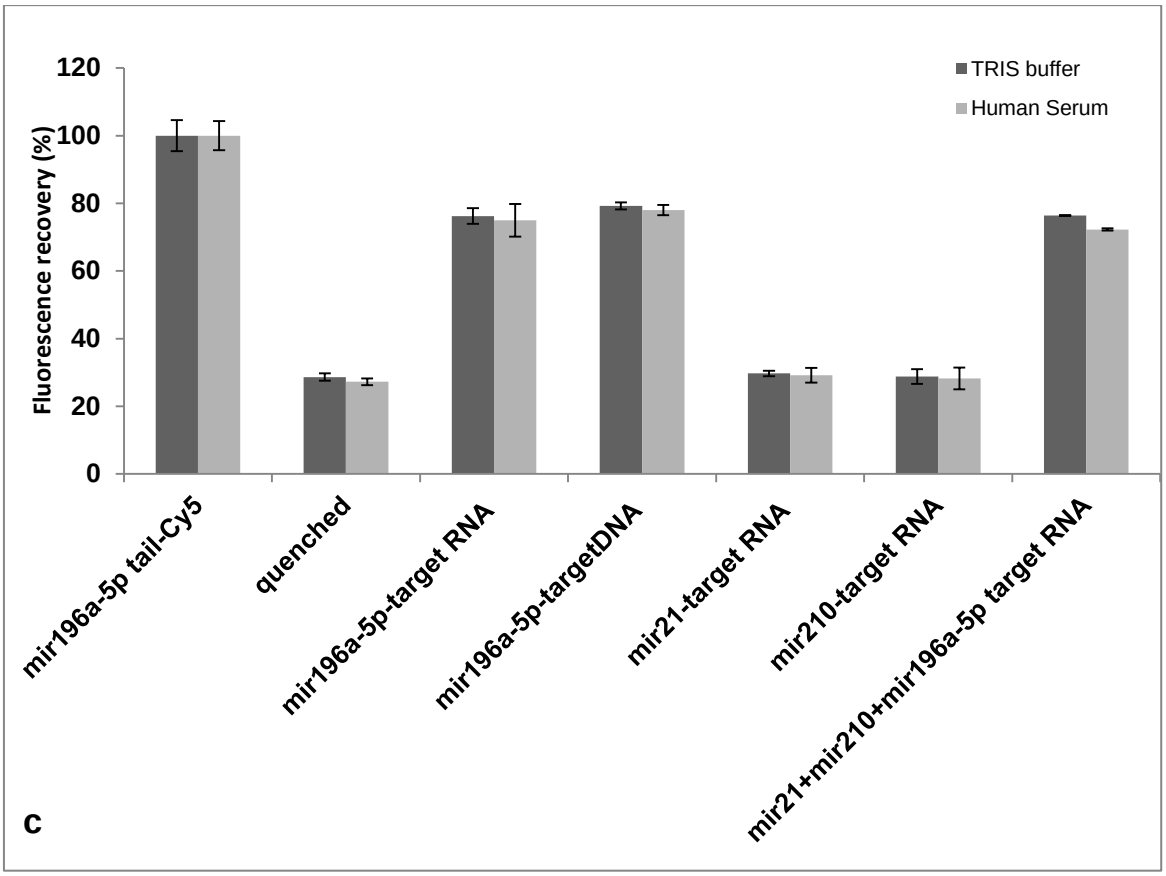

Figure 3.8 Set up of the ds displacement assay for miRNAs detection. Evaluation of efficiency, specificity and selectivity for miR21, miR210, miR196a-5p target in homogeneous assay by spectrofluorometer measurements. The Cy5 emission intensities are normalized versus the DNA tail Cy5 emission.

Within this context, we have demonstrated a homogeneous dsDNA probe to rapidly detection RNA/DNA target in nanomolar concentratrion.

As demonstrated in this study, the probe has good specificity against other common nonspecific DNA/RNA targets and complex sample matrix like human serum. Compared to other hybridization assays the dsDNA probe dramatically simplifies the assay protocol with procedures that are easy to implement for disease diagnostic applications.

3.4 Conclusion

The current work gives an overview on the double-stranded molecular probe design and itsapplication for oligonucleotides detection. The flexibility of

the design allows the probe to be applied in a wide spectrum of applications. The specificity of the molecular assay provides a useful tool in different biomedical applications. For instance, the molecular probe can be adopted for detecting small DNA and quantification of mRNA.

Our results show that as little as (100 nM) of target DNA/RNA can be detected in solution and in complex matrices.

This method is an improvement over common solid-phase methods in that no wash steps to eliminate unbound probe are needed. The simplicity of the assay is also beneficial for microfluidic-based point-of-care diagnostic systems.

Bibliography

[1] Marras, S. A. *Mol Biotechnol*, **2008**, *38*, 247–255.

[2] Morrison, L. E.; Halder, T. C.; Stols, L. M. *Analytical Biochemistry*, **1989**, *183*, 231–244.

[3] 16. Li, Q., Luan, G.; Guo, Q.; Liang J. *Nucleic Acids Research*, **2002**, *30*, E5.

[4] Marras, S. A *Methods in Molecular Biology*, **2006**, *335*, 3–16.

[5] Chen, C., Tan, R., Wong, L., Fekete, R. and Halsey J., *Methods in Molecular Biology*, **2011**, *687*, 113-134.

[6] Meserve, D.; Wang, Z.; Zhang, D. and Wong, P. *Analyst*, **2008**, *133*, 1013–1019.

[7] Bishop, J.; Blair, S. and Chagovetz, A. M. *Biophys. J.*, **2006**, *90*, 831–840.

[8] Bishop, J.; Blair, S. and Chagovetz, A. M, *Biophys. J.*, **2007**, *92*, L10–L12.

[9] Markham, N. R. and Zuker, M. *Nucleic Acids Res.*, **2005**, *33*, W577–W581.

[10] Horejsh, D. *et al. Nucleic Acids Res*, **2005**, *33*, e13.

[11] Lin, C., Liu, Y. and Yan, H. *Nanolett*, **2007**, *7*, 507-512.

[12] Si, M.L. *et al*. *Oncogene*, **2006**, *26*, 2799-2803.

[13] Wang, J. *et al Cancer Prev Res* (Phila Pa), **2009**, *2*, 807-813.

[14] Baker, B. and Milam, V. *Nucleic Acid Res*, **2011**, 1-13.

[15] Riahi, R., Mach, K. E., Mohan, R., Liao, J.C., and Wong, P.K. *Anal. Chem.* **2011**, *83*, 6349-6354.

[16] Broyles, D.; Cissel,K. and Kumar, M. *Anal. Bioanal. Chem.*, **2012**, *402*, 543-550.

[17] Chan, H.;Chan, L.; Wong, R. and Li, H. *Anal. Chem.*, **2010**, *82*, 6911-6918

[18] Xiang, D.;Zhou, G.; Luo, M.; Ji, X. and He, Z. Analyst, **2012**, *137*, 3787-3793.

[19] Reynaldo,L.P., Vologodskii,A.V., Neri,B.P. and Lyamichev,V.I. J. *Mol. Biol.*, **2000**, *297*, 511–520.

[20] Zhang,D.Y. and Winfree,E. *J. Am. Chem. Soc*., **2009**, *131*, 17303–17314.

[21] Genot,A.J., Zhang,D.Y., Bath,J. and Tuberfield, A.J. *J. Am. Chem. Soc*., **2011**, *133*, 2177–2182.

[22] Sugimoto, N.; Nakano, S.; Matsumura, A.; Sasaki, M. *Biochemistry*, **1995**, *34*, 11211-11216.

[23] Varallyay E.; Burgyan J.; Havelda Z. *Nat Protoc*, **2008**, *3*, 190–196 .

[24] Calin GA.; Croce GM. *Nat Rev Cancer*, **2006**,*6*, 857–866.

[25] Cissell KA.; Rahimi Y., Shrestha S.; Junt EA.; Deo SK. *Anal Chem*, **2008**, *80*, 2319–2325.

[26] Matthews JC.; Hori K.; Cormier MH.; Biochemistry, 1977, 16, 85–91

[27] Gao Z.; Yu YH. *Biosens Bioelectron*, **2007**, *22*, 933–940.

[28] Gao Z, Yang Z *Anal Chem* **2006**, *78*, 1470–1477.

[29] Driskell JD, Seto AG, Jones LP, Jokela S, Dluhy RA, Zhao YP, Tripp RA *Biosens Bioelectron*, **2008**, *24*, 923–928.

[30] Shi R, Chiang VL *Biotechniques* **2005**, *39*, 519–525.

Chapter IV

Surface conjugation & **M**icrogel **E**nhanced **Di**splacement **A**ssay

4.1 Introduction

Conventional approaches based on strand hybridization and reporting needs amplification of target to improve detection sensitivity and purification procedures to reduce interference of other biomolecules. For the oligonucleotides detection, we present a platform, named named in this study **M**icrogel **E**nhanched **Di**splacement **A**ssay (MEDiA), based on the combination of the polymeric microgels and the double strand probes previously described. The MEDiA is capable to enhance fluorescence signal by concentrating emission events on reduced particle surface, thus lowering the limit of detection down to femtomolar concentration, to perform the assay directly on serum without additional purification steps and provide an adequate multiplex capability. The MEDiA detects in specific and selective manner distinctive region of viruses genome as well as different miRNA.

4.2 Experimental

4.2.1 Material

DNA and RNA oligonucleotides were purchased from Diatech Pharmacogenetics srl (Ancona, IT) with HPLC purification. All nucleotides were suspended in rnase-free water molecular grade (Applichem) and diluted to the appropriate concentration. Tris buffer 1M, pH 8 was supplied by Applichem GmbH (Darmstadt, DE). The buffer solution for the dsDNA probe contains 10 mM Tris HCl pH 8and 200 mM NaCl. Human serum was supplied by Lonza. 1-ethyl-3-(3-dimethylaminopropyl) carbodiimide (EDC) and MES were all purchased from Sigma-Aldrich (St. Gallen, CH) and used as received. MirVana PARIS kit was purchaised from Ambion (Life Technologies Ltd, Paisley, UK).
Purezol (Biorad), miRNA-specific stem-loop primers and other primers, TaqMan MicroRNA Reverse Transcription Kit and mature miR-21-specific TaqMan MicroRNA Assays were obtained from Applied Biosystem.

4.2.2 Single particle displacement assay (MEDiA) set up

4.2.2.1 Microgel surface functionalization.

1 mg of encoded microgels was dissolved in 250 μL of coupling buffer, 100 mM MES pH 4.8, and kept at 4°C with occasional vortexing for at least 1 h to disperse the colloidal particles. To this suspension, EDC (500 mM, final concentration, dissolved in the coupling buffer that was freshly prepared just before use) was added, followed by addition of tail-Cy5 DNA. Total reaction volume was approximately 500 μL. The reaction mixture was carried on in dark and left at 4°C in a shaker overnight. The DNA conjugate-microgel was precipitated down by centrifugation at 6000 rpm for 15 min at room temperature. The supernatant was removed carefully with a pipette and the precipitant was re-suspended in 1ml of Tris HCl, pH 8 buffer by agitating with a pipette tip and brief vortexing. This washing step was repeated three more times.

A control experiment was done using the same procedure but without EDC being added.

To estimate the coupling efficiency on the microgel, different amounts of tail-Cy5 DNA (15, 150, 1500, 3000 pmol) were tested for the coupling procedure and the unbound tail-Cy5 DNA was estimated by comparing the fluorescence from the retrieved probe solution to standards. The amount of immobilized tail-Cy5 DNA was calculated from the difference between the initially added tail-Cy5 DNA and the free tail-Cy5 DNA in solution after coupling. A confocal microscope with excitation wavelength of 633 nm and emission range wavelengths of 650 and 720 nm, respectively, was used to measure the fluorescence intensity of solutions.

The saturation concentration probe for coupling was found at 1500 pmol of tail-Cy5 DNA.

4.2.2.2 Quenching and DNA Displacement assay

Approximately, 50 μg of tail-Cy5 DNA-coupled microgel (in 250 μl Tris HCl pH8 hybridization buffer) was mixed with 11 pmol of Quencher-DNA (250 μl) probe sequences. The mixture was incubated at room temperature overnight. The microgels were then washed with hybridization buffer and resuspended in 1mL of buffer at final concentration of 0.05μg/μl. 50μl (0.5 μg) of quenched microgel were mixed to 450 μl of a solution containing target sequence at different concentrations ranging from 10^{-15} to 10^{-9} M and incubated at room temperature overnight. The microgel was precipitated down by centrifugation at 6000 rpm for 15 min at 4°C. The supernatant was removed carefully with a pipette and the precipitant was re-suspended in 50μl of Tris HCl, pH 8 buffer by agitating with a pipette tip and brief vortexing.

4.2.2.3 Fluorescence characterization and data analysis for MEDiA assay

30 µl of microgels after target contact were loaded onto µ-slide channels (Ibidi, Martinsried, DE), illuminated at confocal laser scanning microscope Leica SP5 using Helium neon laser 543 nm and 633 nm , Argon laser 488 nm and fluorescence images of microgel were collected. Objective: HCX PL APO CS 100.0x1.40 oil, section thickness 1µm, scan speed 8000 Hz, Excitation Laser Argon 633 nm, λem range 654-710 nm, image size 77.5x77.5 μm^2

For microgel experiments, 200 microparticles were selected for each sample (i.e. different target concentrations) to be analyzed and their fluorescence quantified.

All captured images were analysed with a public domain image-processing Image J (version1,43i, NIH, Bethesda, MD). Briefly the images were thresholded by Otsu algorithm and then processed with the Image J Analyze Particles function to computationally determine the number of single fluorescent particles sizing in the range of 1µm.

For the displacement assay, the fluorescence mean and standard deviation of each sample were calculated and a t-student test was used to compare them (p value < 0.001). The experimental uncertainty represents the standard error of the mean of three replicates assay. To estimate the limit of detection (LOD) weighted linear regression is applied to analyze the data. The LOD values are determined by extrapolating the concentration from the signal equal to the intercept plus three standard deviations on the background signal. The calibration curves are used to convert the values into the corresponding target concentrations. R^2 is above 0,9 in all experiments, p values range from 0,005 to 0,1 and F values are higher than F critical values in all cases. The results are summarized in following **Table 4.1**

Assay	slope	intercept	LOD (fM)	R-Sq	F value	P>F	P<
SARS MEDiA	$2{,}29\cdot10^{16} \pm 1{,}6\cdot10^{15}$	535 ± 9,54	1,25	0,98	194	0,005	0.005
HCV MEDiA	$2{,}02\cdot10^{16} \pm 1{,}1\cdot10^{15}$	551 ± 6,47	9,61	0,99	318	0,003	0.003
HIV MEDiA	$3{,}85\cdot10^{16} \pm 4{,}2\cdot10^{15}$	595 ± 28,5	2,22	0,96	80	0,012	0.01
miR21 MEDiA	$5{,}22\cdot10^{16} \pm 9{,}5\cdot10^{15}$	592 ± 65,3	3,76	0,91	30	0,031	0.03

Table 4.1 Linear regression data analysis table for MEDiA assay

4.2.3 Homogeneous displacement assay by CLSM imaging

Tail-Cy5 DNA were mixed to quencher DNA (molar ratio 1/1) in Tris HCl, pH 8 buffer. Different amount of DNA or RNA target were added to such solutions in a final volume of 200μL. Fluorescence emission of the solution for the homogeneous ds displacement assay was acquired by confocal laser microscope imaging for the detection of HCV, SARS, HIV DNA target and miR21 RNA target over a dynamic range concentration of 10^{-11} – 10^{-6} M.

The experimental uncertainties indicated represent the standard deviation of three replicates.

4.2.3.1 Fluorescence characterization and data analysis for homogeneous displacement assay by CLSM imaging

50 μl of solutions after target contact were loaded onto μ-slide channels (Ibidi, Martinsried, DE), illuminated at confocal laser scanning microscope Leica SP5 using Helium neon laser 543 nm and 633 nm , Argon laser 488 nm and fluorescence images of microgel were collected. Objective: HCX PL APO CS 100.0x1.40 oil, section thickness 1μm, scan speed 8000 Hz, Excitation Laser Argon 633 nm, λem range 654-710 nm, image size 77.5x77.5 μm^2

Six images were selected for each sample (i.e. different target concentrations) to be analyzed and their fluorescence quantified. All captured images were analysed with a public domain image-processing Image J (version1,43i, NIH, Bethesda, MD). Briefly the images were thresholded by Otsu algorithm and then processed with the Image J Analyze.

To estimate the limit of detection, weighted linear regression is applied to analyze the data. The LOD values are determined by extrapolating the concentration from the signal equal to the intercept plus three standard deviations on the background signal. The calibration curves are used to convert the values into the corresponding

target concentrations. R^2 is above 0,9 in all experiments, p values range from 0,005 to 0,1 and F values are higher than F critical values in all cases. Plot of fluorescence recovery of the homogeneous ds displacement assay for the detection of HCV, SARS, HIV DNA target and miR21 RNA target over a dynamic range concentration of 10^{-11} – 10^{-6} M are reported in **Figure 4.1 (a)**. Instead, **Figure 4.1 b** shows the fluorescence recovery response of the ds displacement assay for HCV, SARS, HIV DNA target and miR21 RNA target in linear-linear space over 10^{-9}-10^{-7} M linearity range. The homogeneous ds displacement assay was performed in buffer tris for the viral DNA target detection and for the miR21 RNA target detection in order establish the same conditions used for the ds displacement assay on microgel.

The results are summarized in following **Table 4.2**

Assay	slope	intercept	LOD (pM)	R-Sq	F value	P>F	P<
SARS ds displ assay homogeneous	$6{,}31\cdot10^{9} \pm 4{,}7\cdot10^{6}$	417 ± 0,28	137	0,99	23788	0,004	0.004
HCV ds displ assay homogeneous	$1{,}49\cdot10^{9} \pm 3{,}4\cdot10^{6}$	257 ± 0,43	340	0,99	192	0,04	0.04
HIV ds displ assay homogeneous	$1{,}19\cdot10^{9} \pm 7{,}3\cdot10^{6}$	232 ± 0,51	170	0,99	148	0,05	0.05
miR21 ds displ assay homogeneous	$2{,}42\cdot10^{9} \pm 8{,}5\cdot10^{6}$	460 ± 0,49	230	0,96	53	0,08	0.08

Table 4.2 Linear regression data analysis table for homogeneous ds displacement assay by CLSM imaging

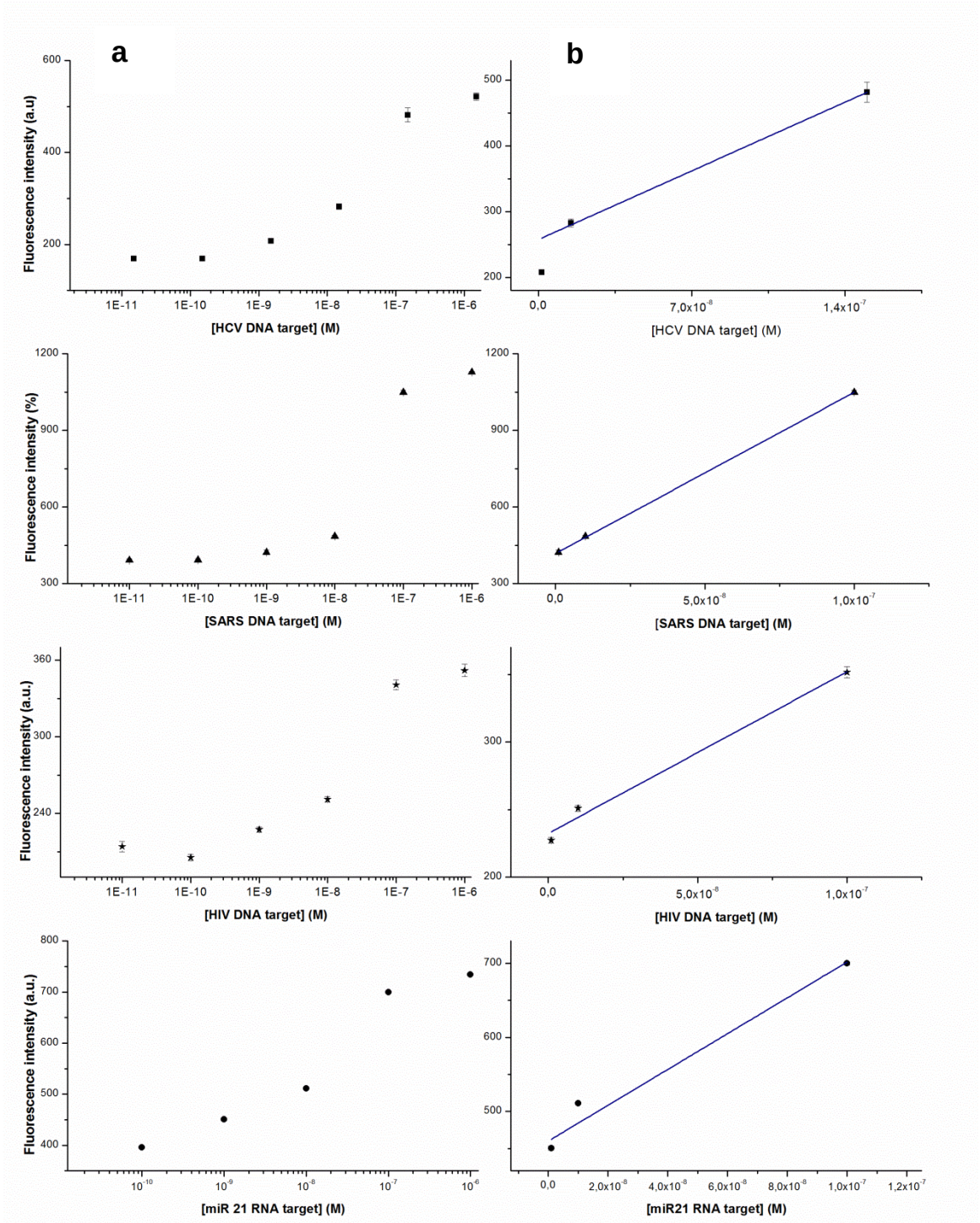

Figure 4.1 (a) Plot of fluorescence recovery of the homogeneous ds displacement assay for the detection of HCV, SARS, HIV DNA target and miR21 RNA target by CLSM imaging ; **(b)** Linear fitting of the Fluorescence recovery response of the ds displacement assay for HCV, SARS, HIV DNA target and miR21 RNA target in linear-linear space over 10^{-9}-10^{-7} M linearity range.

4.2.4 RNA isolation and quantitative RT-PCR in serum

4.2.4.1 Total RNA isolation

Total RNA (including miRNAs) was extracted from 400 μL of serum. Denaturation and phase separation were conducted using Purezol according to manufacturer's protocol, with a minor modification: 10 fmol of a *C. elegans* cel mir-54 was spiked-in.

1 mL of Purezol reagent was mixed with 400 μL of and incubated for 5 minutes. After the addition of chloroform, tubes were shaken well and centrifuged to separate the upper aqueous phase, which was carefully transferred to a fresh tube. Isopropanol was then added to the aqueous phase for 5 minutes followed by centrifugation at 12,000× g for 10 minutes. The RNA precipitate was washed with 75% ethanol and centrifuged at 7,500× g for 5 minutes. The ethanol was discard and the RNA was resuspended in 80 μL of H_2O RNase free.

4.2.4.2 Quantification of miR21 in Human Serum by Quantitative Real Time PCR (qRT-PCR)

Subsequently, Reverse Transcriptase reaction was performed with an CFX96 Touch™ Real-Time PCR Detection System (Biorad). RT mix: (1×) 10 mM dNTPs (0.15 μL), Multi-Scribe Reverse Transcriptase (1 μL), 10× RT buffer (1.5 μL), RNase Inhibitor (0.19 μL), nucleasefree water (7.66 μL), RNA sample (1.5 μL), 5× RT primer (3 μL); 16 ℃ for 30 min, 42 ℃ for 30 min, 85 ℃ for 5 min, 4 ℃ forever.

Real time PCR system: 2× TaqMan Universal PCR Master Mix (10 μL), 20× PCR Primer (1 μL), nuclease-free water (7.67 μL) and miRNA RT product (1:50 dilution) (1.33 L). qRT-PCR was then performed at 95 ℃ for 10 minutes, 95 ℃ for 15 seconds and 60 ℃ for 60 seconds, with the last two steps repeated for a total of

40 cycles. Each reaction was performed in triplicate. miRNA expression was defined based on the threshold cycle (Ct), and expression levels were calculated after calibration.

4.2.4.3 Establishment of miR21 Calibration by qRT-PCR

A mixture of synthetic RNA oligonucleotides was used to generate a standard curve for miR-21 and cel mir-54. The RNA oligonucleotides representing mature miRNA ranging from 300 copies to $3*10^9$ copies were reverse transcribed, also using TaqMan MicroRNA Reverse Transcription Kit and mature miR-21-specific TaqMan MicroRNA Assays. The PCR amplification of the cDNA was then performed using same materials as mentioned above. Three independent experiments were performed, and each experiment was run in duplicate. Calibration curve was shown in **Figure 4.2**

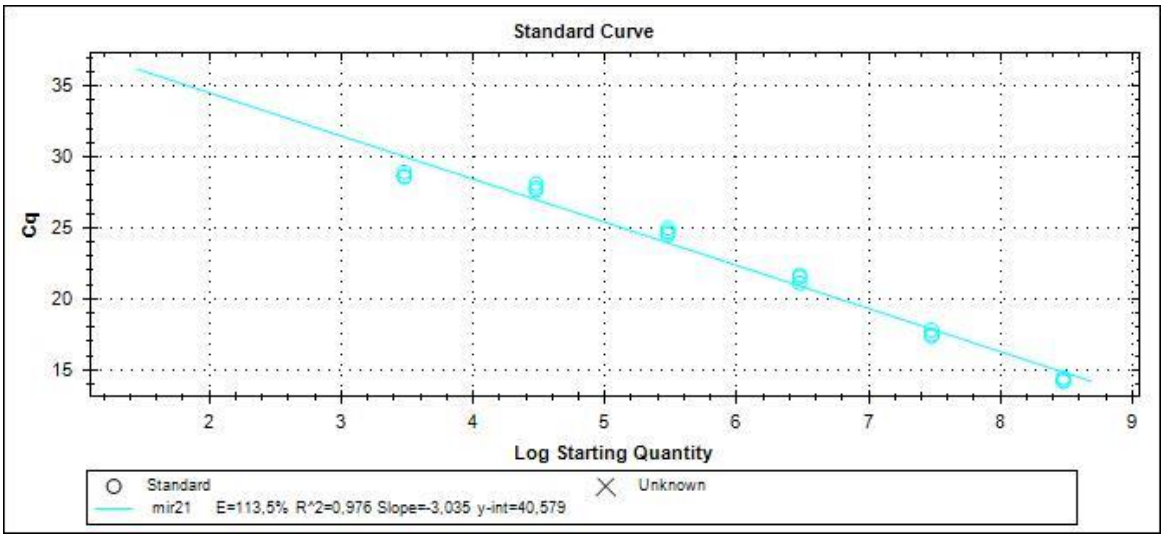

Figure 4.2 miR 21 calibration by qRT-PCR

4.2.5 Quantification of miR21 by MEDiA

50µl (0.5 µg) of quenched microgel were mixed to 80 µl of human serum extract, diluted until a final volume of 500 µl and incubated at room temperature overnight. The microgel was precipitated down by centrifugation at 6000 rpm for 15 min at 4°C. The supernatant was removed carefully with a pipette and the precipitant was re-suspended in 50µl of Tris HCl, pH 8 buffer by agitating with a pipette tip and brief vortexing.

For the fluorescence characterization see 4.3.3. To quantified the amount of miR21, the fluorescent emission of the microgel was correlated to the linear regression previously calculated for the miR21-LOD determination. Three independent experiments were performed, and each experiment was run in duplicate.

4.3 Result and discussion

To further improve the sensitivity of the assay, the double strand probe was assembled on encoded microgel particles surface. The conjugation on the particles surface combines the advantages of oligonucleotide-based probes with a tridimensional element which functions as: i) "concentrator" for the enhancement of response signal upon low abundant target binding;[1-3] ii) non-fouling and bioinert gel-based substrate for bioassays in complex biological media; iii) barcode provided carrier for scalable multiplex assays.[4-6]

Indeed, the conjugation on particle surface brings a large number of fluorophore probes into a small region which significantly increases the intensity and facilitates further manipulation. [7]

Several studies have already focused their attention on new particles for bio-molecule quantification provided with nonfouling properties, high target and encoding capacity and solution-like hybridization thermodynamics. [8] As material, hydrogels are proving to be excellent substrates for biomolecule capture and quantification. The surface immobilization of double strand assay on the bio-inert, PEG-based encoded microgel provides solution-like capture kinetics and high

degrees of both specificity and sensitivity, leading to significant advantages over surface-based immobilization strategies employed in microarrays and existing particle systems. [3-6]

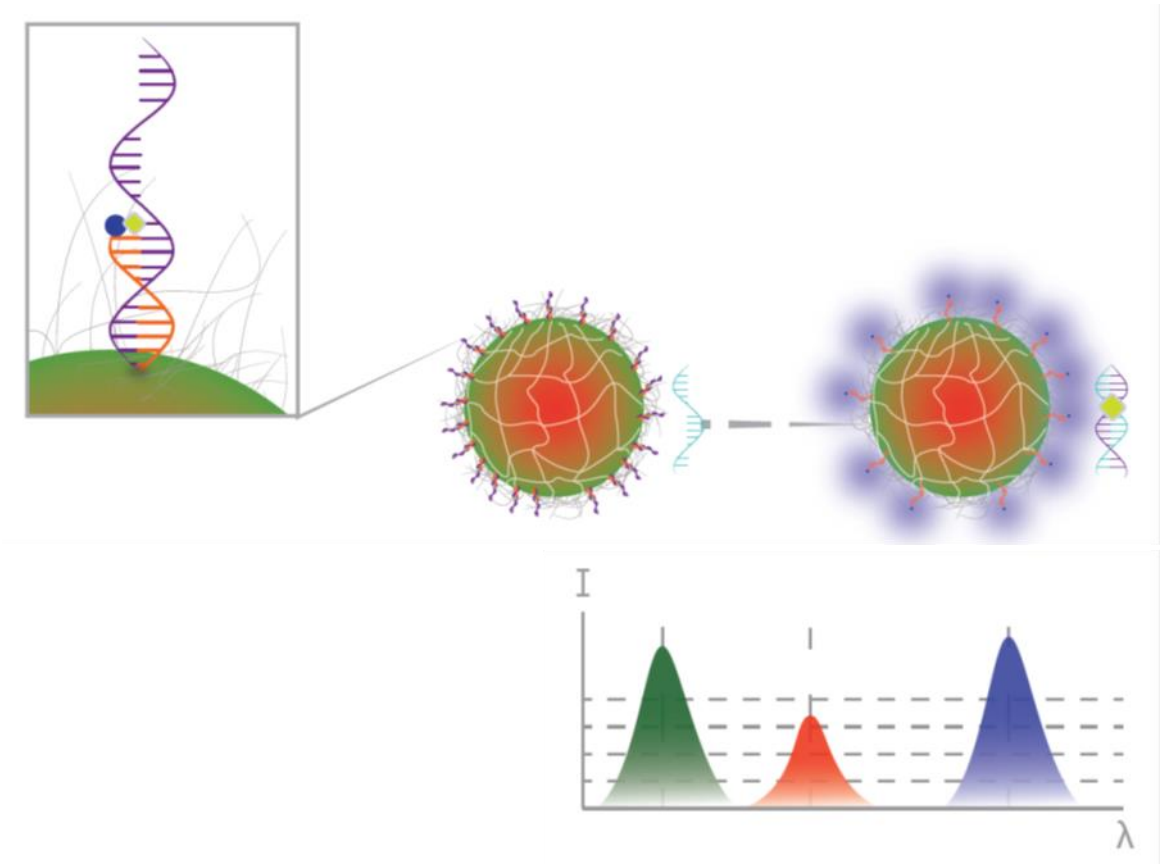

Figure 4.3 Conceptual scheme showing detection mechanism of MEDiA. The identity of each DNA/RNA target is revealed correlating the microgel code to the rhodamine/fluoresceine fluorescence emission ratio. The probe displacement is evaluated by Cy5 emission recovery.

The performance of the double strand probes already tested in homogenous assays (Chapter III) was then evaluated on microgel particles by CLSM imaging analysis.

The suspension assay, named in this study **M**icrogel **E**nhanched **Di**splacement **A**ssay (MEDiA), is based on multiplexed fluorescent microgels (described in Chapter II) provided with the double strand engineered for fluorescence detection upon target binding (described in Chapter III).

Small nucleotide tail (12nt) labeled with Cy5 at the 5’ end and properly functionalized at the 3’ end was used to enable the attachment on the outer shell of

the microgel. The fluorescence of DNA tail Cy5 is previously quenched by a partial hybridization with DNA quencher sequence. In presence of targets, the quencher DNA is thermodynamically driven to hybridize the target, which displace the DNA tail Cy5, leading a fluorescence recovery. The presence of the target is detected by the Cy5 fluorescence recovery after the displacement assay. The rhodamine B emission at λ=560 nm and fluoresceine emission at λ=510 nm ratio identify the encoded microgel. (**Figure 4.3**).

The first step of the assay set up includes the covalent coupling of the nucleotide tail -Cy5 by amino group at the 3' to carboxylic groups of encoded microgel by EDC protocol (**Figure 4.4 a, b**).[9-12] To determine the density of DNA on the microbead surface, the beads were exposed to the DNA-tail labeled with Cy5 (see **Experimental Section 4.2**).

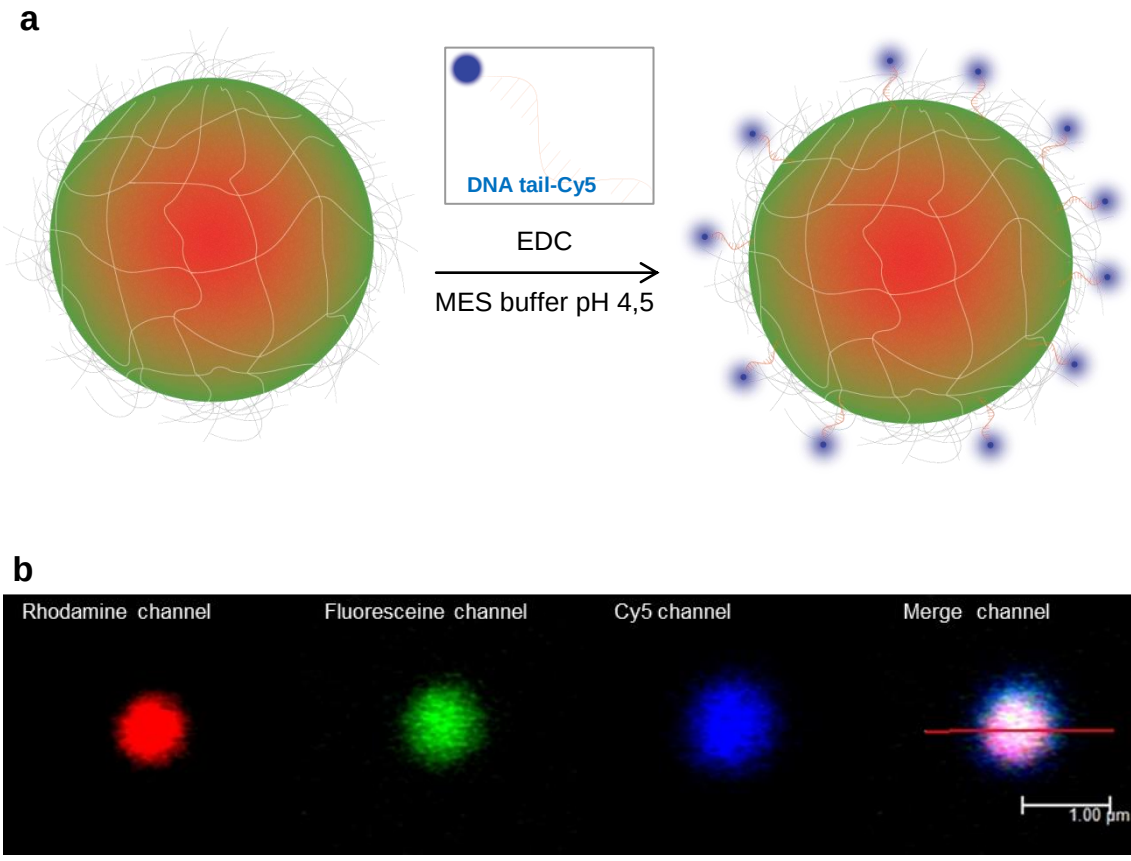

Figure 4.4 a) DNA tail Cy5 coupling reaction; **b)** CLSM image of fluorescence emission for the code and the Cy5 emission on microgel surface.

After immobilization of a fraction of this oligonucleotide, the remaining free DNA was retrieved and quantified by measuring the fluorescence of the resulting solution.

In this condition, the measured probe density was $4.7 \cdot 10^4$ DNA copies/microgel corresponding to $6{,}2 \cdot 10^{12}$ probes/cm^2 of microgel surface area. This was chosen as suitable an optimal surface-probe density since at higher surface densities repulsive electrostatic interactions and steric hindrance between oligonucleotides could reduce hybridization efficiency. [13-16]

Considering that our goal is the detection of oligonucleotide target in a femtomolar concentration (maximum volume of 500 μl), in this condition the total amount of target is in the order of 10^{-18} moles ($1.5 \cdot 10^6$ copies). To enable at least one detection event/particle, we decide to use $1.5 \cdot 10^6$ microgel for each displacement assay.

The next step was to test MEDiA to further increase the number of detectable copies of nucleic acids and to provide a tool for a multiplexed assay. The performance of the ds displacement assay in homogenous and MEDiA was first compared (by CLSM imaging).

As proof of concept, MEDiA was performed with three different fluorescent "barcode" corresponding to microgel decorated for SARS, HCV, HIV detection (see **Experimental section 4.2.3**). **Figure 4.5, panel a** shows Cy5 fluorescence recovery on single microgel with different concentration of target over a dynamic range of 10^{-9}-10^{-15} M.

To estimate the LODs of the assays, linear regression is applied for the data analysis (see **Experimental section 4.2.3**). Data analysis shows that, using MEDiA the minimum target concentration, distinguishable from the background noise, is fM. In particular, for the HCV, SARS and HIV DNA target the calculated LOD is respectively 9,6 fM, 1,2 fM and 2,2 fM (**Figure 4.5 a**). Instead a LOD in a pM concentration range was reported for double displacement assay alone (see **Experimental section 4.2.3, Figure 4.1 a, b**).

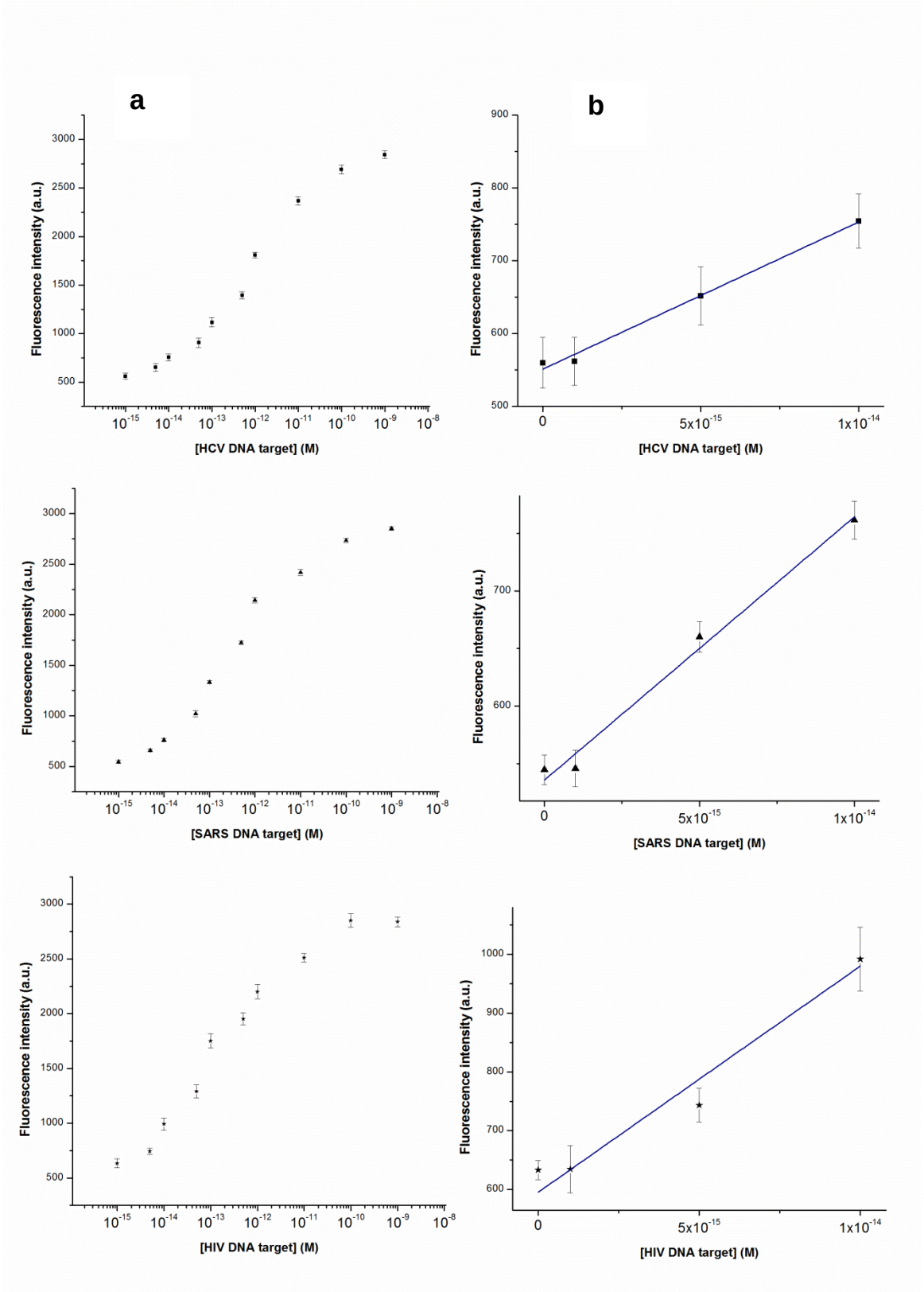

Figure 4.5 a) The plots show the response of MEDiA over a concentration range 10^{-15} to 10^{-9} M for SARS, HCV and HIV virus DNA target by CLSM measurements. **b)** The LOD values are determined by extrapolating the concentration from the signal equal to the intercept plus three standard deviations on the background signal. The LODs for HCV, SARS and HIV MEDiA assay are respectively 9.6, 1.2 and 2.2 fM.

Our results show that the combination of microparticles and dsDNA probes leads to an enhancement of the sensitivity of the detection system if compared with the homogeneus assay performance. This result suggests that the microgel provides a simple and effective approach to enhance the sensitivity of the dsDNA probe assay without target amplification. The single based particle assay permits the detection of very low concentration of small nucleic acids by confining the fluorescence recovery generated by target to the small volume represented by microgel (~0.9 fl) with intensity strictly related to the target amount. [7,17-19]

The MEDiA enhanced assay was also evaluated for its capability to detect RNA target: miR21 sequence was chosen as RNA target model. **Figure 4.6,** shows the fluorescence recovery for the mir21 MEDiA in a dynamic range of 10^{-15} - 10^{-9} M and the linearity of response with a LOD of fM, which is drastically lower than that achieved by ds probe itself (230 pM) (see **Table 4.2).** When the molecular probes are localized with microparticles, the sensitivity of the probe can be improved for over 1000-fold.

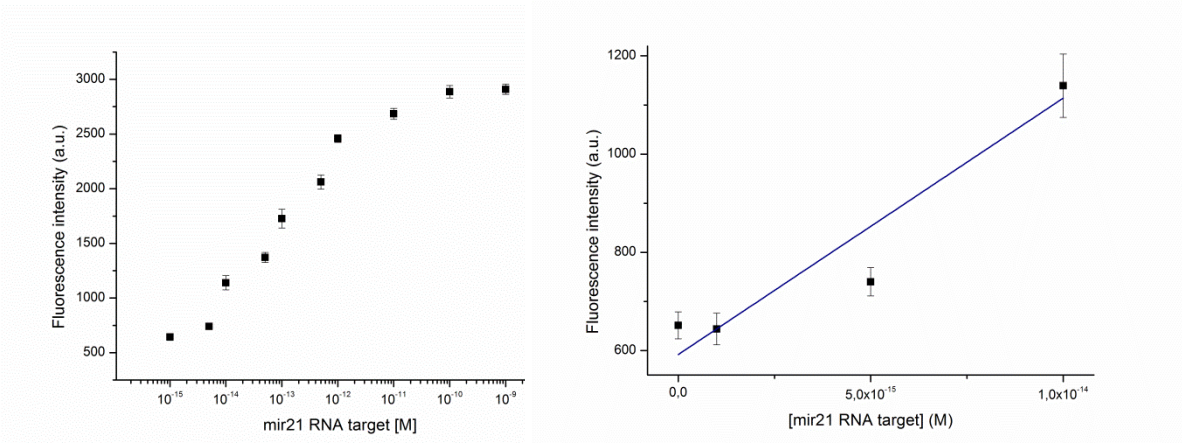

Figure 4.6 The plot on the left hand side shows the fluorescence recovery of miR21 MEDiA over a target concentration range 10^{-15} to 10^{-9} M by CLSM measurements. On the right hand side is reported the linear regression applied to the collected data in a dynamic range concentration of 10^{-15} to 10^{-13} M. The calculated LOD for the miR21 detection is 3,7 fM.

One of the major challenge of this study is the exploitation of a direct miRNAs detection system directly on biological samples without any amplification. The microgels are composed of bioinert PEG, they are nonfouling and have minimal

nonspecific binding, making them favorable for assays of targets in complex biological samples that may contain an excess of background protein species [4].

Since miR-21 has been validated as a key oncomir in breast cancer carcinogenesis [20, 20], we choose to test MEDiA in human serum extract in order to quantify miR21 amount (**Fig.4.7**). The same serum was used for RT-PCR quantification and the sensitivity of the two technologies has been compared.

For the purpose of result validation, we quantified the endogenous content of miR-21 in the human serum extract using the same batch of serum by qRT-PCR method. [22,23] Quantitative RT-PCR is a technique commonly adopted as a standard method for miRNA profiling. It is superior to other detection assays for its high specificity and minute amounts of starting materials used in the detection. Amplification steps however are involved. The output of qRT-PCR is usually expressed in terms of fold-change and so the raw data is semiquantitative. Additional calibration curve has to be established for quantitation purpose. The result is quantitative and obtained by applying standard addition methods. The standardization curve by qRT-PCR is shown in the **Figure 4.2**.

Figure 4.7 displays the contents of miR-21 in human serum determined by the MEDiA assays and those by qRT-PCR with calibration standardization. The MEDiA result ($1 \cdot 10^6 \pm 0.07$ miR21 copies) agrees very well with the outcome of qRT-PCR ($1.3 \cdot 10^6 \pm 0.5$ miR21 copies). The high correlation with the accredited qRT-PCR methods demonstrated that the pretreatment- free MEDiA system developed here is of high potential in detection of miRNAs applicable in early cancer diagnosis.

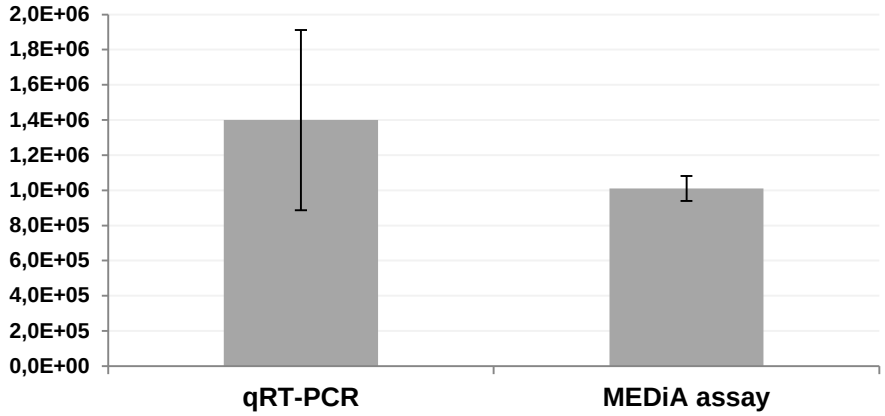

Figure 4.7 miR21 copies detection in human serum by qRT-PCR and by MEDiA. The values do not present significant statistical difference according to Turkey's test

By detecting single strand nucleic acids, MEDiA enables clinically important diagnosis in serum of viral DNA [24-26] or miRNA to be measured at femtomolar concentrations. We believe that such improvement in sensitivity of MEDiA, from pM to fM concentration range, will translate into diagnostic benefits if compared to the other biosensing technologies like direct microarray and qRT-PCR. [27-29]

For example, detection of RNA virus (or DNA one after inverse transcriptase) at lower concentration can bring to the diagnosis of viral pathologies difficult to predict in early stage like HIV and HCV [24-26].

The possibility of a multiplex approach, combined to the high sensitivity, provide a powerful tool for miRNA detection of selected panel, such as miRNA 21, 155, 106, for breast cancer, miRNA 196a-5p, 21, 210 for pancreas cancer, enabling the identification of a wide range of cancer pathologies [26]. Moreover MEDiA allows to reduce the sample processing (purification, amplification) routinely required for nucleic acid based biomarkers by means of PEG-hydrogel providing antifouling properties in biological complex matrixes.

4.4 Conclusion

The proposed MEDiA assay present the following characteristics: i) multiplex-ability with low costs; ii) a probe design capable to detect nucleotides with high

sensitivity and with a great flexibility to adapt the probe to different targets; iii) specificity and feasibility for blood test.

MEDiA assay can allow the direct detection in solution of ssDNA or RNA in the length range between 20 to 100bp with a low limit detection down to$1E^{-15}$M, and an upper limit of detection up to $1E^{-9}$M without the need of intermediate steps of amplification. This can fit the range where the use of more complicated and expensive RT-PCR or PCR is mandatory. Here we provide the proof of concept of the assay by using genetic material specific for viruses such as SARS, HIV, HCV and RNA, i.e. miRNAs. Further, the conjugation of such encoded microgel and the nucleic probe molecules represent an integrated platform able to detect at same time more than one target sequences the use of multiplex approach is possible thanks to encoded microgels. Those characteristics bring MEDiA assay towards the point-of-care analysis, where the sensitivity could not a stringent requirement or an ultra-sensitive quantification by using fluorescent microscopy or miniaturized systems (lab-on-chip).

Bibliography

[1] Birtwell, S.W. and Morgan, H. *Integr. Biol*. **2009**,*1*, 345-362.

[2] Chapin, S.C., Pregibon, D., and Doyle, P.S. *Angew. Chem. Int. Ed.* **2011**, *50*, 2289-2293.

[3] Helgeson, M., Chapin, S.C., and Doyle, P.S. *Curr. Opin. Colloid Interface Sci.* **2011**, *16*, 106-117.

[4] Chapin, S.C., and Doyle, P.S. *Anal. Chem.*, **2011**, *83*, 7179-7185.

[5] Appleyard, D., Chapin, S.C., Srinivas, R., and Doyle, P.S. *Nat. Protoc.*, **2011**, *6*, 1761-1774, 2011.

[6] Appleyard, D., Chapin, S.C., and Doyle, P.S., *Anal. Chem.*, **2010,** *83*, 193-199.

[7] Riahi, R., Mach, K. E., Mohan, R., Liao, J.C., and Wong, P.K. *Anal. Chem.* , **2011**, *83*, 6349-6354.

[8] Pregibon, D.C., and Doyle, P.S. *Anal. Chem.*, **2009**, *81*, 4873-4881, 2009.

[9] Ali, M.; Su, S.; Filipe, C.; Pelton, R. and Li, Y. *Chem. Commun*., **2007**, 4459–4461.

[10] Basinska,T. *Macromol. Biosci*., **2005**, *5*, 1145–1168;

[11] Ellaissari, A.; Ganachaud, F. and Pichot, *C. Top. Curr. Chem*., **2003**, *227*, 169–193;

[12] Pichot, C. *Curr. Opin. Colloid Interface Sci*., **2004**, *9*, 213–221.

[13] Kim,J.; Heo,J. and Crooks, R. *Langmuir* , **2006,** *22*, 10130-10134

[14] Herne, T. M.; Tarlov, M. J. *J. Am. Chem. Soc.* **1997**, *119*, 8916-8920.

[15] Steel, A. B.; Herne, T. M.; Tarlov, M. J. *Anal. Chem.* **1998**, *70*, 4670-4677.

[16] Peterson, A. W.; Heaton, R. J.; Georgiadis, R. M. *Nucleic Acids Res*.**2001**, *29*, 5163-5168.

[17] Wang, L.; Zhang, Y.; Tian, J. and Sun, X. *RSC Advances*, **2011**, *1*, 1318-1323.

[18] Song, S.; Qin, Y.; He, Y.; Huang, Q.; Fan, C. and Chen, H. *Chem. Soc. Rev*., **2010**, *39*, 4234-4243.

[19] Horejsh, D.; Martini, F.; Poccia, F.; Ippolito, G.; Di Caro, A.; Capobianchi, M. R. *Nucleic Acids Res*., **2005**, *33*, e13.

[20] Si, M.L. *et al*. *Oncogene* **2006**, *26*, 2799-2803.

[21] Wang, J. *et al Cancer Prev Res* (Phila Pa) **2009**, *2*, 807-813.

[22] Chan, H.; Chan,L.; Shun Wong, R. and Li, W. *Anal. Chem.* **2010**, *82*, 6911–6918.

[23] Cuk, K.; Zucknick, M. et al. *Int. J. Cancer*, **2013**, *132*, 1602–1612.

[24] Gibellini, D. et al. *Mol. Cell. Probes* **2006**, *20*, 223-229.

[25] Baghat, A.A.S., kuntaegowdanahalli, S.S., Kaval, N., Seliskar C.J. and Papautsky I. *Biomed Microdevices* **2010**, *12*, 187-195.

[26] Tyagi, S., Bratu, D.P. and Kramer, F.R. *Nat. Biotecnol.* **1998**, *16*, 49-53.

[27] Lin, C., Liu, Y. and Yan, H. *Nanolett*, **2007**, *7*, 507-512.

[28] Asaga, S. *et al*. *Clinic Chem* **2011**, *57*, 84-91.

[29] Volinia S, Calin GA, Liu CG, et al. *Proc Natl Acad Sci USA* **2006**, *103*, 2257–61.